# A Study of the Conformational Distribution of Substituted 2,2'-Spirobiindan-1,1'-diones in Ferroelectric Liquid Crystals

by

**Qian Cui**

A thesis submitted to the Department of Chemistry

in conformity with the requirements

for the degree of Master of Science

Queen's University

Kingston, Ontario, Canada

September, 2007

*For my parents, Mr. Peisheng Cui and Ms. Wei Guo.*

# Abstract

Ferroelectric liquid crystals (FLCs) exhibit a bulk electric polarization ($P_S$) that can be coupled to an electric field to produce an ON-OFF light shutter, and are being investigated as an alternative to nematic liquid crystals in display applications. Commercial FLC mixtures normally consist of a small amount of chiral dopant in an achiral smectic C (SmC) liquid crystal host. Because the switching time of FLC display is inversely proportional to the induced polarization, the design of chiral dopants with high polarization powers ($\delta_p$) is a key aspect of FLC research. Such work requires an understanding of the relationship between molecular structure and polar order in the chiral SmC* phase.

Previous work in the Lemieux group focused on 2,2'-spirobiindan-1,1'-diones dopants, and a conformational model was proposed to explain the observed host dependence of the polarization power ($\delta_p$) of these dopants. In order to test this model, the 2,2'-spirobiindan-1,1'-dione core has been modified by introducing polar substituents and by modifying the functional groups linking the core to the alkyl side-chains. Specifically, this thesis focuses on implementing this approach via the synthesis and characterization of chloro- and methyl-substituted 2,2'-spirobiindan-1,1'-dione dopants.

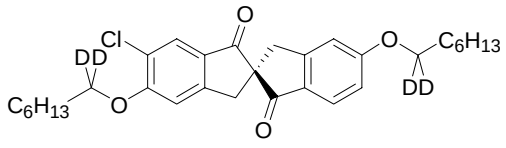


**2.1a**

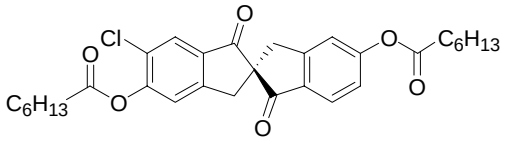


**2.1b**

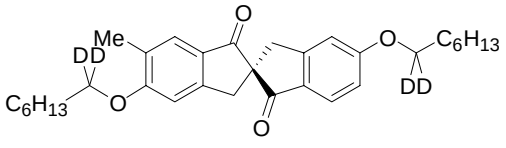


**2.2a**

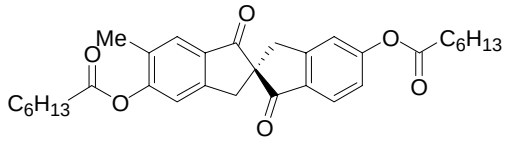


**2.2b**

Four chiral dopants (**2.1a**, **2.1b**, **2.2a** and **2.2b**) were synthesized, resolved and their absolute configurations assigned by CD spectroscopy. Their polarization powers were measured in four SmC hosts with different core structures. For both the ether-linked and ester-linked dopants, the addition of a substituent at the 6-position of one indanone ring results in lower polarization powers regardless of the size and polarity of the substituent, which is contrary to the original conformational distribution model.

A comparative study of the data suggests that the ester-linked dopants exert much stronger perturbations on the host environment than the ether-linked dopants, especially when the 6-position is substituted. We postulate that this perturbation is chiral in nature, and that the feedback effect of chirality transfer causes a shift in the conformational distribution of the dopant favoring conformers with negative polarity. Probe experiments were performed to detect the effect of chirality transfer feedback (CTF) in the case of the chloro-substituted diester dopant (**2.1b**), showing consistent results with the postulate.

## Acknowledgements

First of all, I would like to thank my supervisor Dr. Robert P. Lemieux for his support and guidance. Bob has set a fantastic example not only as a scientist but also as a successful person. His personality and thought will affect me for a life time.

A special acknowledgement is given to Dr. Derek Pratt and Dr. Suning Wang for being my committee members, and for offering valuable suggestions and help.

I feel greatly honored working together with the many 'nice' group-mates of the Lemieux lab, especially Dr. Jeff Roberts, Carl Carling, Christa Huntley, Eagranie Yuh, Jeremy Finden, Li Li, Linli Fang, Mark Moran, Matt Thompson, Markus Ohlin, Qingxiang Song, Sunny Lai and Wei Gan. Your friendship and help are appreciated and will never be forgotten.

I would also like delicate my grace to all the people who work behind the scenes, especially Dr. Françoise Sauriol in the NMR facility, Dr. Bernd Keller and Jie Sui in the mass spectrometry lab, Ed Maracle and Robin Roberts in the electronics shop, all the faculty members who taught me in courses and the many other people in the department whom I got help from and had fun with.

Last but not the least, I would like thank Shubin Zhao for his love and support as a husband, help and suggestion as a co-worker and strict requirement as a senior. I would love to thank my parents, who always love me, believe in me, and pray for me on the other half of the earth.

# Table of contents

# List of Tables

# List of Figures

# Abbreviations

| | |
|---|---|
| $\delta$ | Chemical shift |
| $\Delta\varepsilon$ | Difference in molar extinction coefficients between left- and right-handed circularly polarized light |
| $\Delta\nu$ | Quadrupolar splitting |
| $\Delta\Delta\nu$ | Difference between quadrupolar splitting values for two different $^2$H atoms |
| $\delta_P$ | Polarization power |
| $\delta_{probe}$ | Polarization power of probe dopant |
| $\lambda$ | Wavelength |
| $\lambda_{max}$ | Wavelength of maximum absorption |
| $\eta$ | Orientational viscosity |
| $\theta$ | Tilt angle |
| $\tau_r$ | Electro-optical rise time |
| $\mu_\perp$ | Transverse dipole moment |
| $2V_{ij}$ | Davydov split |
| $A$ | Amplitude of bisignate CD curve |
| Ac | Acetyl |
| AC | Alternating current |
| AIBN | Azo-bis-isobutylonitrile |
| AM1 | Austin model 1 semi-empirical method |
| aq | Aqueous |

| | |
|---|---|
| B3LYP | Becke's three parameter hybrid functional using the Lee, Yang, and Parr correlation functional (density functional theory method) |
| Bu | Butyl |
| **$C_2$** | $C_2$-symmetric conformer |
| calc'd | Calculated |
| CD | Circular dichroism |
| CTF | Chirality transfer feedback |
| DCC | 1,3-Dicyclohexylcarbodiimide |
| **DFT** | 2',3'-Difluoro-4"-heptyl-4-nonyl-[1,1';4',1"]terphenyl |
| dec. | Decomposed |
| DMAP | *N*,*N*-Dimethylaminopyridine |
| DMF | *N*,*N*-Dimethylformamide |
| EI | Electron impact ionization |
| ESI | Electrospray ionization |
| Et | Ethyl |
| $Et_2O$ | Ether |
| EtOAc | Ethyl acetate |
| EtOH | Ethanol |
| FLC | Ferroelectric liquid crystal |
| h | Hours |
| HPLC | High performance liquid chromatography |
| HRMS | High resolution mass spectrometry |
| I | Isotropic |

| | |
|---|---|
| ITO | Indium-tin oxide |
| *J* | Coupling constant |
| LC | Liquid crystal |
| LCD | Liquid crystal display |
| **MDW950** | 5-(2*S*,3*S*-difluorooctyloxy)-2-(4-octyloxyphenyl)pyridine |
| MeI | Methyl iodide |
| min | Minutes |
| mp | Melting point |
| MS | Mass spectrometry |
| N | Nematic |
| N* | Chiral nematic |
| $\hat{\mathbf{n}}$ | Director |
| NBS | *N*-Bromosuccinimide |
| **NCB76** | 4-(4'-heptyl[1,1'-biphenyl]-4-yl)-1-hexylcylohexanecarbonitrile |
| NMR | Nuclear magnetic resonance |
| **P** | Planar conformer |
| *p* | Helical pitch |
| Ph | Phenyl |
| ppm | Parts per million |
| $P_0$ | Reduced polarization |
| $P_S$ | Spontaneous polarization |
| **PhBz** | 4-[(±)-(4-methylhexyl)oxy]phenyl 4-decyloxybenzoate |
| **PhP1** | 2-(4-butyloxyphenyl)-5-(octyloxy)pyrimidine |

| | |
|---|---|
| rt | Room temperature |
| sat | Saturated |
| SmA | Smectic A |
| SmA* | Chiral smectic A |
| SmC | Smectic C |
| SmC* | Chiral smectic C |
| SSFLC | Surface-stabilized ferroelectric liquid crystal |
| $T$ | Temperature |
| $T_i$ | Polarization inversion temperature |
| $T_C$ | Curie point |
| THF | Tetrahydrofuran |
| TOF-MS | Time of flight mass spectrometry |
| UV-vis | Ultraviolet-visible |
| $\chi$ | Mole fraction |
| $\chi_d$ | Mole fraction of dopant |
| $\hat{\mathbf{z}}$ | Layer normal |

# Chapter 1. Introduction

Intermolecular interactions in liquid crystals play a crucial role in their performance in display applications. Research based on understanding this structure-property relationship is of particular interest in terms of ferroelectric liquid crystals (FLC), which have been investigated as an alternative to nematic liquid crystals in display applications due to their low power requirement and fast switching time. Typically, commercial FLC mixtures are composed of a small amount of a chiral additive (dopant) and a large amount of achiral liquid crystal host. The chiral dopant induces a spontaneous electric polarization ($P_S$) in the SmC phase that can be coupled to an applied electric field to produce an ON-OFF light shutter. The switching time of such devices is inversely proportional to $P_S$. Therefore, the design of chiral dopants that can induce high ferroelectric polarizations is a key aspect of FLC research and requires an understanding of the relationship between molecular structure and polar order in the chiral SmC* phase.

Previous work in the Lemieux's lab has led to a conformational distribution model for 2,2'-spirobiindan-1,1'-dione dopants in a SmC host. In order to test this model, the 2,2'-spirobiindan-1,1'-dione core has been modified by introducing polar substituents and by modifying functional groups linking the core to the alkyl side-chains. This thesis focuses an implementing this approach via the synthesis and characterization of chloro- and methyl-substituted 2,2'-spirobiindan-1,1'-dione dopants.

## 1.1. Background

Liquid crystals are intermediate phases between ordered crystalline and disordered liquid phases; while maintaining some degree of order, they also exhibit the fluid property

of liquids. First discovered by Reinitzer in 1888[1], liquid crystals have become a focus of research interest due to their potential applications, including liquid crystal display (LCD). Molecules that form liquid crystalline phases are referred to as mesogens, and there are two types. *Lyotropic* mesogens form liquid crystal phases as a function of their concentration in a solvent and temperature; *thermotropic* mesogens form liquid crystalline phases only as a function of temperature, and are the main focus of our research.

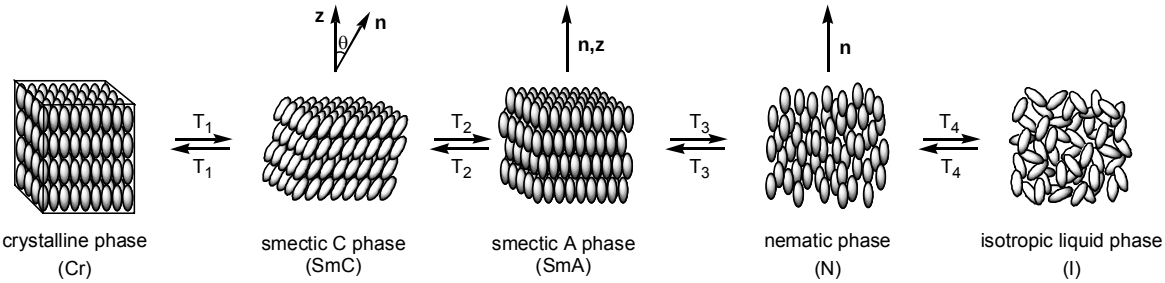


**Figure 1-1.** Phase transitions between crystal, liquid crystal, and isotropic liquid phases for a calamitic material as a function of temperature.

One of the most important types of thermotropic mesophases are calamitic liquid crystals, which are formed by rod-like molecules consisting of a rigid core and flexible alkyl side-chains. As shown in Figure 1-1, calamitic mesogens can form two main classes of liquid crystal phases: nematic and smectic. On the time average, molecules in the nematic phase have orientational order along the molecular long axis but are otherwise disordered. However, molecules in the smectic phase have both orientational and lamellar order. Despite the existence of many types of smectic mesophases, the smectic A (SmA) and smectic C (SmC) phases are the most commonly observed. The major difference between the two phases is that the orientation of molecular long axes ($\hat{\mathbf{n}}$) is parallel to the layer normal $\hat{\mathbf{z}}$ in the SmA phase, whereas $\hat{\mathbf{n}}$ is tilted by an angle $\theta$

with respect to $\hat{\mathbf{z}}$ in the SmC phase. For mesogens forming both the SmA and SmC phases, the SmC phase always forms at lower temperatures.

The liquid crystal phases described so far are achiral phases formed by achiral molecules. However, chiral mesophases are of particular interest because of their potential use in a broad range of technological applications, including a variety of electro-optical ON/OFF light shutters. Currently, most liquid crystal display applications are based on ON/OFF light shutters formed by chiral nematic liquid crystals.

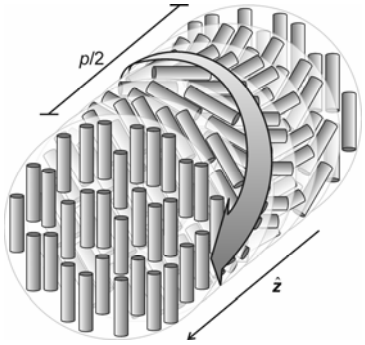


**Figure 1-2.** Structure of the chiral nematic phase showing the helical twist of $\hat{\mathbf{n}}$ along $\hat{\mathbf{z}}$ over ½ of the helical pitch, p.

The chiral nematic phase (N*) is also known as cholesteric phase for historical reasons.[1] By virtue of chirality, molecules in the N* phase are not uniformly organized along one direction, but instead twist along an axis $\hat{\mathbf{z}}$ perpendicular to $\hat{\mathbf{n}}$ to give a helical structure in the bulk that minimizes free energy, as shown in Figure 1-2. The length corresponding to a full rotation ($360^{o}$) of $\hat{\mathbf{n}}$ about $\hat{\mathbf{z}}$ is defined as the helical pitch (p), which is temperature dependent and reflects the degree of twisting.

Despite the many virtues of N* liquid crystal, chiral smetic (SmC*) liquid crystals have been investigated as an alternative to twisted nematic liquid crystal display (TN-LCD) due to their low power requirement and fast switching time ($10^2$~$10^3$ times faster than TN-LCD). [2~5]

## 1.2. Ferroelectric Liquid Crystals (FLCs)

Under certain alignment conditions, SmC* liquid crystals possess a spontaneous electric polarization whose orientation can be switched by application of an external electric field. This property is referred to as *ferroelectricity*, by analogy to ferromagnetism. The ferroelectricity in SmC* mesophase was first predicted by Meyer and coworkers in 1973 at the macroscopic level based upon a reduced symmetry argument. Shortly afterwards, its existence was confirmed experimentally.[6] The symmetry of the achiral SmC phase is $C_{2h}$ on the time average; it includes a $\sigma$ plane congruent to the tilt plane (defined by the molecular long axis $\hat{\mathbf{n}}$ and the layer normal $\hat{\mathbf{z}}$) and a $C_2$ axis perpendicular to the tilt plane (Figure 1-3). In the case of chiral SmC* phases, the reflection symmetry element vanishes, and transverse molecular dipoles may no longer cancel out along the $C_2$ axis, which results in a *spontaneous polarization* ($P_S$). This polarization is a chiral property intrinsic to each SmC* layer with a handedness (sign), i.e., enantiomeric materials give opposite signs of $P_S$. According to the physics convention, which defines an electric dipole as going from negative to positive, the spontaneous polarization is positive if it points in the same direction as the cross-product $\hat{\mathbf{z}} \times \hat{\mathbf{n}}$. [7]

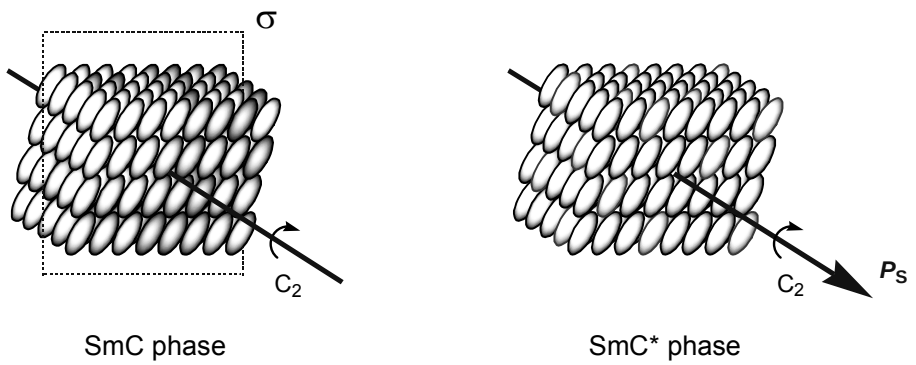


**Figure 1-3.** Symmetry elements of the achiral SmC and chiral SmC* phases.

However, as with the chiral nematic phase, another supramolecular manifestation of molecular chirality in the SmC* phase is a helical structure defined by the precession of $\hat{\mathbf{n}}$ about the layer normal $\hat{\mathbf{z}}$ from one layer to the next (Figure 1-4(a)). Since $P_S$ is oriented along $\hat{\mathbf{z}} \times \hat{\mathbf{n}}$, it rotates periodically from one layer to the next, thus averaging to zero in the helical state over a full precession of $\hat{\mathbf{n}}$ about $\hat{\mathbf{z}}$.

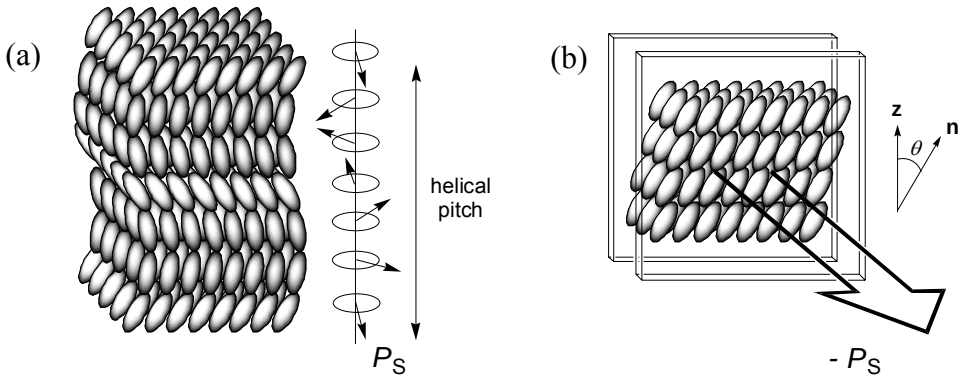


**Figure 1-4.** (a) Helical structure of the SmC* phase in the absence of external constraints, and (b) surface stabilized ferroelectric liquid crystal sandwiched between two glass slides.

A solution to this problem was reported by Clark and Lagerwall in 1980.[8] They observed that constraining the SmC* material between two glass plates with rubbed polyimide alignment layers and a spacing on the order of the helical pitch (usually a few microns) causes the SmC* helix to spontaneous unwind to give a *surface-stabilized ferroelectric liquid crystal* (SSFLC) with a net spontaneous polarization oriented perpendicular to the glass plate (Figure 1-4(b)). When the plates are coated with a transparent conducting material, such as indium-tin oxide (ITO), the polarization can be coupled to an applied electric field, and the tilt orientation of the molecules can be driven between two opposite states by switching the sign of the electric field (Figure 1-5). Because liquid crystals are birefringent, this device forms an effective ON/OFF light shutter when placed between crossed polarizers.

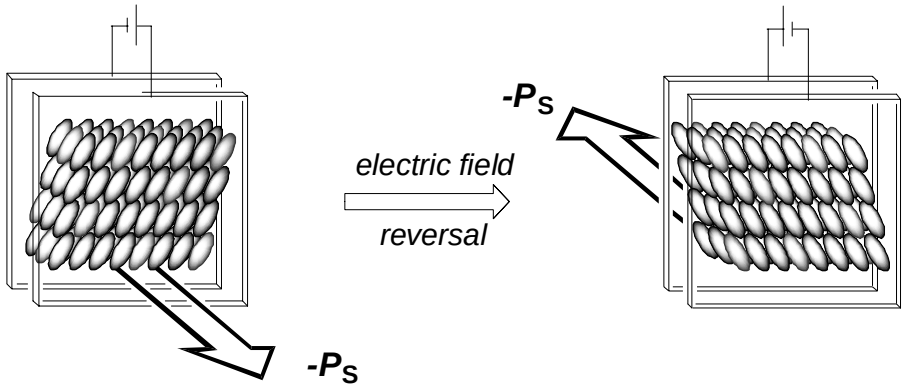


**Figure 1-5**. Switching of SSFLC by changing the direction of an applied external electric field.

The ON/OFF switching of a SSFLC electro-optical device is achieved by the mesogens collectively precessing about $\hat{\mathbf{z}}$ from one tilt orientation to the other, and can take place on the microsecond time scale. The switching time ($\tau_r$) of this so-called "Goldstone-mode", is proportional to the rotational viscosity of the material ($\eta$) and inversely proportional to the magnitude of $P_S$ and the strength of the applied field ($E$) according to eq. 1-1[9]:

$$\tau_r \propto \frac{\eta}{|P_S|E} \tag{1-1}$$

For high-performance devices, it is therefore desirable to create materials with large polarizations and low viscosity. Unfortunately, there is an inevitable conflict between $P_S$ and viscosity for pure SmC* materials, since the introduction of lateral polar groups that favors large polarizations also tends to increase the rotational viscosity. [10]

However, in 1980, Kuczynski and Stegemeyer showed that ferroelectricity can be induced by adding a small amount of chiral dopant in achiral SmC materials.[11] Later on, Beresnev and co-workers observed that dopants which are structurally similar to the liquid crystal host induce polarizations that scale linearly with the dopant

concentration.[12, 13] The dopant itself does not have to be liquid crystalline, but it must be soluble in the host. Hence, commercial FLC formulations normally consist of achiral SmC liquid crystal mixtures with low viscosity and wide temperature range as host, and a highly compatible chiral dopant with the ability to induce optimum polarizations (based on the desired $\tau_r$) at low concentration. This ability of a chiral dopant to induce a spontaneous polarization is expressed by its *polarization power,* $\delta_P$ [14]:

$$\delta_P(\Delta T) = \left( \frac{dP_0(\chi_d)}{d\chi_d} \right)_{\chi_d \to 0} \tag{1-2}$$

$$P_0 = P_S / \sin\theta \tag{1-3}$$

where $\chi_d$ is the mole fraction of the chiral dopant, $\Delta T$ is the reduced temperature $T - T_C$, and $T_C$ is the Curie point referring to the phase transition temperature from the ferroelectric SmC* phase to a non-ferroelectric phase at higher temperature. $P_0$ is the reduced polarization, a normalized form of $P_S$ that takes into account variations in tilt angle from one host to the next, and is therefore a material constant that reflects the polar ordering of molecular dipoles. The polarization power is used to compare materials in terms of structure-property relationship. In order to effectively design chiral dopants with extremely large polarization powers, which is a key aspect of FLC applications, a detailed understanding of the molecular origins of the spontaneous polarization is required.

## 1.3. Molecular Origin of $P_S$

### *1.3.1. The Boulder Model*

The Boulder model [7, 15], proposed in 1986 by Walba and Clark, describes the origins of the spontaneous polarization in the SmC* phase at the molecular level using

conformational analysis. This model is particularly useful in qualitatively predicting the direction (sign) and relative magnitude of $P_S$ in doped and neat SmC* materials. More recently, computational models have been developed to make semi-quantitative predictions of $P_S$ values. [16, 17]

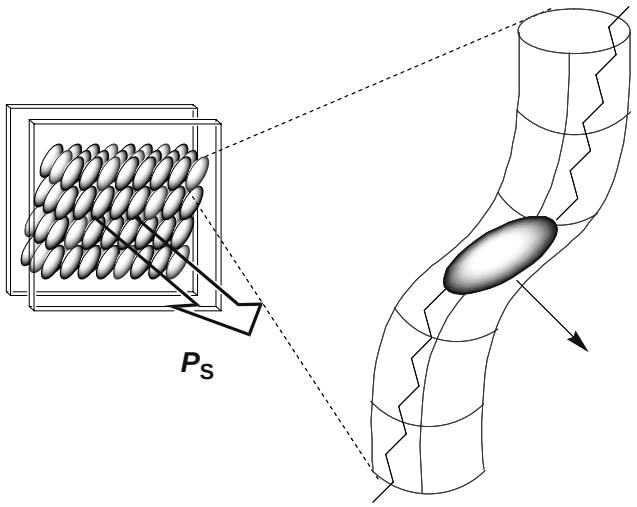


**Figure 1-6.** The bent-cylinder shaped binding site of the SmC phase according to the Boulder model.

The Boulder model assumes that the ordering imposed by the SmC phase on individual molecules can be modeled by a *bent cylinder* with $C_{2h}$ symmetry (Figure 1-6). The shape of this "binding site" is consistent with experimental evidence derived from powder X-ray diffraction [18], polarized optical microscopy and deuterium NMR studies[19,20], suggesting that the core of a calamitic molecule in the SmC phase is more tilted than the side-chains.

The zigzag shape of this binding site is also consistent with the rotational order of molecules about the director $\hat{\mathbf{n}}$, which is the origin of polar order in the SmC phase. This can be understood based on a molecular view of the SmC layers, as shown in Figure 1-7.

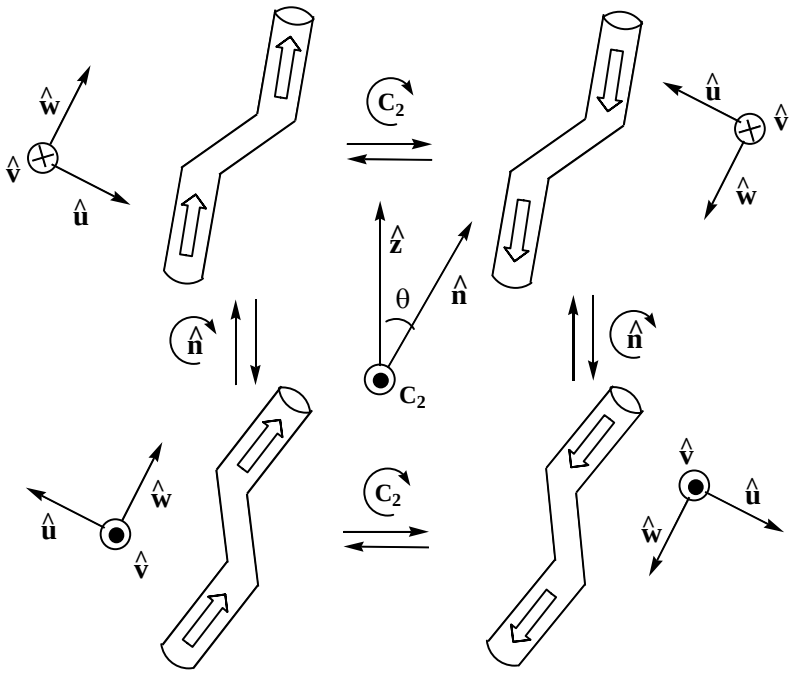


**Figure 1-7.** Polar order in the SmC* phase for a generic mesogen. The components of the molecular dipole are defined by the axes $\hat{\mathbf{u}}$, $\hat{\mathbf{v}}$, and $\hat{\mathbf{w}}$. Horizontally, the states differ by rotation about the $C_2$ axis. Vertically, the states differ by rotation about $\hat{\mathbf{n}}$, the molecular long axis.

Consider a generic SmC mesogen with three orthogonal dipole components: $\hat{\mathbf{u}}$, $\hat{\mathbf{v}}$, and $\hat{\mathbf{w}}$. Both the top and the bottom two states with the molecules pointing in opposite directions are degenerate, with respect to the $C_2$ operation, and dipole components along $\hat{\mathbf{u}}$ and $\hat{\mathbf{w}}$ cancel out. However, interconversion between the upper and lower states is restricted in the SmC phase because these two rotational states are not energetically equivalent: the upper state with the core more tilted than the side-chains is favoured in the SmC phase. Hence, a bulk polarization may exist along $\hat{\mathbf{v}}$ (the $C_2$ axis) if the molecule is chiral (*i.e.* the average projection of $\hat{\mathbf{v}}$ onto the $C_2$ axis is non-zero). For doped SmC* material, the achiral SmC host acts as a supramolecular host, in which the guest dopant molecules adopt a zigzag conformation with the core more tilted than the side-chains, as if they were confined by the zigzag binding site. Therefore, transverse molecular dipoles

in a chiral dopant may contribute to $P_S$ in an induced SmC* phase provided that they are coupled to a stereogenic center *(vide infra*).

In order to predict the sign and magnitude for $P_S$ of a particular SmC* material, a general expression for $P_S$ in terms of molecular dipoles is required [15]:

$$P_S = \sum_i \frac{D_i \mu_{\perp i} ROF_i}{\varepsilon} \tag{1-4}$$

where ε is the dielectric constant for the material and, for the *i*th conformation, $D_i$ is the molecular number density, $\mu_{\perp i}$ is the projection of its dipole moment along the polar $C_2$ axis, and $ROF_i$ is its *rotational orientation factor* reflecting the degree of rotational order imposed on the conformation by the binding site. Since more than one polar functional group is usually found in a chiral molecule, this expression is especially useful because it includes only those polar functional groups which are sterically coupled to the stereocenter (*stereo-polar coupling*, $ROF_i \neq 0$). Other polar functional groups with no stereo-polar coupling have no orientational bias ($ROF_i = 0$) and therefore do not contribute to $P_S$. A well-studied class of liquid crystals containing a chiral 2-octyloxy side-chain (*i.e*. **1.1**) is a perfect example. [21]

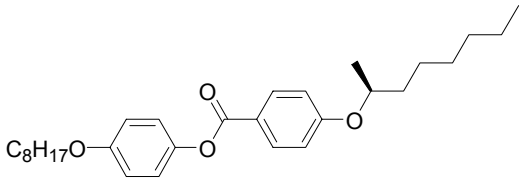


(*S*)-**1.1**

Although there are three polar functional groups present in **1.1**, only the ether group coupled to the stereogenic center contributes to $P_S$; the ester and 1-octyloxy groups are too far away from the stereocenter and are therefore expected to have symmetrical conformational distributions. When confined to the SmC binding site, the 2-octyloxy unit

in **1.1** can adopt three different staggered conformations about the $C_2$-$C_3$ bond with the ether group being coplanar with the aromatic ring and the side-chains fully extended in an all-*anti* conformation. However, only two of the three conformations contribute to the polarization, because the alkoxy dipole in one conformation lies in the tilt plane. As shown in Figure 1-8, the two conformations **A** and **B** have opposite polarities, but conformer **A** is energetically favored by virtue of the *anti* relationship between the methyl group and the rest of the alkyl side-chain. The magnitude of $P_S$ should be a function of the energy difference between conformations **A** and **B**. As a result, this analysis predicts that dopant (*S*)-**1.1** should produce a negative $P_S$, which is consistent with experimental results.

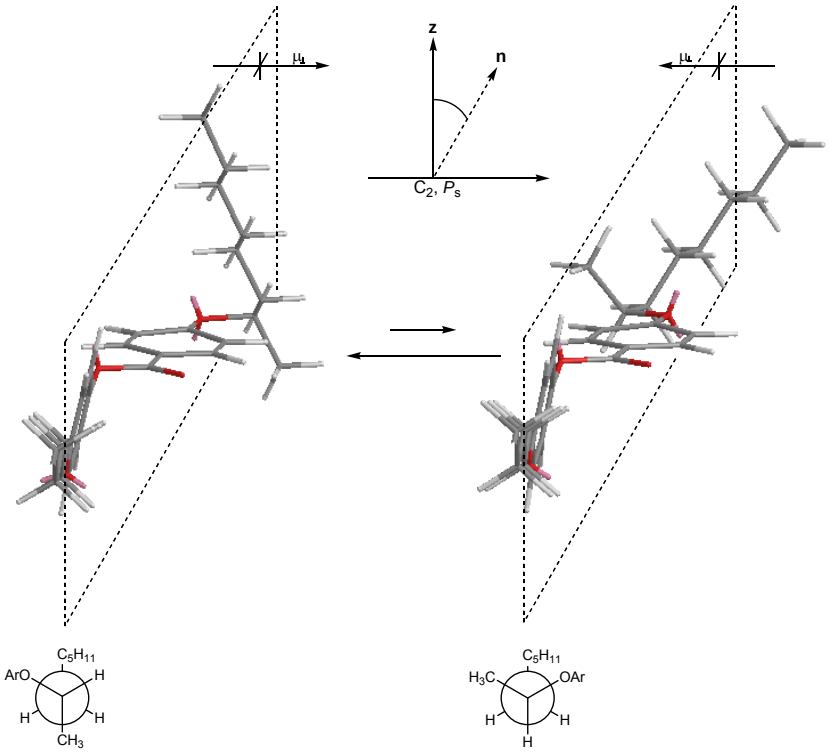


**Figure 1-8.** Conformations of (*S*)-**1.1** contributing to $P_S$ according to the Boulder model. The tilt plane is represented by the dashed box where $\hat{\mathbf{n}}$ points back into the page. The direction of the transverse dipole moment is indicated (pointing from negative to positive consistent with the physics convention). This model correctly predicts a negative $P_S$. From ref. 21.

*1.3.2. Limitation of the Boulder Model: Two Types of Dopants*

As with many models, the Boulder Model has its limitations. At a first approximation, the dopant molecules are considered to be *passive* guests with conformational distributions that provide the best fit to the binding site of the SmC host, which is assumed to have $C_{2h}$ symmetry and the same shape for all SmC hosts. This assumption is certainly reasonable for most conventional dopants, which have the stereo-polar unit (coupled polar group and stereogenic center, SPU) located in one of the side chains (Type I, *e.g.* **1.1**).[22] The polarization power of Type I dopant is generally invariant of the host structure, which is consistent with the liquid-like nature of the paraffinic regions of the SmC layer structure.[23] Moving the SPU closer to the core or having two adjacent stereogenic centres (*e.g.* **MDW950**) increases its conformational rigidity, and some host dependence of $\delta_P$ may be observed.[16, 17, 24] Finally, chiral dopants with SPUs located in the rigid core (*i.e.* **1.2**) generally have polarization powers that vary strongly with the structure of the host (Type II).[22, 16, 17] Such a manifestation of molecular recognition is consistent with the crystal-like nature of the core region of the SmC layer structure. In some cases, a Type II dopant may behave as an *active* guest by perturbing the binding site topography (*vide infra*). Under these circumstances, the original Boulder model needs to be refined.

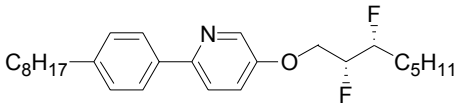


**MDW950**

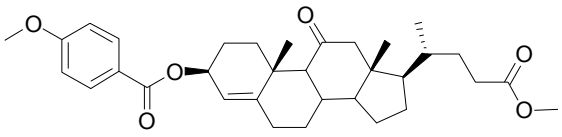


**1.2**

Stegemeyer and co-workers developed two models to explain the host dependence behavior of Type II dopants. In the first model, the dopants are assumed to be passive

guests and the polarization they induce is described in terms of the orientational distribution of the tranverse dipole moment $\mu_\perp$ and its polar ordering term according to eq. 1-5:

$$P_S = N\mu_\perp \cos\Psi_o \langle \cos\Psi \rangle \tag{1-5}$$

where $N$ is the dopant number density, $\mu_\perp$ is the transverse dipole moment of the dopant, $\psi_o$ is the angle between $\mu_\perp$ and a molecular reference axis, and $\langle cos\psi \rangle$ is the polar ordering term (Figure 1-9(a). For example, dopants that have poor miscibility with the host tend to induce small polarizations, because a destabilization of the SmC phase will lower the polar ordering term. Likewise, for a given degree of polar ordering, a dopant may induce a low polarization in one host if the transverse molecular dipole $\mu_\perp$ lies closer to the tilt plane ($\psi$ is big), and high polarization in another host if $\mu_\perp$ lies closer to the polar axis ($\psi$ is small) (Figure 1-9(b)). This model can be adapted to the Boulder model by assuming that the topography of the central part of the binding site varies with the host structure.

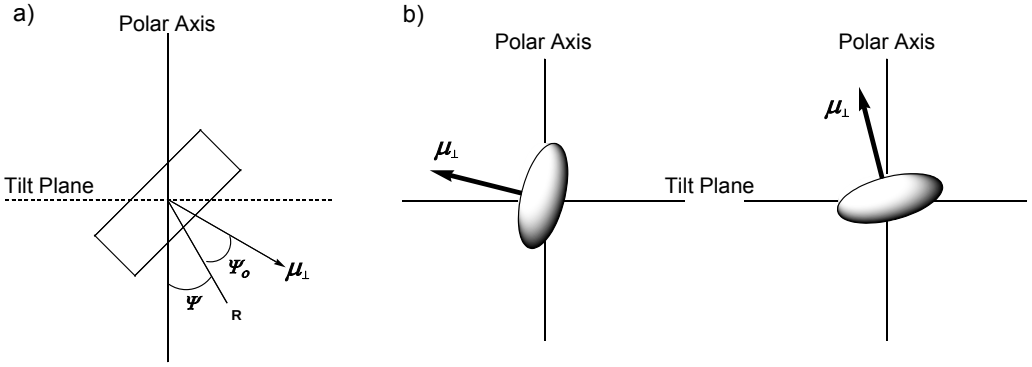


**Figure 1-9.** (a) Orientation of the dipole moment of a Type II chiral dopant with respect to a molecular reference axis (R); and (b) different rotational distributions of a Type II chiral dopant and its transverse dipole moment ($\mu_\perp$) viewed along the molecular long axis.

In the second model, the notion of intermolecular chirality transfer similar to that described in induced N* phase is introduced, and the dopant is assumed to be an *active* guest that exerts a chiral perturbation on surrounding host molecules, resulting in a polar ordering of the host that contributes to the observed polarization. In this case, two possibilities exist: the dopant and host transverse dipoles may point in the same direction, resulting in a larger polarization, or in opposite directions, resulting in a smaller polarization, or a polarization of opposite sign.

## 1.4. Axially Chiral Dopants with Atropisomeric Biphenyl Cores

Unlike most type II dopants with stereogenic centers located in the core, research in the Lemieux group has focused on a class of unconventional dopants with an axis of chirality. The core structure of one dopant family features *ortho*-tetrasubstituted biphenyl units whose rotation about the biphenyl bond is restricted (atropisomerism).

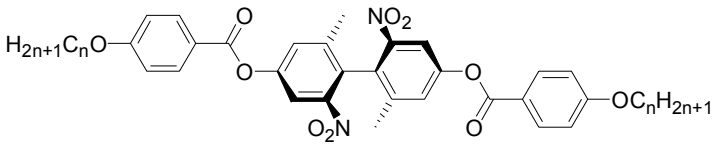


**1.3a**, n = 8; **1.3b**, n = 9

The initial design of these atropisomeric biphenyl dopants featured polar nitro groups *ortho* to the biphenyl bond (i.e. **1.3a** and **1.3b**).[25, 26] As expected, the $\delta_P$ of these dopants showed a significant host dependence, which is consistent with Stegemeyer's observations, but the absolute values of $\delta_P$ were smaller than anticipated considering the large transverse dipole moment of the core (~5D according to AM1 calculation). This observation can be explained by considering the Boulder model. Figure 1-10(a) shows an energy-minimized conformation of the dopant molecule that approximates the shape of

the zigzag binding site. Assuming that the 4-alkoxybenzoate groups lie in the tilt plane and do not contribute to the $P_S$, four conformational energy minima are obtained based on AM1 calculations using a simplified model compound of **1.3a** (Figure 1-10(b)). Only the upper two conformations with opposite polarities can contribute to $P_S$, because the lower conformations have polar groups equally distributed on each side of the tilt plane. The energy difference between conformers (a) and (b) is quite small in the gas phase (on the order of 0.2 kcal/mol), which suggests that the biphenyl core can rotate almost freely with respect to the 4-alkoxybenzoate side-chains with minimal distortion to the overall zigzag shape. Because such a low conformational bias would correspond to a low $ROF_i$, the $P_S$ is small even though the molecular transverse dipole moment $\mu_\perp$ is large.

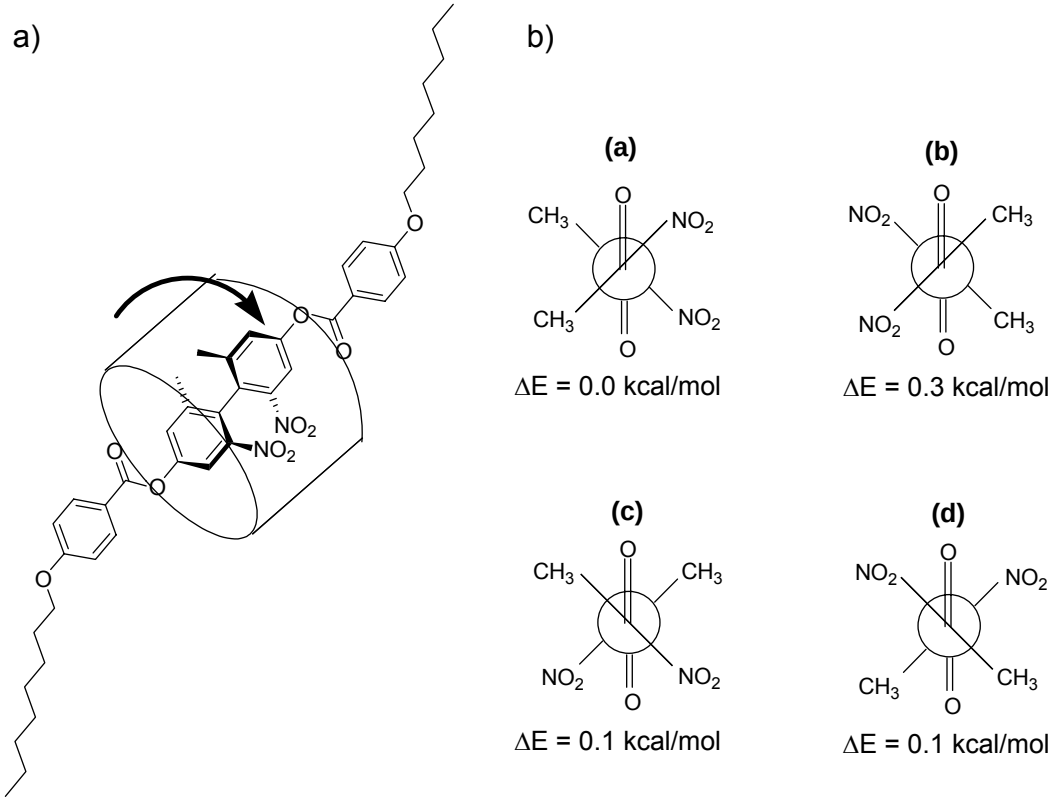


**Figure 1-10.** Conformations predicted by the Boulder model and AM1 calculation for **1.3a**. Only conformations (a) and (b) contribute to $P_S$.

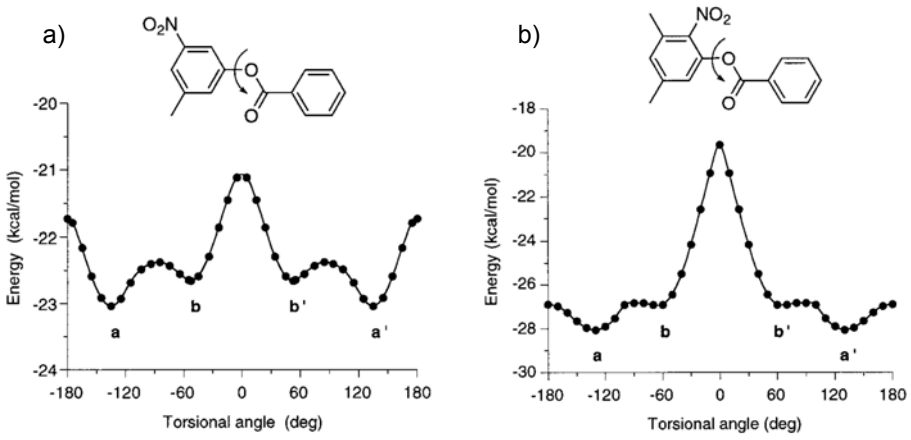


**Figure 1-11.** Energy profiles for (left) 3-methyl-5-nitrophenyl benzoate and (right) 3,5-dimethyl-2-nitrophenyl benzoate as a function of the torsional angle defined by C-6, C-1, O, C(O) and C-2, C-1, O, C(O), respectively, according to AM1 calculations. From ref. 27.

In order to increase the asymmetric conformational bias of the chiral core in the binding site, better coupling between the core and the side-chains was sought. Therefore, in subsequent designs of the atropisomeric biphenyl dopants, the symmetry-breaking groups were moved *ortho* to the side chains. According to AM1 calculations (Figure 1-11), shifting the nitro group from the 2- to the 3-position increases the energy difference between conformation (a) and (b) by a factor of 3 (1.2 vs. 0.4 kcal/mol) for the model compounds. A series of dopants were synthesized (**1.4a–j**, **1.5–1.9**) to study the effects of structural variations on the sign and magnitude of $\delta_P$ (side-chain length, polar functional group, relative position of the core) in different hosts. [27~30]

As shown in Table 1-1, the absolute value of $\delta_P$ for the 3,3'-dinitro dopant **1.4d** is significant larger than the 2,2'-dinitro analogue **1.3a** in every host (except for **PhBz**, in which $\delta_P$ is below the detection limit for both dopants), which is consistent with the enhanced bias predicted by the conformational analysis. Remarkably, the $\delta_P$ value for **1.4d** in **PhP1** (1738 nC/cm$^2$) is the highest reported in the literature for a chiral dopant of

any kind, and this value is more than 10 times larger than the $\delta_P$ value of **1.3a** in the same host (161 nC/cm$^2$). Given that $\delta_P$ for **1.4d** is only twice the value for **1.3a** in **NCB76** and **DFT**, the predicted increase in conformational asymmetry may not be the only factor responsible for the extremely large polarization power observed for dopant **1.4d** in **PhP1**.

**Table 1-1.** Polarization powers for selected dopants in four LC hosts.

| Dopant (X) | $\delta_P$ (nC/cm$^2$)$^{a,b}$ | | | |
|---|---|---|---|---|
| | **PhP1** | **PhBz** | **NCB76** | **DFT** |
| (*R*)-**1.3a** | 161 (-) | < 30 (+) | 170 (-) | 63 (-) |
| (*S*)-**1.4d** | 1738 ± 95 (+) | < 30 (-) | 373 ± 54 (+) | 124 (+) |
| (*R*)-**1.6** | 255 ± 36 (-) | < 40 (+) | 94 ± 3 (+) | 59 ± 6 (+) |
| (*S*)-**1.7** | 197 ± 28 (+) | < 30 (+) | 116 ± 7 (+) | 60 ± 7 (+) |
| (*S*)-**1.8** | 34 (+) | < 20 (+) | 83 ± 4 (+) | 42 ± 1 (+) |
| (*S*)-**1.9** | 46 ± 6 (-) | < 26 (-) | < 43 (-) | < 60 (-) |

[a]Uncertainties are ±1 standard deviation. [b]Sign of $P_S$ indicated in parentheses. From ref. 26, 27, 30.

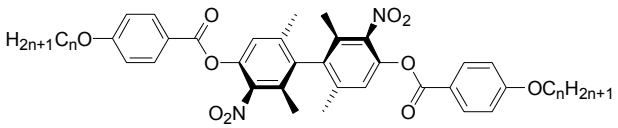

**1.4a**, n = 1; **1.4b**, n = 4; **1.4c**, n = 6; **1.4d**, n = 8; **1.4e**, n = 9; **1.4f**, n = 12; **1.4g**, n = 14; **1.4h**, n = 16; **1.4i**, n = 18; **1.4j**, n = 20

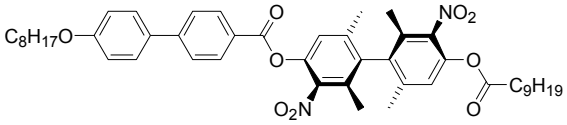

**1.5**

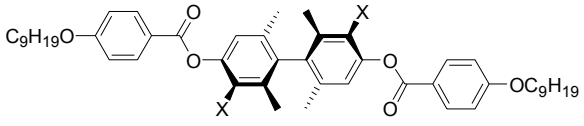

**1.6**, X = F; **1.7**, X = Cl; **1.8**, X = Br; **1.9**, X = $CH_3$

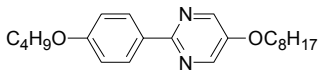

**PhP1**: Cr 58 SmC 85 SmA 95 N 98 I

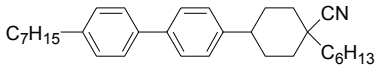

**NCB76**: Cr 66 (SmG 55) SmC 73 SmA 116 N 125 I

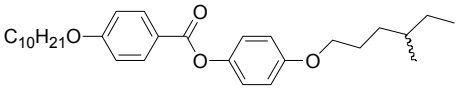

**PhBz**: Cr 35 SmC 70.5 SmA 72 N 75 I

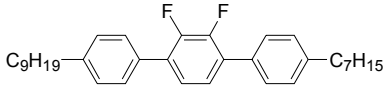

**DFT**: Cr 49 SmC 77 SmA 93 N 108 I

## 1.5. The Chirality Transfer Feedback Model (CTF)

A series of experiments correlating alkoxy chain length in series **1.4a–j** to $\delta_P$ and the helical pitch of the induced SmC* phase provided evidence suggesting that $\delta_P$ in **PhP1** may be a function of the degree of chirality transfer taking place via core-core interactions between the dopant and host molecules.[27] Gottarelli and co-workers pointed out that a good structural match between dopant and host molecules is essential for chirality transfer to occur in the induced N* phase [31~33], in which a dopant molecule distorts its neighboring host molecule towards a homochiral conformation, and the host molecule then passes this conformation to its next neighbor and so on. A similar argument can be applied to the induced SmC* phase. In the case of dopant **1.4d**, the best structural match between dopant and host molecules is with **PhP1**, which accounts for the very large $\delta_P$ observed (Figure 12(a)).

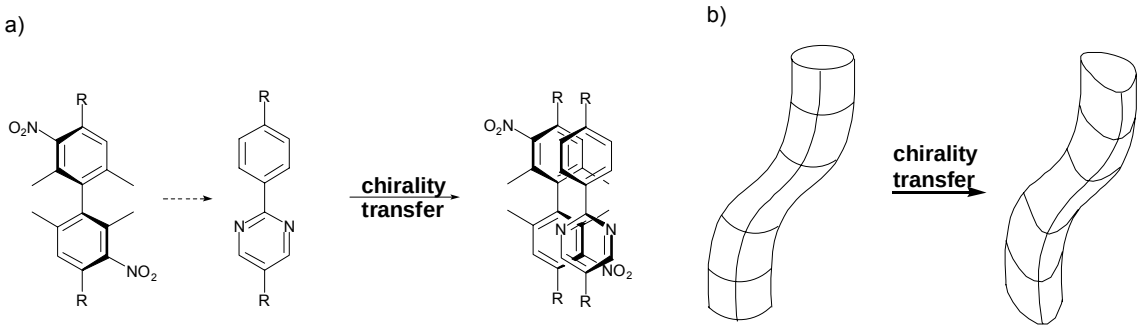


**Figure 1-12.** (a) Proposed model for chirality transfer via core-core interactions; and (b) chirality transfer resulting in a chiral distortion of the SmC binding site.

However, considering that the core structure of **PhP1** is unlikely to contribute to $P_S$ based on Stegemeyer's model, the Lemieux group proposed the *Chirality Transfer Feedback* (CTF) model [34] to account for the very large $\delta_P$ values of **1.4d** in this host. According to this model, dopants such as **1.4d** exert a chiral perturbation on surrounding

host molecules via core-core interactions, which causes a reduction in symmetry of the SmC binding site from $C_{2h}$ into $C_2$, as shown in Figure 1-12(b). As a feedback effect, this chiral distortion may cause a shift in the conformational distribution of the dopant because of the diastereomeric relationships between the various chiral conformers and the chiral binding site. The CTF model can be thought of as intermolecular, solvent-mediated stereo-polar coupling, or as a dynamic form of chiral molecular imprinting. The validity of this model in this particular example was confirmed by probe experiments (*vide infra*).[35, 36]

### 1.6. Detecting Chirality Transfer Feedback Using Probe Experiments

The first direct evidence for chirality transfer in the SmC* phase was obtained by formulating mixtures of dopant **1.4d**, **PhP1**, and **MDW950**, a second chiral dopant that structurally mimics the SmC host.[35] The polarization power of **MDW950** was measured in the presence of (*R*)- or (*S*)-**1.4d** in **PhP1**as a constant mole fraction of 0.04. A similar set of experiments were conducted in **PhBz**, using **1.10** as the probe instead of **MDW950** to mimic the host.

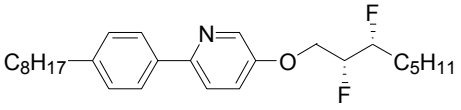


**MDW950**

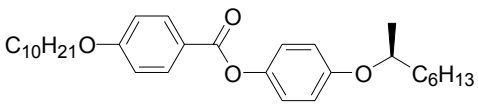


**1.10**

Any conclusion derived from the results is based on the assumption that any perturbation exerted by **1.4d** on the SmC host will affect the polarization power of the probe ($\delta_{probe}$). If **1.4d** is passive, one would expect the induced $P_0$ from **1.4d** and the probe to be simply additive and $\delta_{probe}$ to remain unchanged. On the other hand, if **1.4d** is

active and perturbs the host, $\delta_{probe}$ measured in the presence of **1.4d** would be different from the $\delta_{probe}$ value obtained in the absence of **1.4d**. Whether the perturbation exerted by **1.4d** is chiral or not can be determined by comparing $\delta_{probe}$ values obtained with the (*R*) and (*S*) forms of the dopant. If the perturbation is achiral in nature, both enantiomers should affect $\delta_{probe}$ to the same extent. Otherwise, if the perturbation is chiral in nature, $\delta_{probe}$ measured with the (*R*) enantiomer should be different from that measured with the (*S*) enantiomer because of the diastereomeric pairs formed by the dopant and probe molecules.

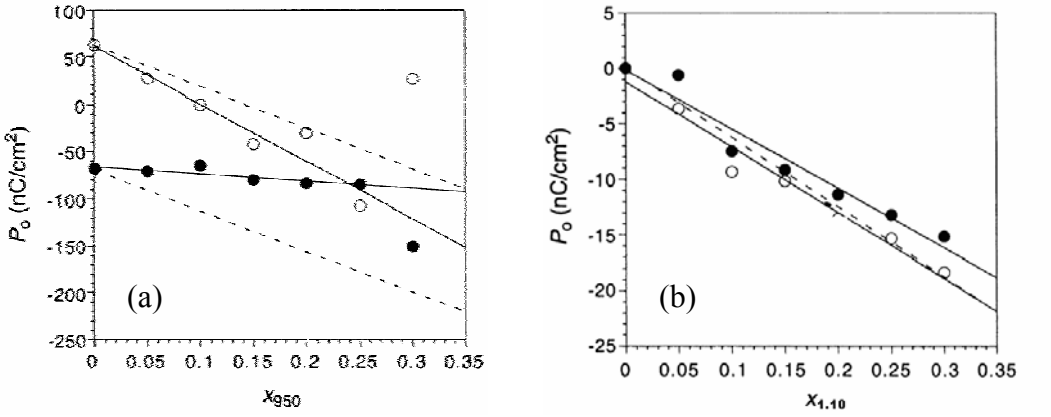


**Figure 1-13**. Reduced polarization, $P_0$, versus mole fraction of probe molecule, $x_{probe}$, at $T$-$T_C$ = –5 K in the presence of (*S*)-**1.4d** (○) and (*R*)-**1.4d** (●) at a constant mole fraction $x_{4d}$= 0.04 for (a) **MDW950** in **PhP1** and (b) **1.10** in **PhBz**. The slope of the dashed lines corresponds to the polarization power of the probe in pertinent host in the absence of the chiral dopant. From ref. 35.

As shown in Figure 1-13 (a), the plots of $P_0$ versus $\chi_{950}$ in **PhP1** gave good linear fits expect for the very last point, which might be the result of a cooperative effect between probe molecules. The values of $\delta_{950}$ with (*R*)-**1.4d**, (*S*)-**1.4d** and without **1.4d** are –78 ± 23 nC/cm$^2$, –605 ± 88 nC/cm$^2$, and –435 ± 11 nC/cm$^2$, respectively. The results strongly suggest that **1.4d** is an active dopant in **PhP1**, and that the perturbation is chiral in nature. On the other hand, in the plots of $P_0$ versus $\chi_{1.10}$ in **PhBz** (Figure 1-13 (b)),

$\delta_{1.10}$ in the presence of either (*S*)-**1.4** or (*R*)-**1.4** ($\delta_{1.11}$ = –59 ± 5 nC/cm$^2$ and –53 ± 6 nC/cm$^2$ for (*S*)- and (*R*)-**1.4d**, respectively) did not vary much from its value in the absence of **1.4d** (–62 ± 7 nC/cm$^2$), which suggests that little or no chiral perturbation is exerted by **1.4d** in **PhBz**.

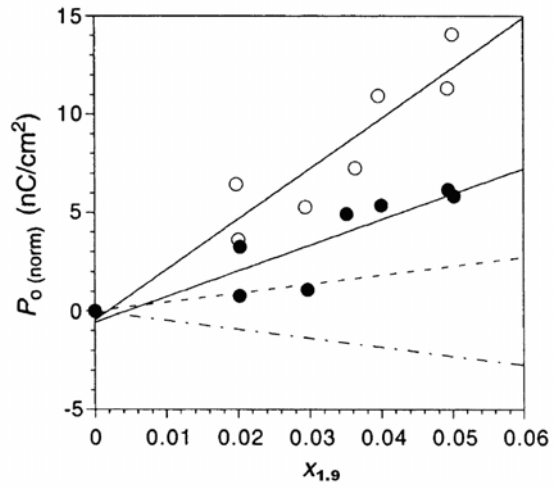


**Figure 1-14.** Normalized reduced polarization ($P_{0(norm)}$) vs. mole fraction of (*R*)-**1.9** (○) and (*S*)-**1.9** (●) in **PhP1** in the presence of 4.1-3.9 mol% (*S*)-**1.4d** 5 K below the SmA*-SmC* transition temperature. The $P_{0(norm)}$ values are obtained by subtracting the calculated reduced polarization induced by (*S*)-**4d** from the total reduced polarization. The solid lines represent least-squares fits of the two data sets and the dashed lines represent reference plots for (*R*)- and (*S*)-**1.9** (short and long dashes respectively) in the absence of **1.4d**. From ref. 36.

In order to address the "feedback" effect of the CTF mechanism, the probe dopants was modified to mimic the structure of **1.4d** to determine whether any chiral perturbation exerted by **1.4d** on **PhP1** can amplify the polarization power of another atropisomeric dopant. [36] Therefore, a third probe experiment was carried out in **PhP1** using optically pure **1.9** as the probe dopant, which was shown to exert little chiral perturbations in **PhP1** (Figure 1-14). Least-squares fits of the plots give $\delta_{1.9}$ values of +256 ± 36 nC/cm$^2$ and +130 ± 28 nC/cm$^2$ for (*R*)- and (*S*)-**1.9** respectively, compared to $\delta_{1.9}$ values of +46 and –46 ± 6 nC/cm$^2$ in the absence of **1.4d**. These results not only

support the feedback effect of the CTF model, but also are consistent with the particularly large polarization power of **1.4d** in **PhP1**, suggesting that chirality transfer may enhance a conformational bias, as the chiral perturbation exerted by (*S*)-**1.4d** on **PhP1** causes a 5.5-fold increase in $\delta_{1,9}$ for (*R*)-**1.9**, and a 2.8-fold increase in $\delta_{1,9}$ combined with a sign reversal of the polarization for (*S*)-**1.9**.

## 1.7. Dopants with a Substituted 2,2'-Spirobiindan-1,1'-dione Core

### *1.7.1. Dopants with a 2,2'-Spirobiindan-1,1'-dione Core*

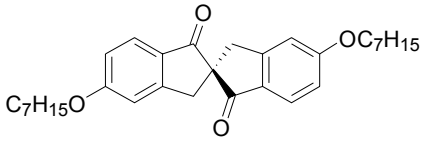


(*R*)-**1.11a**

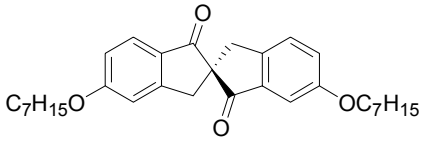


(*S*)-**1.12**

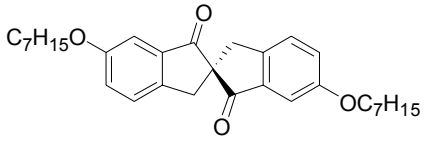


(*R*)-**1.13**

Dopants with high $\delta_P$ need to have a large transverse dipole moment and high orientational and conformational order. However, despite the very large $\delta_p$ of **1.4d** in **PhP1**, molecular modeling suggests that the biphenyl core can rotate almost freely with respect to the ester side chains, and that the conformational bias between two conformers of opposite polarities is small, on the order of only 1 kcal/mole in the gas phase. Hence, we postulated that even larger polarization powers might be achieved by designing dopants with polar chiral cores that are conformationally more restricted when confined to the zigzag binding site of the Boulder model. Hence, three isomers of the diheptyloxy derivative of 2,2'-spirobiindan-1,1'-dione were synthesized and characterized as chiral

dopants: 5,5'-diheptyloxy-2,2'-spirobiindan-1,1'-dione (**1.11a**), 5,6'-diheptyloxy-2,2'-spirobiindan-1,1'-dione (**1.12**), and 6,6'-diheptyloxy-2,2'-spirobiindan-1,1'-dione (**1.13**).[37]

It was shown that the polarization power of the three dopants depends strongly on the nature of the host (Table 1-2). Despite their similarity in structure, (*R*)-**1.11a** induces uniformly positive polarizations in all four hosts, whereas the 6-6'-isomer (*R*)-**1.13** induces uniformly negative polarizations and shows different trend in $\delta_p$ versus host. The unsymmetrical dopant (*S*)-**1.12** behaves as a hybrid of the two symmetrical dopants, showing a strong host dependence and both negative and positive values of $\delta_p$.

**Table 1-2.** Polarization powers for dopants (*R*)-**1.11a**, (*S*)-**1.12** and (*R*)-**1.13** in four LC hosts.

| Dopant (X) | $\delta_P$ (nC/cm$^2$)[a,b] | | | |
|---|---|---|---|---|
| | **PhP1** | **PhB** | **NCB76** | **DFT** |
| (*R*)-**1.11a** (5,5') | 749 ± 35 (+) | 460 ± 13 (+) | 363 ± 30 (+) | 21 ± 3 (+) |
| (*S*)-**1.12** (5,6') | > 11(+) | 130 ± 7 (–) | 144 ± (7) (–) | 220 ± 5 (–) |
| (*R*)-**1.13** (6,6') | > 160 (–) | 79 ± 9 (–) | 1037 ± 100 (–) | 285 ± 26(–) |

[a] Uncertainties are ±1 standard deviation. [b] Sign of $P_S$ indicated in parentheses. From ref. 37.

A conformational analysis of (*R*)-**1.11a** was conducted at the AM1 level based on assumptions consistent with the Boulder model: (1) the dopant was treated as a passive guest, adopting a zigzag shape with the core more tilted than the side-chains; (2) the alkoxy side chains are fully extended in an all-*anti* conformation; (3) the ether linking groups are coplanar with the aromatic rings. This analysis only involves rotation about two bonds, C-5–O and O–C-1 on each side of the dopant molecule (Figure 1-15). The calculations suggest that, in the gas phase, the dopant is in equilibrium between two types of conformations: one is the **P** conformation, in which one indanone fragment lies in the

tilt plane defined by $\hat{\mathbf{n}}$ and $\hat{\mathbf{z}}$; the other is the $C_2$-symmetric conformation ($\mathbf{C_2}$), in which the $C_2$ axis is coincident with the polar axis of the SmC* phase.

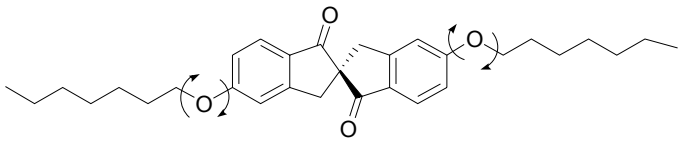

(*R*)-**1.11a**

**Figure 1-15.** Conformational degrees of freedom for (*R*)-**1.11a** corresponding to rotation about C-5–O and O–C-1 bonds.

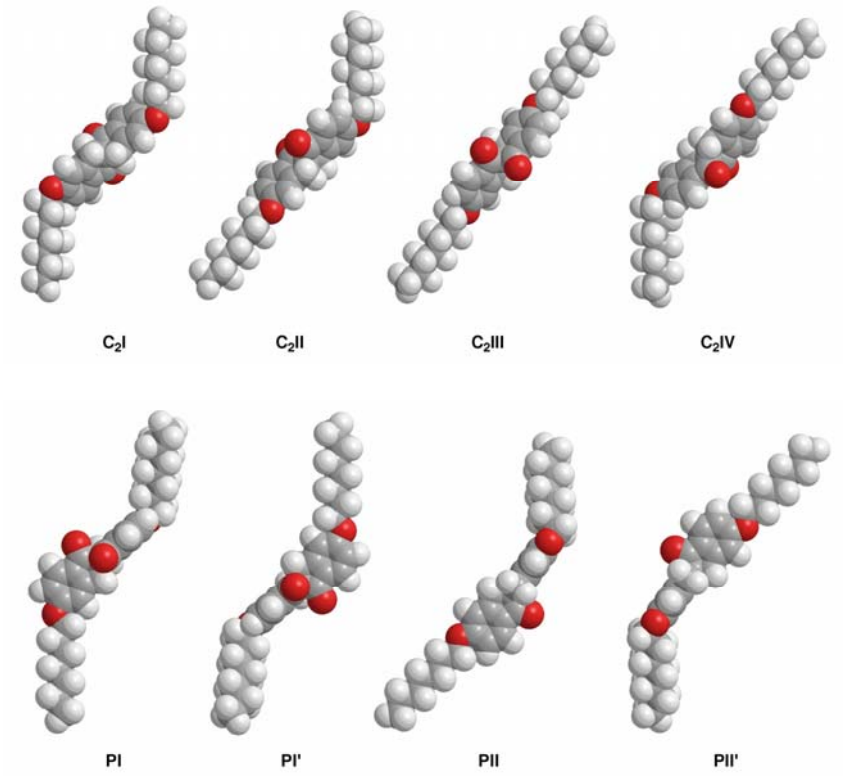


**Figure 1-16.** Space-filling models showing conformational distributions of (*R*)-**1.11a** as side-on views with the spirobiindandione core in **P** and $\mathbf{C_2}$ orientations. From ref. 37.

Eight possible conformations were identified for (*R*)-**1.11a** which are shown in Figure 1-16. However, five of them ($\mathbf{C_2II}$, $\mathbf{C_2III}$, $\mathbf{C_2IV}$, **PII** and **PII'** ) were neglected due to their shape, which do not conform to the zigzag binding site imposed by the host according to the Boulder model. Among the remaining three conformations, **PI** and **PI'** are degenerate, which suggests that, in the binding site of the SmC host, dopant **1.11a** is

in dynamic equilibrium between two conformations of opposite polarities (**P** and **C$_2$**). Similar conformational analyses were performed for (*R*)-**1.12** and (*R*)-**1.13**, and the end-on views of the **P** and **C$_2$** conformers for all three dopants are shown in Figure 1-17. The conformational analysis of (*R*)-**1.13** is very similar to that of (*R*)-**1.11a**, but gives opposite signs of $P_S$ despite having the same absolute configuration. Due to its unsymmetrical structure, (*R*)-**1.12** showed three possible conformations since the two **P** conformers are no longer degenerate.

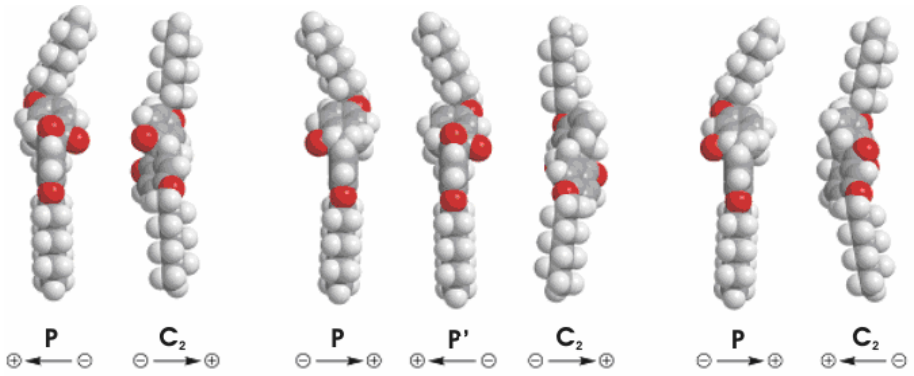


**Figure 1-17.** Space-filling models showing minimized zigzag conformations of (*R*)-**1.11a**, (*R*)-**1.12,** and (*R*)-**1.13** as end-on views with the spirobiindandione core in **P** and **C$_2$** orientations. From ref. 37.

In order to explain the host dependence of $\delta_p$ exhibited by each dopant, an initial hypothesis was made based on a difference in excluded volume of the core fragment of the two conformations, as shown in Figure 1-18. The core section of the **C$_2$** conformer is established to be *ca.* 1.5 Å longer than that of the **P** conformer. Therefore, the conformational equilibrium should shift towards the **P** conformer (positive $\mu_\perp$) as the core length of the host becomes shorter. This hypothesis is consistent with the experimental data for (*R*)-**1.11a**, but cannot account for the host-dependence trend of (*R*)-**1.12** and (*R*)-**1.13**, indicating that other factors (*i.e.* chirality transfer feedback) may also need to be considered for these dopants.

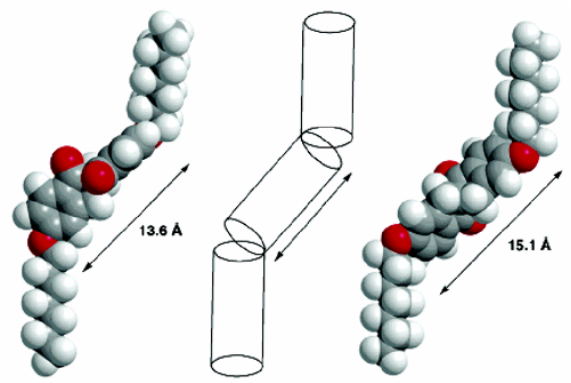


**Figure 1-18.** Space-filling models of the conformations **P** (left) and $\mathbf{C_2}$ (right) for (*R*)-**1.11a** in relation to a simplified form of the zigzag binding site according to the Boulder model. From ref. 37.

### *1.7.2. Detecting Chiral Perturbations for the 2,2'-Spirobiindan-1,1'-dione Dopants*

Initially, $^2$H NMR experiments were designed to investigate dopant-host compatibility for the three dopants. The interaction of the quadrupolar moment of a deuterium nucleus with the electric field gradient tensor produces a quadrupolar doublet with a splitting $\Delta\nu$ that is directly proportional to the orientational order parameter of the C–D bond. In an isotropic liquid environment, there is no order associated with the C–D bond ($\Delta\nu = 0$), and therefore a singlet is observed in the corresponding spectrum. However, in an anisotropic liquid crystal phase, this quadrupolar doublet is visible, and the splitting $\Delta\nu$ reflects the order parameter of deuterated mesogens [38], or the local environment of dopants in liquid crystal hosts. [39]

$^2$H NMR studies of the racemic dopants **1.11a**-$d_4$, **1.12**-$d_4$, and **1.13**-$d_4$ with dideuterated side-chains ($-OCD_2C_6H_{13}$) showed some interesting results besides dopant-host compatibility: more than one pair of quadrupolar doublets were observed for **1.12**-$d_4$, and **1.13**-$d_4$ (Figure 1-19). It was shown that the presence of quadrupolar doublet pairs was due to non-equivalence of the methylene deuterons instead of phase separation. Even

though the methylene deuterons are formally diastereotopic, they should not be distinguished in an achiral liquid crystal host considering their distance to the stereogentic centre, *unless* a chiral perturbation exerted by the dopant on the host via core-core interaction create a local chiral environment strong enough to make the two deuterons unequivalent. According to this explanation, the difference in $\Delta\nu$ between two quadrupolar doublets ($\Delta\Delta\nu$) should reflect the degree of chiral transfer from the dopant to the host. Thus, $^2$H NMR experiments suggest that (*R*)-**1.13** exerts stronger chiral perturbation than (*R*)-**1.11a** in the SmC* phase, which may account for the different host-dependence trend exhibited by (*R*)-**1.12** and (*R*)-**1.13**.

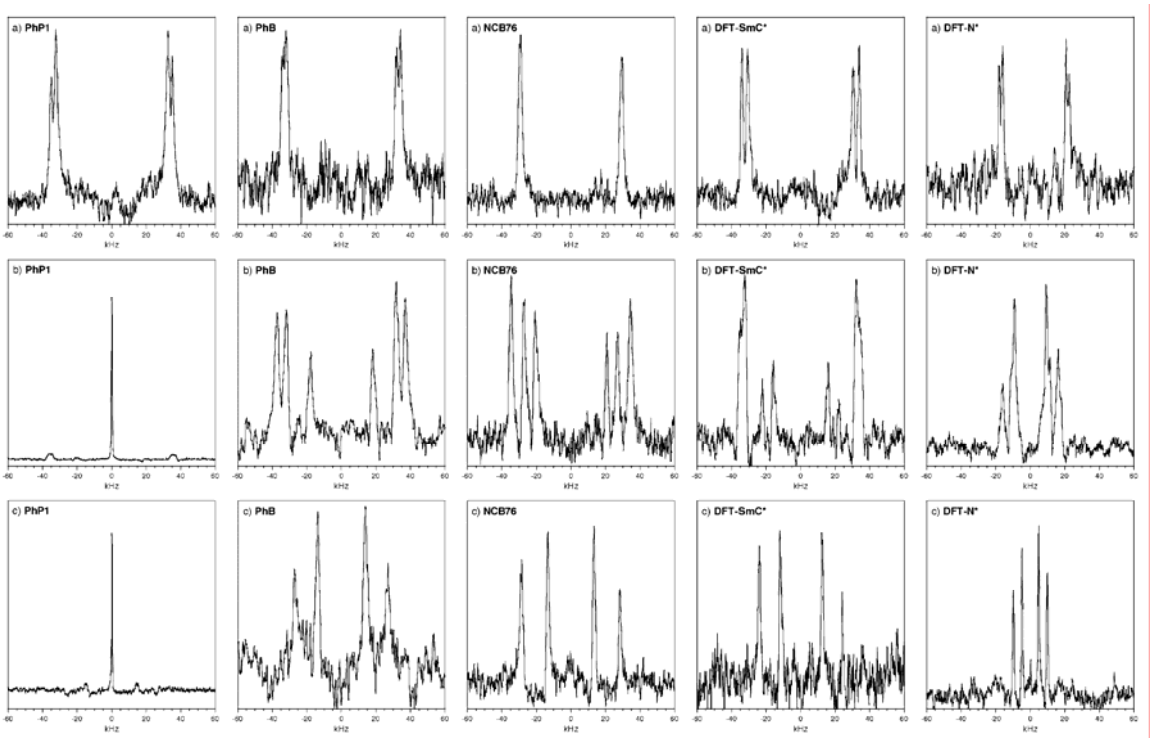


**Figure 1-19**. $^2$H NMR spectra (92.13 MHz) of (a) 10 mol % mixtures of (*RS*)-**1.11a**-$d_4$ in the four liquid crystal hosts, (b) 10 mol % mixtures of (*RS*)-**1.12**-$d_4$ in the four liquid crystal hosts, and (c) mixtures of (*RS*)-**1.13**-$d_4$ in the four liquid crystal hosts at the following concentrations: 2.6 mol % (**PhP1**), 3 mol % (**PhB**), 5 mol % (**NCB76**), and 3 mol % (**DFT**). Each spectrum was taken in the SmC* phase at $T$-$T_C$ = -10 K, except those in the fifth column, which were taken in the N* phase. From ref. 37.

Probe experiments were also attempted to support the results of $^2$H NMR showing that that the 6,6'-diether 2,2'-spirobiindan-1,1'-dione dopant (*R*)-**1.13** exerts stronger chiral perturbations than the 5,5'-diether analogue (*R*)-**1.11a** in the SmC* phase. Since **MDW950** proved to be a useful probe to detect CTF, similar probe experiments were conducted in **NCB76**, in which the largest difference in $\Delta\Delta\nu$ between **1.11a**-$d_4$ (0 kHz) and **1.13**-$d_4$ (30 kHz) was observed.

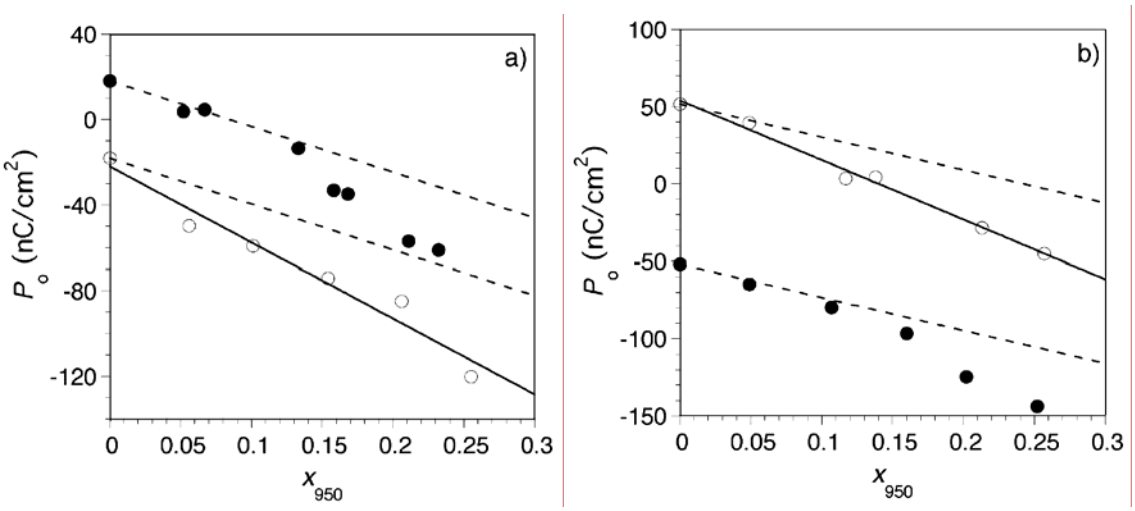


**Figure 1-20**. Reduced polarization, $P_0$, versus mole fraction of **MDW950**, $x_{950}$, in **NCB76** at $T$-$T_C$ = –10 K: (a) in the presence of (*R*)-**1.11a** (●) and (*S*)-**1.11a** (○) at $x_{1.11a}$ = 0.05; (b) in the presence of (*R*)-**1.13** (●) and (*S*)-**1.13** (○) at $x_{1.13}$ = 0.05. The slope of the dashed lines (-212 nC/cm$^2$) corresponds to the polarization power of **MDW950** in **NCB76** in the absence of the chiral dopant. From. ref. 37.

The results in Figure 1-20 show that $\delta_{950}$ increases by approximately the same amount in the presence of (*S*)-**1.11a** and (*S*)-**1.13** in **NCB76** within error, ($\delta_{950}$ = –355 ± 37 nC/cm$^2$ and –369 ± 24 nC/cm$^2$, respectively, versus $\delta_{950}$ = –212 ± 12 nC/cm$^2$ in the absence of chiral dopant). Similarly, (*R*)-**1.11a** and (*R*)-**1.13** caused an increase in $\delta_{950}$ to about the same extent, although the plots of $P_0$ versus $\chi_{950}$ are non-linear. Combined with the result of $^2$H NMR, it was postulated that dopant **1.13** exerts stronger *local* chiral

perturbation than **1.11a**, but that the two dopants exert less significant long-range perturbation in **NCB76** than what is observed for atropisomeric biphenyl dopants in **PhP1**.

### *1.7.3. Dopants with a 6-Fluoro-2,2'-Spirobiindan-1,1'-dione Core*

Conformational analysis consistent with the Boulder model suggests that dopant **1.11a** is equilibrium between two conformations with opposite polarizations, and that the observed host dependence of $P_S$ may be explained by a shift in this conformational distribution as a response to changes in the binding site topography. Despite the **P** conformer being predominant in all four hosts, the calculated energy difference between **P** and $\mathbf{C_2}$ is very subtle, on the order of 0.2 kcal/mol at the AM1 level. The only difference between the two conformers is the conformation of one alkoxy side-chain: in the $\mathbf{C_2}$ conformer, the alkoxy group on both sides are *syn*-periplanar relative to the carbonyl group, and adopt a *gauche* bend along the O–C-1 bond axis so as to maintain a zigzag shape; in the **P** conformer, one alkoxy group is *syn*-periplanar with a *gauche* bend while the other is *anti*-periplanar relative to the carbonyl group, with no *gauche* bend.

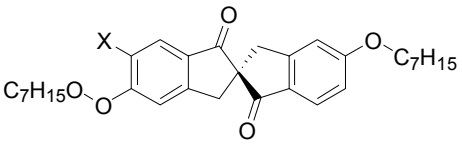


(*R*)-**1.11a**, X = H; (*R*)-**1.14a**, X = F;

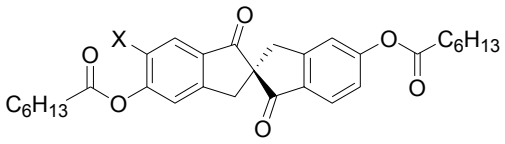


(*R*)-**1.11b**, X = H; (*R*)-**1.14b**, X = F;

In order to increase the conformational bias so as to maximize $\delta_P$, as well as test this conformational distribution model, the original dopant **1.11a** was modified by introducing a fluoro group *ortho* to one of the heptyloxy side-chains (**1.14a**), and by modifying the ether linkages into esters (**1.11b** and **1.14b**).[40] The former should bias the

**P**/**C$_2$** conformational distribution towards **P** conformer by forcing one alkoxy group in an *anti* conformation relative to the carbonyl group, thus resulting in more positive polarization powers for the (*R*) enantiomer (Figure 1-21), while the latter should change the nature of the conformational distribution altogether.

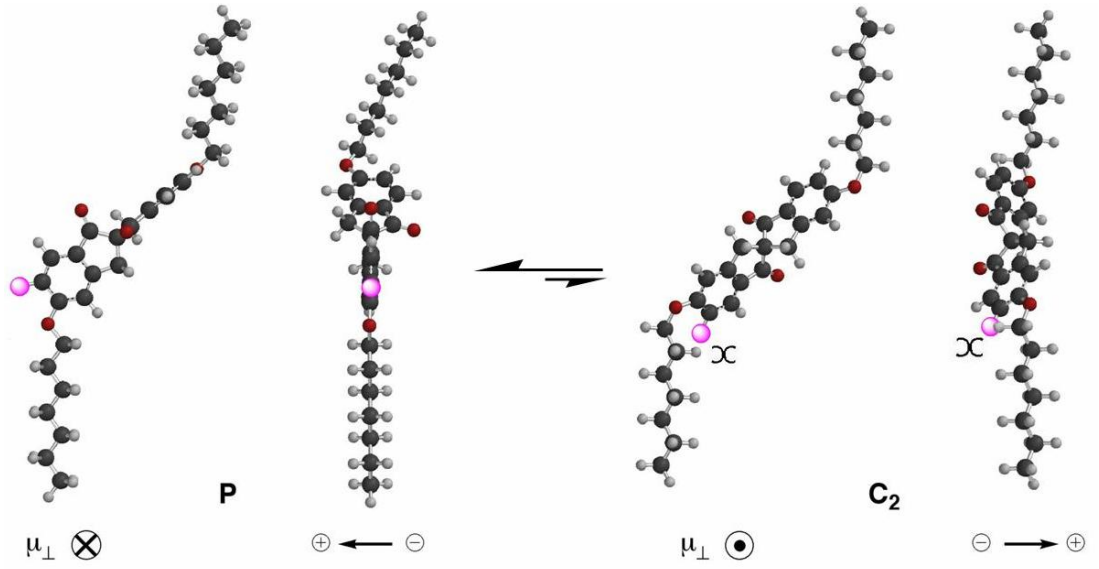


**Figure 1-21**. Molecular models showing the AM1-minimized zigzag conformations **P** and **C$_2$** of 6-substituted dopant (*R*)-**1.11a** as side-on (left) and end-on views (right). Introducing a substituent on the 6-position of one indanone ring should disfavor the **C$_2$** conformer by promoting additional string but should accommodate with the **P** conformer.

**Table 1-3.** Polarization powers for dopants (*R*)-**1.11a**, (*R*)-**1.11b**, (*R*)-**1.14a** and (*R*)-**1.14b** in four LC hosts.

| linking group | dopant | $\delta_p$ (nC/cm$^2$)$^{a,b}$ | | | |
|---|---|---|---|---|---|
| | | **PhP1** | **PhB** | **NCB76** | **DFT** |
| ether | (*R*)-**1.11a** | 749 ± 35 (+) | 460 ± 13(+) | 353 ± 30 (+) | 21 ± 3 (+) |
| ether | (*R*)-**1.14a** | 298$^c$ (+) | 144 ± 11 (+) | (–)/(+)$^d$ | 209$^c$ (–) |
| ester | (*R*)-**1.11b** | 314 ± 30 (+) | 242 ± 24 (+) | 446 ± 46 (+) | (+)/(–)$^e$ |
| ester | (*R*)-**1.14b** | 147 ± 18 (+) | (–)/(+)$^d$ | (–)/(+)$^d$ | 334 ± 15 (–) |

$^a$ Sign of polarization in parentheses. $^b$ Uncertainty is ± standard error from least-squares fit. $^c$ Extrapolated value from single measurement taken for 1 mol% mixture of dopant in host. $^d$ Inversion from $-P_S$ to $+P_S$ upon cooling was observed. $^e$ Inversion from $+P_S$ to $-P_S$ upon cooling was observed. From ref. 40.

Contrary to the above analysis, experimental data showed that the addition of a fluoro group results in less positive values of $\delta_P$ for the (*R*) enantiomer of both the diheptyloxy dopant (**1.11a** vs. **1.14a**) and its diester analogue (**1.11b** vs. **1.14b**), as shown in Table 1-3.

Considering that fluorine is nearly isosteric with hydrogen, it was postulated that the fluoro group is too small to exert a significant steric bias, and that the primary effect of the fluoro moiety is to increase the transverse dipole moment of the $C_2$ conformer, that is, to become more negative, since the dipole moment of the C–F bond points in the same direction as the two carbonyls, as shown in Figure 1-22.

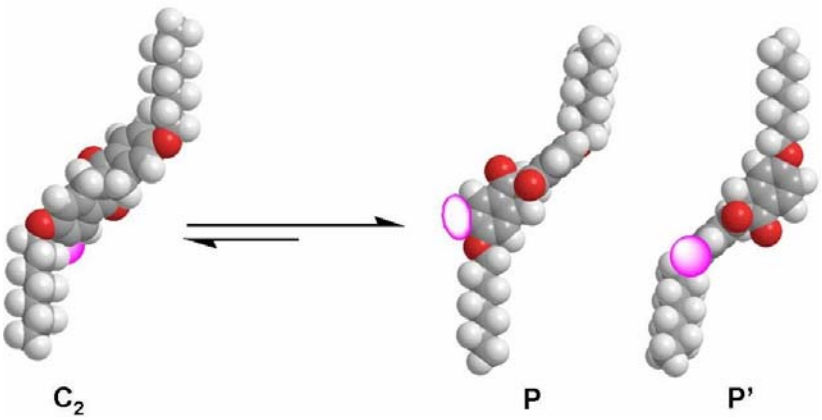


**Figure 1-22.** Modified space-filling models showing zigzag conformations **C₂** (left) and **P** (right) for (*R*)-**1.14a**. Note that the two **P** conformers are no longer degenerate by the addition of a fluorine; the **P** conformer is favored over **P'** by virtue of the *anti*-periplanar relationship of alkoxy tail relative to the carbonyl groups on the fluoro side.

If the original conformational distribution equilibrium is not strongly perturbed by the addition of a fluoro group, we may expect the contribution of the **C₂** conformer to $P_S$ to increase by virtue of its high $\mu_\perp$. Furthermore, the additional dipole moment from the fluoro group should not cause the **P** conformer to become more positive, as the two **P** conformers are no longer degenerate (**P** ≠ **P'**) and the steric bias would favor the alkoxy tail on fluoro side of the molecule to be *anti*-periplanar relative to the carbonyl groups.

This would favor the **P** conformer over the **P'** conformer and the C–F bond would therefore have no contribution to $P_S$.

However, the experimental data for the fluoro-substituted dopants alone is not adequate to support the above explanation to any significant extent. Other factors (*i.e.* chirality transfer feedback, and/or contributions from conformers other than **P** or $\mathbf{C_2}$) may also need to be considered or ruled out. Unfortunately, the results of a $^2$H NMR experiment for **1.14a** to detect the degree of chirality transfer were inconclusive due to poor miscibility of **1.14a** with a variety of hosts. In addition, computational modeling of **1.11b** at the AM1 level was very complicated and attempts to model **1.14b** were abandoned.

## 1.8. Project Outline

The goal of this project is to further test the conformational distribution model proposed in previous studies of dopants with a 2,2'-spirobiindan-1,1'-dione core so as to design a new class of Type II dopant capable of inducing large polarizations. Specifically, the recent study on the 6-fluoro-2,2'-spirobiindan-1,1'-dione dopants suggests that the positive contribution brought by the steric bias of the fluoro moiety is not enough to compensate the negative effect of increasing the transverse dipole moment of an opposite conformer, resulting in a less positive polarization power. In order to provide enough steric bias to the system, substituents bigger than fluorine were sought, but not so big that it would compromise the rod-like shape of the molecule. As a result, a pair of isosteric groups with different polarities, chloro and methyl, were chosen to test this model as well as to improve the miscibility of the dopants.

Firstly, the target molecules were synthesized and resolved by HPLC, and their absolute configuration assigned by circular dichrosim spectroscopy. Next, characterization of the target molecules as chiral dopants were carried out by polarized microscopy, and their polarization powers were measured in the four liquid crystal hosts. Finally, probe experiments were performed to determine the influence of chirality transfer feedback on polar ordering.

## 1.9. References


1) Reinitzer, F. *Monatsh. Chem.* **1888**, *9*, 421.
2) Lagerwall, S. T. Ferroelectric and Antiferroelectric Liquid Crystals; Wiley-VCH: Weinheim, 1999.
3) Lagerwall, S. T. Ferroelectric Liquid Crystals. In Handbook of Liquid Crystals; Demus, D., Goodby, J. W., Gray, G. W., Spiess, H.-W., Vill, V., Eds.; Wiley-VCH: Weinheim, 1998; Vol. 2B, pp 515-664.
4) Walba, D. Science**1995**, 270, 250-251.
5) Goodby, J. W.; Blinc, R.; Clark, N. A.; Lagerwall, S. T.; Osipov, M. A.; Pikin, S. A.; Sakurai, T.; Yoshino, K.; Zeks, B. Ferroelectric Liquid Crystals: Principles, Properties and Applications; Gordon & Breach: Philadelphia, 1991.
6) Meyer, R. B.; Liebert, L.; Strzelecki, L.; Keller, P. *J. Phys. (Paris) Lett.* **1975**, *36*, L69-71.
7) Walba, D. M. Ferroelectric Liquid Crystals: A Unique State of Matter. In *Advances in the Synthesis and Reactivity of Solids*; Mallouck, T. E., Ed.; JAI Press, Ltd.: Greenwich, CT, 1991; Vol. 1, pp 173-235.
8) Clark, N. A.; Lagerwall, S. T. *Appl. Phys. Lett.* **1980**, *36*, 899-901.

9) Handschy, M. A.; Clark, N. A. *Appl. Phys. Lett.* **1982**, *41*, 39-41.

10) Collings, P. J.; Hird, M. *Introduction to Liquid Crystals: Chemistry and Physics*; Taylor & Francis Inc.: London, 1997.

11) Kuczynski, W.; Stegemeyer, H. *Chem. Phys. Lett.* **1980**, *70*, 123-126.

12) Beresnev, L. A.; Blinov, L. M.; Baikalov, V. A.; Pozhidaev, E. P.; Purvanetskas, G. V.; Pavlyuchenko, A. I. *Mol. Cryst. Liq. Cryst.* **1982**, *89*, 327-338.

13) Beresnev, L. A.; Pozhidaev, E. P.; Blinov, L. M.; Pavlyuchenko, A. I.; Étingen, N. B. *JETP Lett.* **1982**, *35*, 531-534.

14) Siemensmeyer, K.; Stegemeyer, H. *Chem. Phys. Lett.* **1988**, *148*, 409-412.

15) Walba, D. M.; Slater, S. C.; Thurmes, W. N.; Clark, N. A.; Handschy, M. A.; Supon, F. *J. Am. Chem. Soc.* **1986**, *108*, 5210-5221.

16) Glaser, M. A. Atomistic Simulation and Modeling of Smectic Liquid Crystals. In *Advances in the Computer Simulations of Liquid Crystals*; Zannoni, C., Pasini, P., Eds.; Kluwer: Dordrecht, 1999, pp 263-331.

17) Glaser, M. A.; Clark, N. A.; Walba, D. M.; Keyes, M. P.; Radcliffe, M. D.; Snustad, D. C. *Liq. Cryst.* **2002**, *29*, 1073-1085.

18) Bartolino, R.; Doucet, J.; Durand, G. *Ann. Phys. (Paris)* **1978**, *3*, 389-396.

19) Samulski, E. T. *Isr. J. Chem.* **1983**, *23*, 329-339.

20) Samulski, E. T.; Dong, R. Y. *J. Chem. Phys.* **1982**, *77*, 5090-5096.

21) Wand, M. D.; Vohra, R.; Walba, D. M.; Clark, N. A.; Shao, R. *Mol. Cryst. Liq. Cryst.* **1991**, *202*, 183-192.

22) Stegemeyer, H.; Meister, R.; Hoffmann, U.; Sprick, A.; Becker, A. *J. Mater. Chem.* **1995**, *5*, 2183-2193.

23) Other examples for Type I dopant: (a) Walba, D. M.; Vohra, R. T.; Clark, N. A.; Handschy, M. A.; Xue, J.; Parmar, D. S.; Lagerwall, S. T.; Skarp, K. *J. Am. Chem. Soc.* **1986**, *108*, 7424-7425. (b) Walba, D. M.; Ros, M. B.; Clark, N. A.; Shao, R.; Robinson, M. G.; Liu, J.-Y.; Johnson, K. M.; Doroski, D. *J. Am. Chem. Soc.* **1991**, *113*, 5471-5474.

24) Thompson, M. Ph.D. Thesis, Queen's University, 2006.

25) Yang, K.; Lemieux, R. P. *Mol. Cryst. Liq. Cryst.* **1995**, *260*, 247-253.

26) Yang, K.; Campbell, B.; Birch, G.; Williams, V. E.; Lemieux, R. P. *J. Am. Chem. Soc.* **1996**, *118*, 9557-9561.

27) Vizitiu, D.; Lazar, C.; Halden, B. J.; Lemieux, R. P. *J. Am. Chem. Soc.* **1999**, *121*, 8229-8236.

28) Vizitiu, D.; Halden, B. J.; Lemieux, R. P. *Chem. Commun.* **1997**, 1123-1124.

29) Vizitiu, D.; Halden, B. J.; Lemieux, R. P. *Ferroelectrics* **1998**, *212*, 257-264.

30) Vizitiu, D.; Lazar, C.; Radke, J. P.; Hartley, C. S.; Glaser, M. A.; Lemieux, R. P. *Chem. Mater.* **2001**, *13*, 1692-1699.

31) Gottarelli, G.; Hilbert, M.; Samori, B.; Solladié, G.; Spada, G. P.; Zimmermann, R. *J. Am. Chem. Soc.* **1983**, *105*, 7318-7321.

32) Gottarelli, G.; Spada, G. P.; Bartsch, R.; Solladié, G.; Zimmermann, R. *J. Org. Chem.* **1986**, *51*, 589-592.

33) Gottarelli, G.; Mariani, P.; Spada, G. P.; Samorí, B.; Forni, A.; Solladie, G.; Hibert, M. *Tetrahedron* **1983**, *39*, 1337-1344.

34) Lemieux, R. P. *Acc. Chem. Res.* **2001**, *34*, 845-853.

35) Lazar, C.; Wand, M. D.; Lemieux, R. P. *J. Am. Chem. Soc.* **2000**, *122*, 12586-12587.

36) Hartley, C. S.; Lazar, C.; Wand, M. D.; Lemieux, R. P. *J. Am. Chem. Soc.* **2002**, *124*, 13513-13518.

37) Boulton, C. J.; Finden, J. G.; Yuh, E.; Sutherland, J. J.; Wand, M. D.; Wu, G.; Lemieux, R. P. *J. Am. Chem. Soc.* **2005**, *127*, 13657-13665.

38) Dong, R. Y. In *Encyclopedia of Nuclear Magnetic Resonance*; Grant, D. M., Harris, R. K., Eds.; John Wiley & Sons: 1996; Vol. 4, pp 2752-2760.

39) Examples for the utility of $^{2}$H NMR to characterize the local environment of dopants in liquid crystal host: (a) Workentin, M. S.; Leigh, W. J. *J. Phys. Chem.* **1992**, *96*, 9666. (b) Workentin, M. S.; Fahie, B. J.; Leigh, W. J. *Can. J. Chem.* **1991**, *69*, 1435. (c) Workentin, M. S.; Leigh, W. J.; Jeffrey, K. R. *J. Am. Chem. Soc.* **1990**, *112*, 7329. (d) Fahie, B. J.; Mitchell, D. S.; Leigh, W. J. *Can. J. Chem.* **1989**, *67*, 148. (e) Fahie, B. J.; Mitchell, D. S.; Workentin, M. S.; Leigh, W. J. *J. Am. Chem. Soc.* **1989**, *111*, 2916. (f) Vlahakis, J. Z.; Lemieux, R. P. *J. Mater. Chem.* **2004**, *14*, 1486. (g) Maly, K. E.; Wu, G.; Lemieux, R. P. *Liq. Cryst.* **2001**, *28*, 457.

40) Yuh, E., M.Sc. Thesis, Queen's University, 2005.

# Chapter 2. Synthesis and Resolution

The chiral dopants with 6-chloro- and 6-methyl-2,2'-spirobiindan-1,1'-dione core (**2.1a**, **2.1b**, **2.2a** and **2.2b**) were synthesized as racemic mixtures by modification of a literature procedure, and resolved by preparative chiral phase HPLC. The absolute configuration of each dopant was assigned by CD spectroscopy, showing that the first eluant corresponds to the (*R*) enantiomer with *P* helicity, which is consistent with other dopants of this class. The dideuterated side-chains were introduced with the intent of performing $^{2}$H NMR experiments on the dopants.

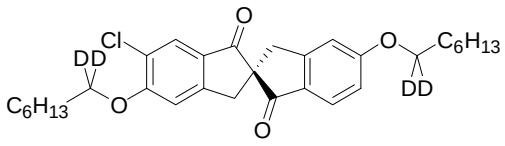


(*R*)-**2.1a**

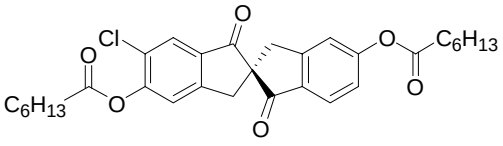


(*R*)-**2.1b**

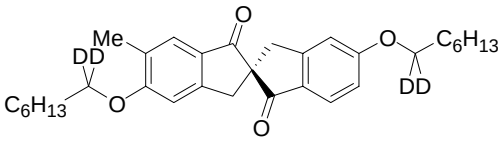


(*R*)-**2.2a**

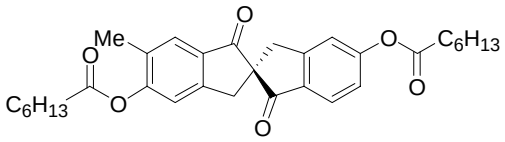


(*R*)-**2.2b**

## 2.1. Synthesis and Resolution

The syntheses of the four chiral dopants were adapted from an approach reported by Nieman and Keay for the synthesis of 2,2'-spirobiindan-1,1'-dione,[1] which involves two building blocks, an indanonecarboxylate and an ethyl 2-(bromomethyl)benzoate. The synthesis of the chloro-substituted dopants **2.1a** and **2.1b** was based on modification of the ethyl 2-(bromomethyl)benzoate building block **2.8,** which was prepared in five steps with an overall yield of 44%. As shown in Scheme 2-1, commercially available 2-chloro-

5-methylphenol (**2.3**) was brominated with $Br_2$ to give **2.4** in 97% yield,[2] and methylated to protect the hydroxyl group to give **2.5** in quantitative yield. Lithium-halogen exchange followed by quenching with $CO_2$ gave the acid **2.6** in 78% yield,[2] and subsequent esterification gave **2.7** in 87% yield. Benzylic bromination with NBS using AIBN as initiator gave the ethyl 2-(bromomethyl)benzoate building block **2.8** in 67% yield.

**Scheme 2-1.**[a]

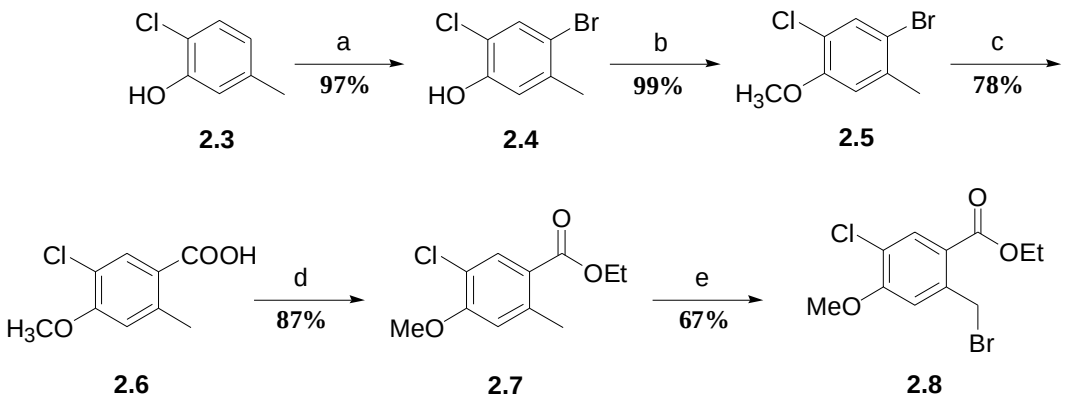


[a] *Reagents and conditions*: (a) $Br_2$, $CHCl_3$, 0 °C ~ rt; (b) (i) NaH, THF, rt ~ reflux, (ii) MeI; (c) (i) $^n$BuLi, THF/hexane/$Et_2O$ (6 : 1 : 1), –98 °C, (ii) $CO_2$; (d) $H_2SO_4$, EtOH, reflux; (e) NBS, AIBN, $CCl_4$, reflux.

Conversely, our strategy for the synthesis of the methyl-substituted dopants **2.2a** and **2.2b** focused on modifying the indanonecarboxylate building block rather than the 2-(bromomethyl)benzoate, because the addition of another methyl substituent on an aromatic precursor would complicate the benzylic bromination step. As shown in Scheme 2-2, commercially available 5-methoxyindan (**2.9**) was brominated at the less sterically hindered position of the aromatic ring with $Br_2$ to give **2.10** in quantitative yield, and subsequent lithium-halogen exchange followed by quenching with excess MeI gave 5-methoxy-6-methylindan (**2.11**) in 90% yield. Noureldin's method [3] was used to selectively oxidize the methylene group *para* to the methoxy group to give 5-methoxy-6-

methylindanone (**2.12**) in 35% yield. The regioselectivity of the oxidation was established by an NOESY experiment. As shown in Figure 2-1, the NOESY spectrum of **2.12** shows that the aromatic proton correlating to the benzylic methylene group also correlates to the methoxy group but not to the methyl group, which is consistent with the *para*-oxidation product relative to the methoxy group. In the case of the other possible regio-isomer, 6-methoxy-5-methylindanone, the aromatic proton correlating to the methylene group would correlate to the methyl group instead of the methoxy group.

**Scheme 2-2.**[a]

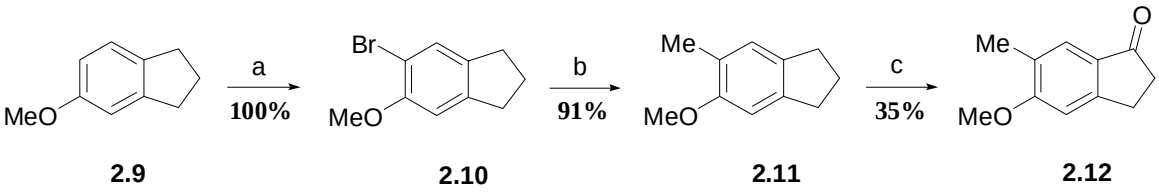


**2.9** **2.10** **2.11** **2.12**

[a] *Reagents and conditions*: (a) $Br_2$, $CHCl_3$, 0 °C ~ rt; (b) (i) $^nBuLi$, THF, –78 °C, (ii) MeI; (c) $KMnO_4$, $CuSO_4 \cdot 5H_2O$, $CH_2Cl_2$, reflux.

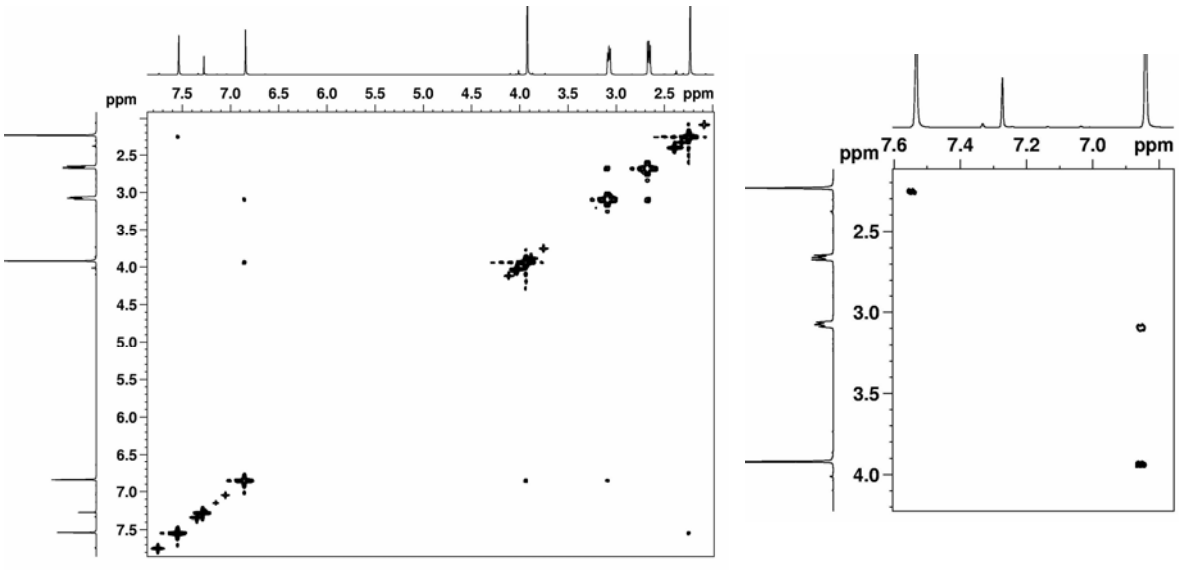


**Figure 2-1.** NOESY spectrum for compound **2.12** (left) and its enlarged view for the aromatic region (right). The proton at 6.9 ppm correlates to the methoxy group at 3.9 ppm and the benzylic methylene group at 3.1ppm.

**Scheme 2-3.**[a]

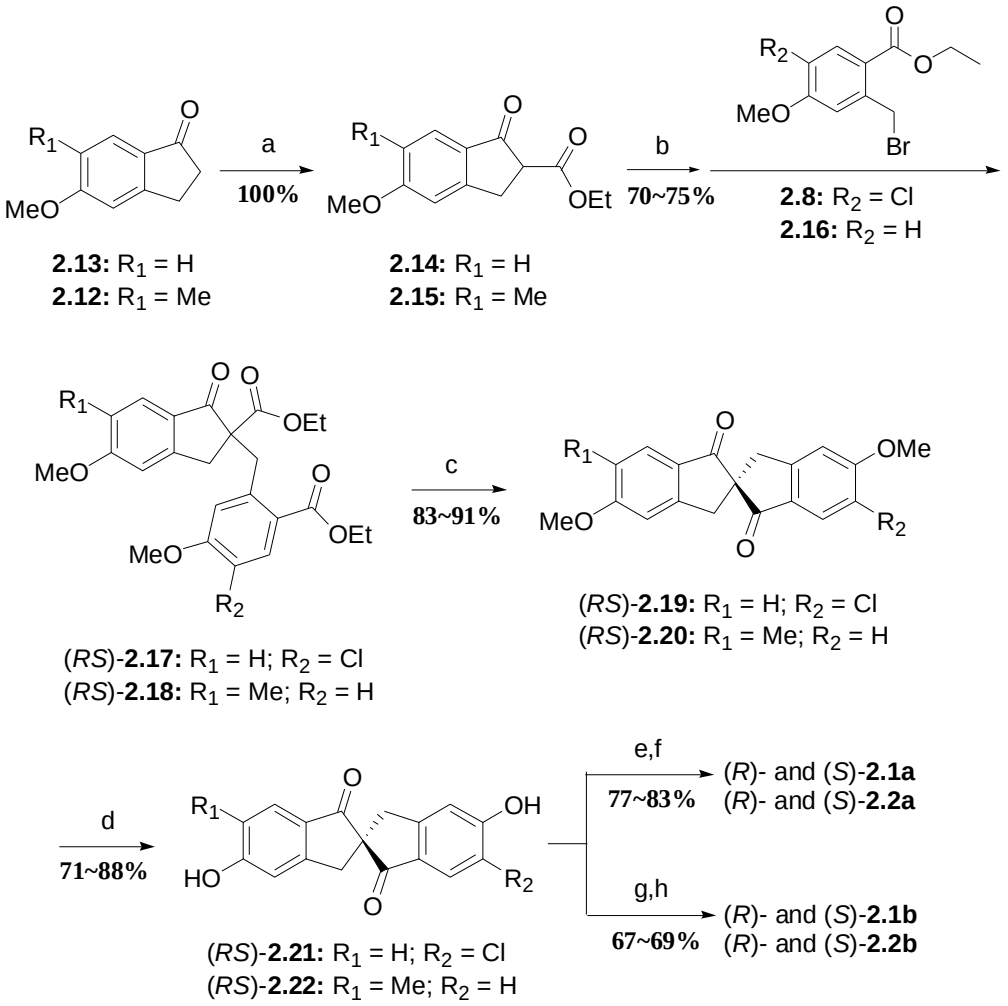


[a] *Reagents and conditions*: (a) NaH, diethyl carbonate, toluene, reflux; (b) NaH, DMF, 60 °C; (c) 40% $H_2SO_4$, 40% EtOH, 20% $H_2O$, reflux; (d) $AlCl_3$, toluene, reflux; (e) 1-bromoheptane-1,1'-$d_2$, $CsCO_3$, DMF, rt ~ 70 °C; (f) prep HPLC resolution, Daicel Chiralpak AS column, 2% EtOH/hexane; (g) heptanoic acid, DCC, DMAP, $CH_2Cl_2$, rt; (h) prep HPLC resolution, Daicel Chiralpak AS column, 5% EtOH/hexane.

To assemble the building blocks, commercially available 5-methoxyindanone (**2.13**) and 5-methoxy-6-methylindanone (**2.12**) were converted to the corresponding indanonecarboxylates **2.14** or **2.15** in quantitative yield (Scheme 2-3). Reactions of the enolates of **2.14** and **2.15** with the appropriate ethyl 2-(bromomethyl)benzoates **2.8** and **2.16** gave the substitution products **2.17** and **2.18** in 70~75% yields. Acid-catalyzed

hydrolysis followed by decarboxylation and cyclization gave the racemic dimethoxyspirobiindan-1,1'-diones **2.19** and **2.20** in 83~91% yields. The methyl groups were cleaved with $AlCl_3$ in 71~88% yields to give the diols **2.21** and **2.22**, which were alkylated with 1-bromoheptane-1,1-$d_2$ to give the racemic dopants **2.1a** and **2.2a** in 77~83% yields. Similarly, esterification of the diols with heptanoic acid via DCC/DMAP gave **2.1b** and **2.2b** in 67~69% yields. The racemic dopants were resolved by preparative chiral phase HPLC using a Daicel Chiralcel AS column, with either 2% ethanol/hexane (**2.1a** and **2.2a**) or 5% ethanol/hexane (**2.1b** and **2.2b**) as the mobile phase.

## 2.2. Assignment of Absolute Configuration

### *2.2.1 The Exciton Chirality Method*

Circular dichroism (CD) spectroscopy can be used to assign the absolute configuration of chiral chromophores, which is known as the *exciton chirality method*.[4~6] When two chromophores are located near each other in space, the coupling of the two excited states (exciton coupling) results in two new excited state levels, as shown in Figure 2-2. Although this so-called Davydov splitting is normally indistinguishable by the UV-Vis spectroscopy, it *does* produce two corresponding bands with opposite signs in the CD spectrum if the two transition dipole moments describe either a left-handed or right-handed turn relative to a given reference axis. This is referred to as a split Cotton effect, which is either positive or negative depending on the handedness of the turn described by the two coupled transition dipoles. A peak at higher wavelength than the trough corresponds to a positive split Cotton effect and describes a *P* helicity, whereas a peak at lower wavelength than the trough corresponds to a negative split Cotton effect and describes an *M* helicity. Provided that the direction of the transition dipole moments

in the chromophore are established, which can be achieved using theoretical calculations, the sign of the split Cotton effect can be related to the absolute configuration of the compound.

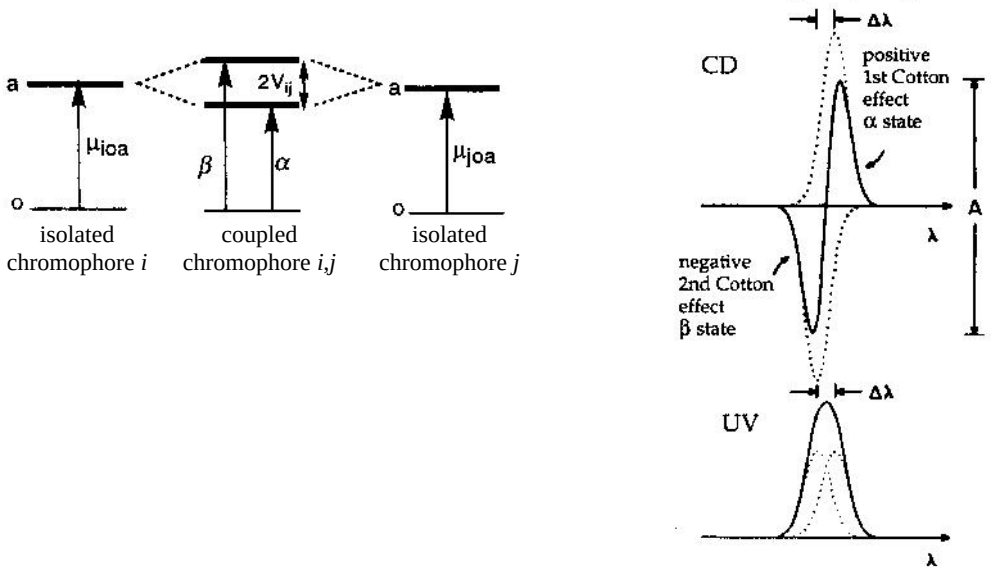


**Figure 2-2.** (a) The splitting of the excited states of isolated chromophores into $\alpha$ and $\beta$ states with Davydov split $2V_{ij}$; (b) summation CD and UV curves (solid line) or two component curves (dotted line) and amplitude *A* of bisignate CD curve. From ref. 4.

### *2.2.2 Assignment of Absolute Configuration*

Using CD spectroscopy, previous work by Schlögl has enabled one to assign the absolute configuration of 2,2'-spirobiindan-1,1'-dione and 5,5'-disubstituted 2,2'-spirobiindan-1,1'-diones with reasonable certainty according to the sign of split Cotton effects corresponding to $L_a$ and $L_b$ exciton couplets.[7, 8] Moreover, this assignment was confirmed by Harada *et al*, who converted 2,2'-spirobiindan-1,1'-dione to the corresponding bis-*p*-dimethylaminobenzoate (Figure 2-3),[9,10] and by Finden, who applied a similar approach to establish the configuration of dopants **1.11a** and **1.13**, showing consistent results with the assignment first made based on the CD spectra of **1.11a** and **1.13**.[11] The absolute configuration assignments of the diester **1.11b** (5,5'-)

and **2.23** (6,6'-) were made by comparison of their CD spectra with those of the corresponding diether **1.11a** and **1.13**, which showed similar split Cotton effect profiles.

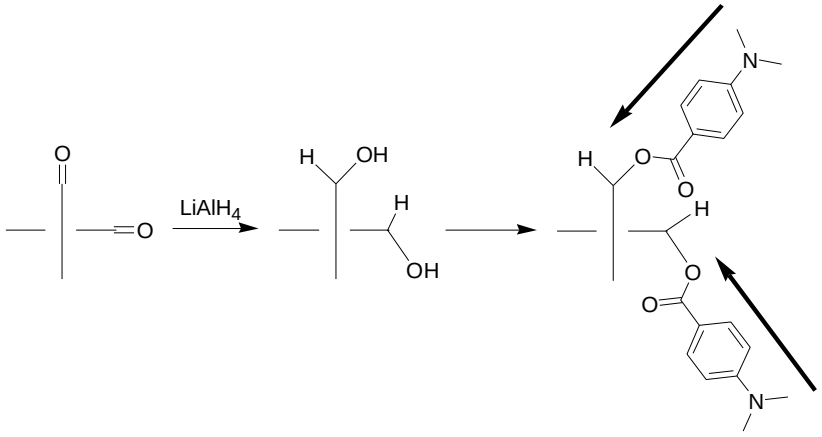


**Figure 2-3**. Reduction of a spirobiindandione core to the *cis*/*trans*-diol and conversion the diol to *p*-dimethylaminobenzoate derivative to maximize chiral exciton coupling. The relative orientation of the transition dipole moments of the two *p*-dimethylaminobenzoate chromophores relative to the helical (reference) axis is shown.

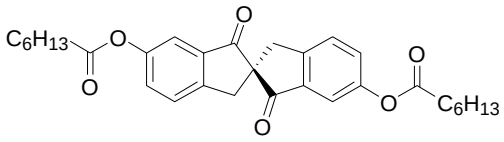


**2.23**

For each of the substituted 2,2'-spirobiindan-1,1'-dione dopants previously investigated (**1.11a**, **1.11b**, **1.12**, **1.13**, **1.14a**, **1.14b** and **2.23**), the helicity of the 2,2'-spirobiindan-1,1'-dione core assigned for the first chiral phase HPLC eluant has been *P*, which corresponds to the (*R*) absolute configuration, expect for dopant **1.12**.

A comparison of the CD spectra for the first HPLC eluants of dopants **2.1a 2.1b**, **2.2a** and **2.2b** with those of the corresponding diether (*R*)-**1.11a** and diester (*R*)-**1.11b** confirms that the new dopants isolated as the first eluants have *P* helicity and (*R*) absolute configuration (Figure 2-4). Prior to doping into liquid crystal mixtures, the dopants were recrystallized from HPLC hexanes after filtration through a 0.45 um PTFE filter.

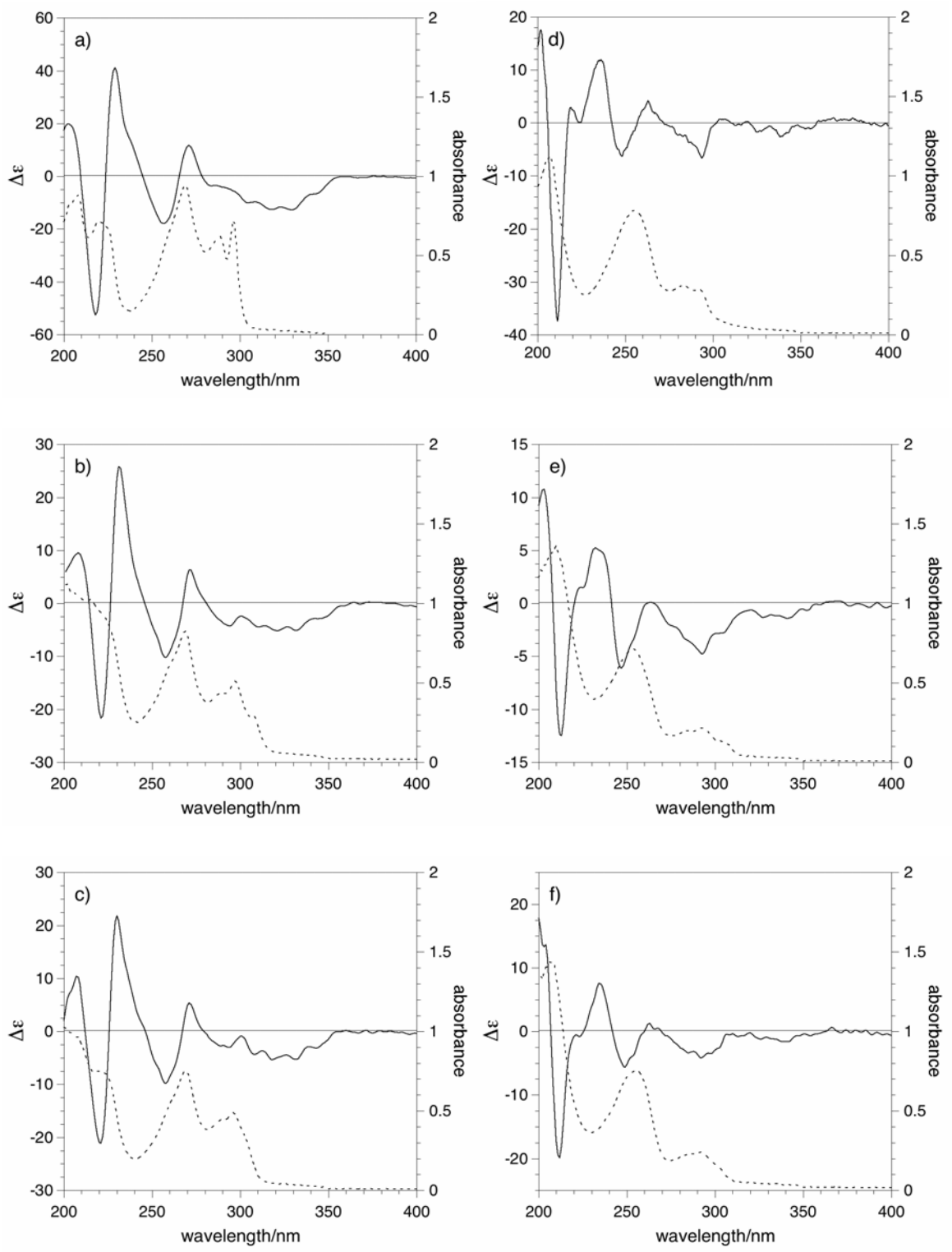


**Figure 2-4.** Comparison of circular dichroism (solid line) and UV (dotted line) absorption spectra of the 6-chloro/methyl substituted 5,5'-diether/diester dopants with their unsubstituted analogues (all first eluants in HPLC reolution): (a) dopant (*R*)-**1.11a** (1.7 x $10^{-5}$ M), from ref. 11, (b) dopant (*R*)-**2.1a** (2.0 x $10^{-5}$ M), (c) dopant (*R*)-**2.2a** (2.0 x $10^{-5}$ M), (d) dopant (*R*)-**1.11b** (2.1 x $10^{-5}$M), from ref. 12, (e) dopant (*R*)-**2.1b** (2.0 x $10^{-5}$ M) and (f) dopant (*R*)-**2.2b** (2.0 x $10^{-5}$ M) in hexanes (spectro grade).

## 2.3. References


1) Nieman, J. A.; Keay, B. A. *Tetrahedron: Asymmetry* **1995**, *6*, 1575.
2) Speicher, A.; Kolz, J.; Sambanje, R. P. *Synthesis*, **2002**, *17*, 2503.
3) Noureldin, N. A.; Zhao, D.; Lee, D. G. *J. Org. Chem*. **1997**, *62*, 8767.
4) Berova, N.; Nakanishi, K. In *Exciton Chirality Methods: Principles and Applications*; Berova, N., Nakanishi, K., Woody, R., Eds.; Wiley-VCH: New York, 2000.
5) Harada, N.; Nakanishi, K. *Circular Dichroic Spectroscopy: Exciton Coupling in Organic Photochemistry*; University Science Books: New York, 1983.
6) Lightner, D. A.; Gurst, J. E. *Organic Conformational Analysis and Stereochemistry from Circular Dichroism Spectroscopy*; Wiley-VCH: New York, 2000.
7) Falk, H.; Fröstl, W.; Hofer, O.; Schlögl, K. *Monatsh. Chem.* **1974**, *105*, 598.
8) Langer, E.; Lehner, H.; Neudeck, H.; Schlögl, K. *Monatsh. Chem.* **1978**, *109*, 987.
9) Harada, N.; Ai, T.; Uda, H. *J. Chem. Soc. Chem. Commun.* **1982**, 232.
10) Harada, N.; Ochiai, N.; Takada, K.; Uda, H. *J. Chem. Soc. Chem. Commun.* **1977**, 495.
11) Boulton, C. J.; Finden, J. G.; Yuh, E.; Sutherland, J. J.; Wand, M. D.; Wu, G.; Lemieux, R. P. *J. Am. Chem. Soc.* **2005**, *127*, 13657.
12) Yuh, E., M.Sc. Thesis, Queen's University, 2005.

# Chapter 3. Polarization Power Measurements

Having our four target dopants (**2.1a**, **2.1b**, **2.2a** and **2.2b**) synthesized, resolved and their absolute configurations assigned, we measured their polarization powers in four SmC hosts, and correlated the sign of induced polarization with the absolute configuration of each dopant.

Both the miscibility of the dopants and their polarization powers show strong host dependence, which is consistent with other dopants in this class. For both the ether-linked and ester-linked dopants, the addition of a substituent at the 6-position of one indanone ring results in lower polarization powers regardless of the size and polarity of the substituent.

A comparative study of the data suggests that the ester-linked dopants exert much stronger perturbations on the host environment than the ether-linked dopants, especially when the 6-position is substituted. We postulate that this perturbation is chiral in nature, and that the feedback effect of this chiral perturbation causes a shift in the conformational distribution of the dopant favoring conformers with negative polarity. This postulate is supported by probe experiments in the case of the chloro-substituted diester dopant (**2.1b**).

## 3.1. Dopant-host Compatibility

The optically pure dopants **2.1a**, **2.1b**, **2.2a** and **2.2b** were mixed in the four standard liquid crystal hosts **PhP1**, **PhBz**, **NCB76** and **DFT** and solubility limits were estimated by polarized microscopy based on the observation of persistent biphasic

SmC*/isotropic domains at 10K below the Curie point of a given mixture ($T - T_C = -$ 10K).

### *3.1.1. Diether Dopants*

As shown in Figure 3-1, both chloro- and methyl-substituted diether dopants (**2.1a** and **2.2a**) showed improved solubilities in all four hosts compared to the fluoro-substituted analogue (**1.14a**), but still not as good as that of the unsubstituted analogue (**1.11a**). The solubility limits of **2.1a** and **2.2a** are quite similar in any given host, ranging from *ca.* 4 to 6 mol% in **PhP1** and **DFT**, to *ca*. 10 to 15 mol% in **PhBz** and **NCB76**. All the diether dopants showed similar solubility trends, with the highest solubility in **NCB76**, followed by **PhBz**, **DFT**, and the lowest in **PhP1**.

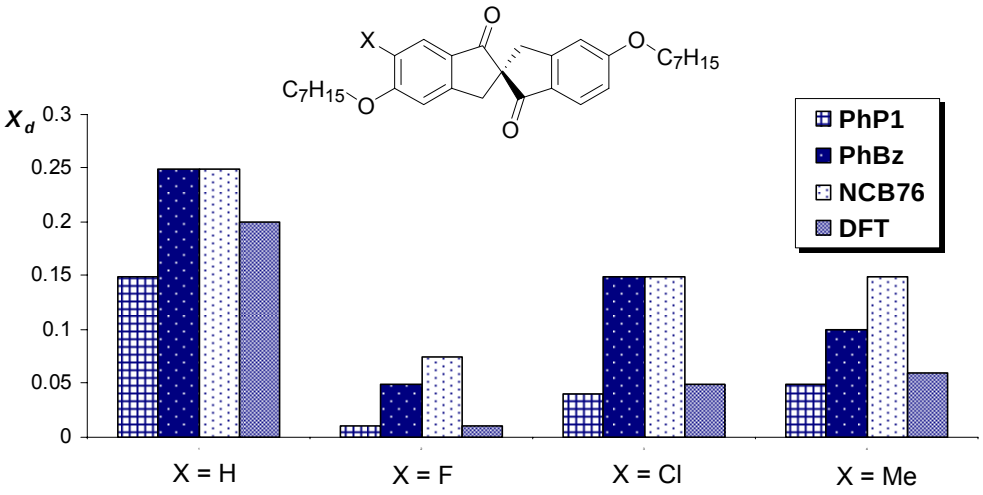


**Figure 3-1**. A comparison of solubility limits for dopants **1.11a**, **1.14a**, **2.1a** and **2.2a** in **PhP1**, **PhBz**, **NCB76** and **DFT**.

The trend in solubility limits can also be derived from phase diagrams, as shown in Figure 3-2 and Figure 3-3. The addition of either **2.1a** or **2.2a** causes a significant destabilization of the SmC* phase in **PhP1**, as indicated by the broad biphasic regions

and depression of the SmA*-SmC* transition temperature with increasing dopant mole fraction ($\chi_d$). A less pronounced destabilization of the SmC* phase in **PhBz** and **DFT** was observed upon addition of **2.1a** or **2.2a**, whereas virtually no effect on the SmA*-SmC* phase transition temperature was observed in **NCB76**, which suggests that the binding site of this host provides a good fit for the dopants. These observations are consistent with those previously reported for dopants **1.11a**[1] and **1.14a**[2].

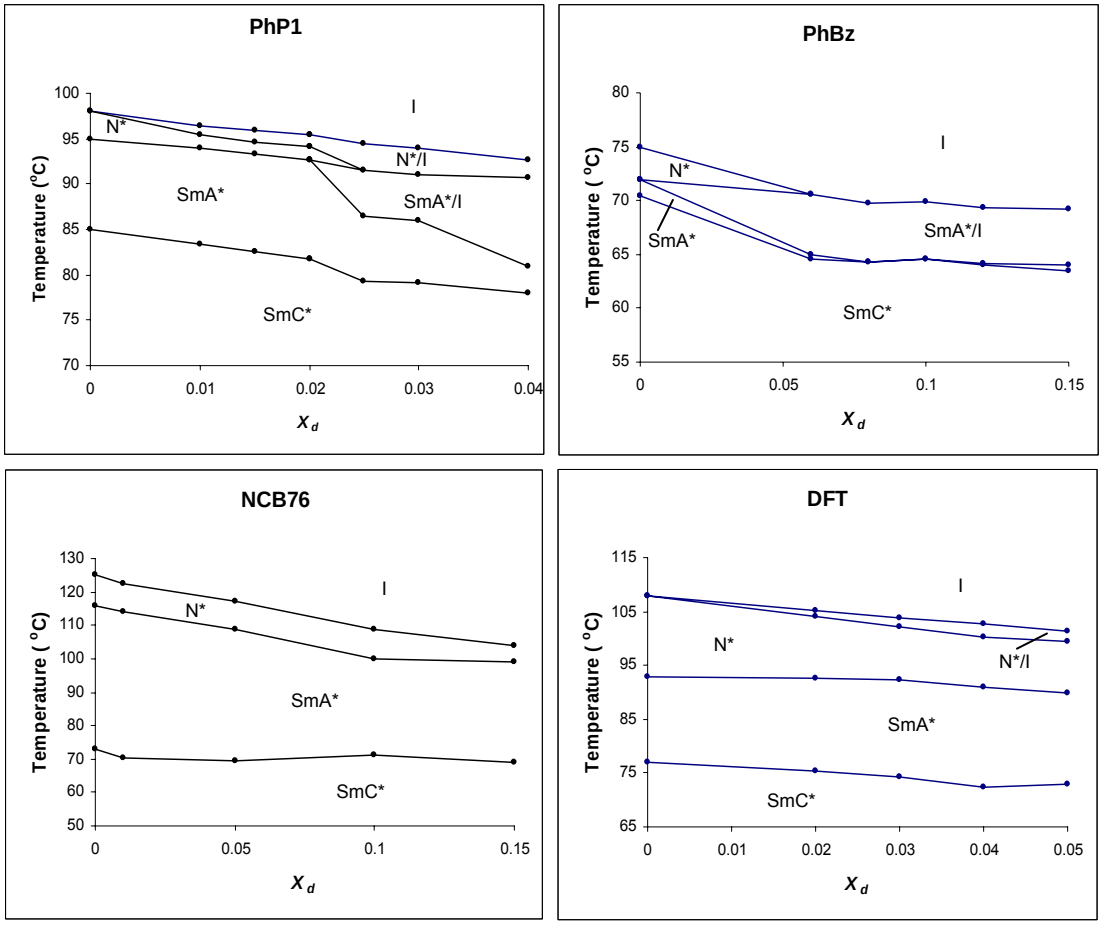


**Figure 3-2.** Partial phase diagrams of **2.1a** in hosts **PhP1**, **PhBz**, **NCB76** and **DFT**. The phase transition temperatures were determined by polarized microscopy upon cooling.

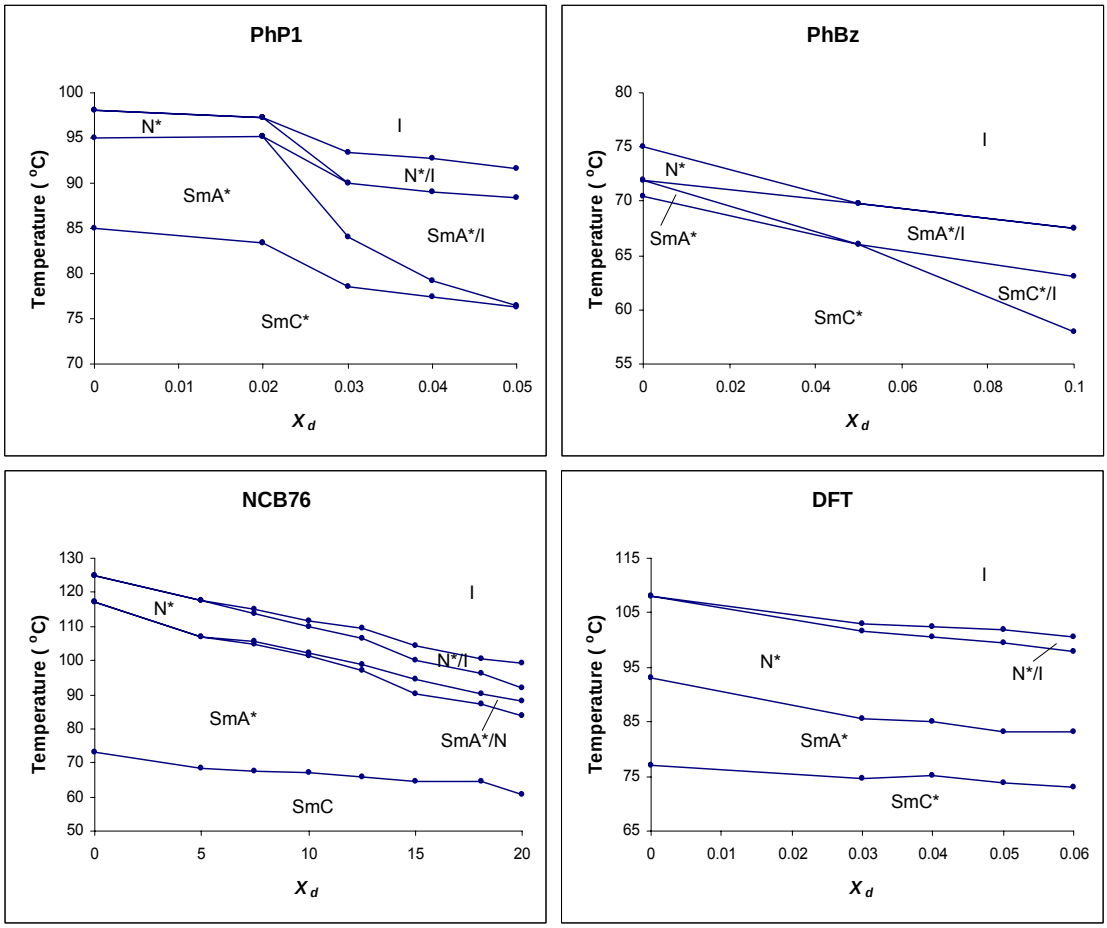


**Figure 3-3.** Partial phase diagrams of **2.2a** in hosts **PhP1**, **PhBz**, **NCB76** and **DFT**. The phase transition temperatures were determined by polarized microscopy upon cooling.

### *3.1.2. Diester Dopants*

A comparison of solubility limits for the chloro- and methyl-substituted diester dopants (**2.1b** and **2.2b**) and for the fluoro-substituted and unsubstituted analogues (**1.14b** and **1.11b**) in the four SmC hosts is shown in Figure 3-4. In contrast to the solubility limit profiles of the diether dopants, the addition of a substitutent at the 6-position of the diester dopant **1.11b** did not cause a dramatic decrease in the dopant solubility. The fluoro- and chloro-substituted diesters **1.14b** and **2.1b** have similar solubility limits in all four hosts, ranging from *ca.* 8 to 10 mol% in **PhP1**, to *ca*. 20% in **PhBz** and **NCB76**. The

methyl-substituted diesters **2.2b** is less soluble in all hosts expect in **NCB76**, in which no phase separation was observed up to 15 mol% of dopant. Similarly to the diether dopants, the diester dopants are most soluble in **NCB76** and least soluble in **PhP1**, which is consistent with trends observed for all other 2,2'-spirobiindan-1,1'-dione dopants previously investigated.[1, 2]

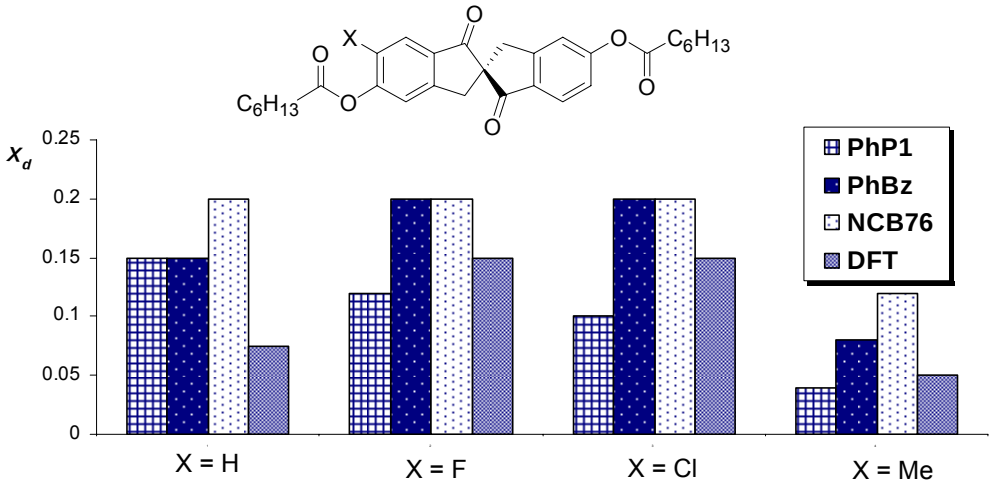


**Figure 3-4**. A comparison of solubility limits for dopants **1.11b**, **1.14b**, **2.1b** and **2.2b** in **PhP1**, **PhBz**, **NCB76** and **DFT**.

As shown in Figure 3-5 and Figure 3-6, both diester dopants **2.1b** and **2.2b** cause significant destabilization of the SmC* phase in **PhP1**. The destabilization of the SmC* phase, as reflected by a decrease in SmA*-SmC* phase transition temperature, is less pronounced in **PhBz**, but a biphasic SmC*/I region is still present. In **DFT**, no depression of the SmA*-SmC* phase transition temperature is evident, but the dopant **2.2b** crystallizes out of solution at mole fractions greater than 6 mol%. Interestingly, both **2.1b** and **2.2b** show a stabilization effect of the SmC* phase in **NCB76** similar to that observed with **1.11b** and **1.14b** (Figure 3-7).[2]

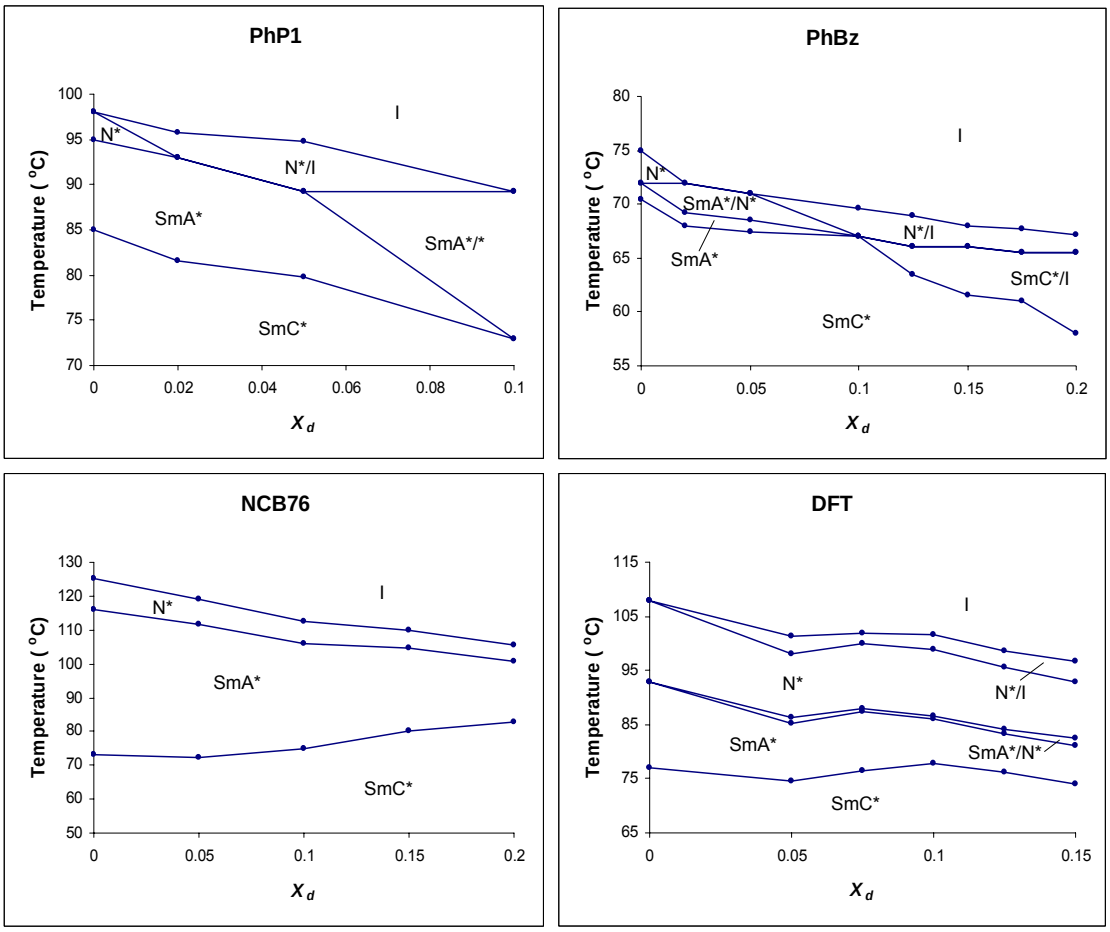


**Figure 3-5.** Partial phase diagrams of **2.1b** in hosts **PhP1**, **PhBz**, **NCB76** and **DFT**. The phase transition temperatures were determined by polarized microscopy upon cooling.

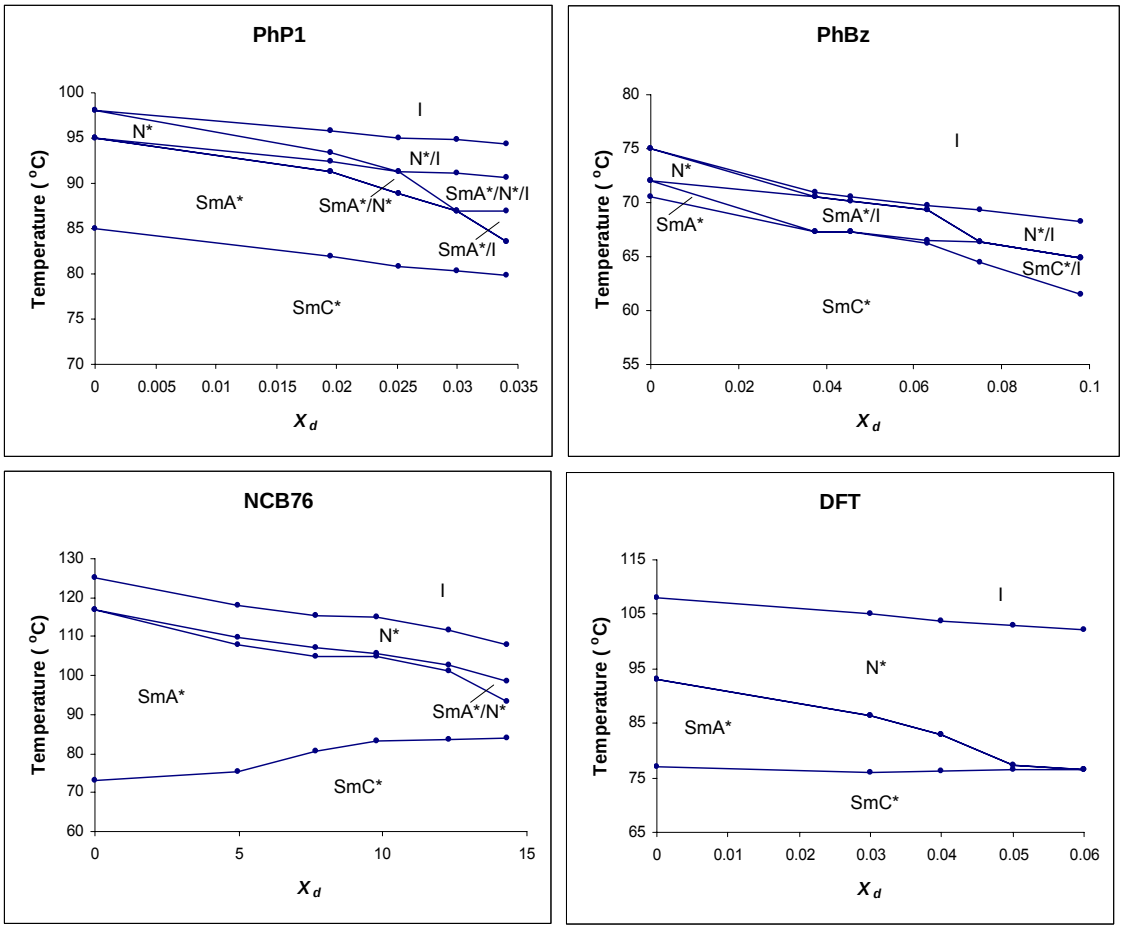


**Figure 3-6.** Partial phase diagrams of **2.2b** in hosts **PhP1**, **PhBz**, **NCB76** and **DFT**. The phase transition temperatures were determined by polarized microscopy upon cooling.

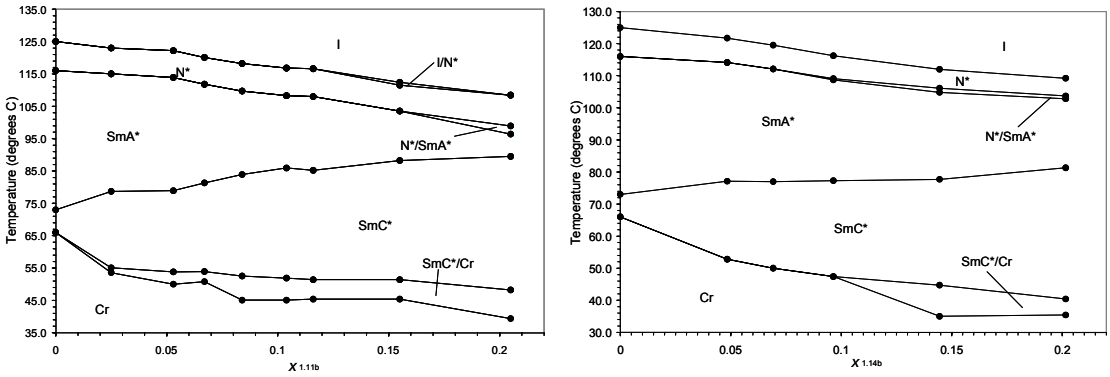


**Figure 3-7.** Phase diagrams of **1.11b** and **1.14b** in **NCB76**. The phase transition temperatures were determined by polarized microscopy upon cooling. From ref. 2.

## 3.2. Polarization Power Measurements

Homogeneous mixtures of optically pure dopants in the four liquid crystal hosts were aligned as surface-stabilized ferroelectric liquid crystal (SSFLC) films using commercial ITO glass cells with rubbed polyimide surfaces and a cell gap of 4 $\mu$m. Spontaneous polarizations ($P_S$) and tilt angles ($\theta$) were measured in the SmC* phase at $T - T_C = -10$ K by the triangular wave method [3] and the corresponding $P_0$ values were calculated according to eq. 1-3. A minimum of three different mixtures were prepared for each dopant/host combination, and the resulting $P_0$ values were plotted as a function of the dopant mole fraction $\chi_d$. The sign of $P_S$ along the polar axis was assigned from the relative configuration of the electric field and the switching position of the SSFLC film according to the established convention. [4]

### *3.2.1. Diether Dopants*

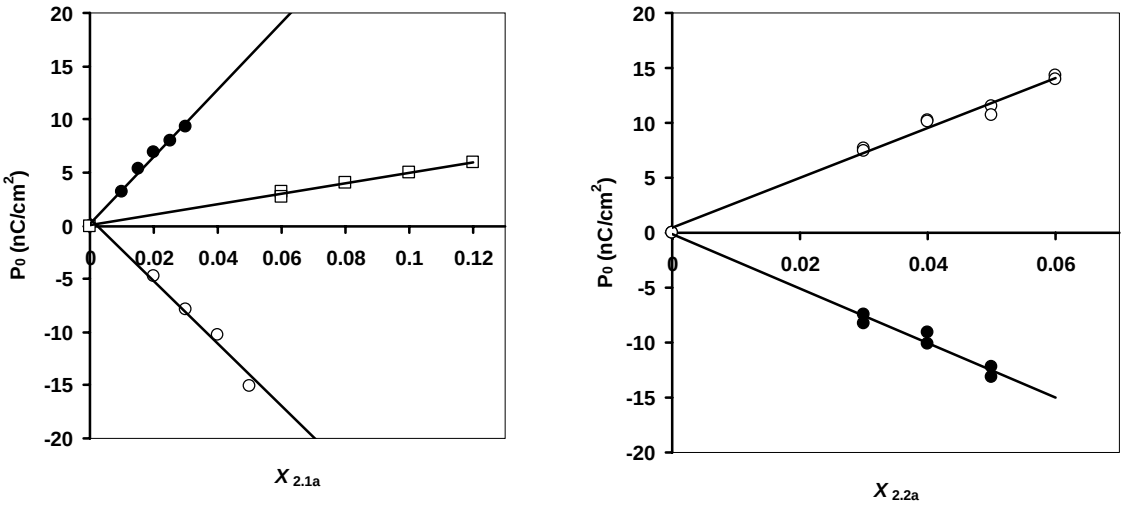


**Figure 3-8**. Reduced polarization $P_o$ versus dopant mole fraction $x_d$ in **PhP1** (●), **PhBz** (□), and **DFT** (○) at $T - T_C$ = -10K for dopant (*R*)-**2.1a** (left) and dopant (*S*)-**2.2a** (right).

As shown in Figure 3-8, the plots of $P_0$ versus $\chi_d$ for (*R*)-**2.1a** and (*S*)-**2.2a** in **PhP1** and **DFT** gave good least-squares fits ($R^2$ = 0.980-0.991), and the polarization power ($\delta_p$) values were derived from the slope of each plot. Moderate $\delta_p$ values with opposite sign were obtained in **PhP1** and **DFT** for each dopant, ranging from 227–315 nC/cm$^2$. The results indicate that the (*R*) enantiomers of **2.1a** and **2.2a** induce a positive polarization in **PhP1** and a negative polarization in **DFT**.

The two dopants gave much smaller $\delta_p$ values in **PhBz**; a value of +50 nC/cm$^2$ ($R^2$ = 0.995) was obtained for (*R*)-**2.1a**. However, (*S*)-**2.2a** failed to give a good linear relationship between $P_0$ and $\chi_d$ in spite of its good miscibility with the host. A small $P_S$ of –0.55 nC/cm$^2$ was detected with a 5 mol% mixture and $P_0$ was extrapolated to a $\delta_p$ value of –28 nC/cm$^2$, but the $P_S$ value was below the limit of detection (< 0.3 nC/cm$^2$) with a 10 mol% mixture, and its sign is negative.

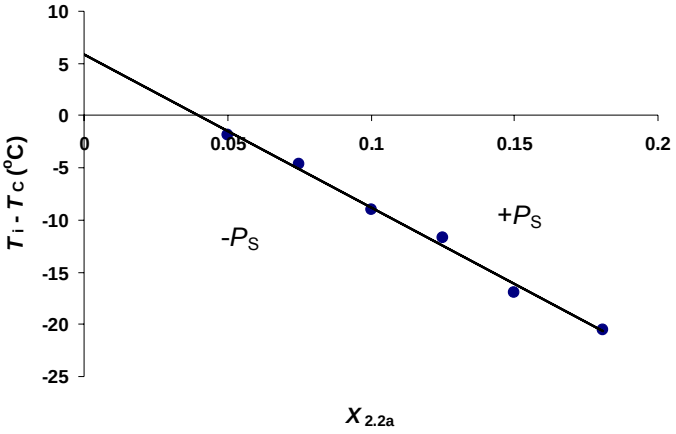


**Figure 3-9**. Reduced Inversion temperature ($T_i$ - $T_C$) versus dopant mole fraction $x_{2.2a}$ for dopant (*S*)-**2.2a** (●) in **NCB76**. The polarization is uniformly positive above $T_i$ - $T_C$ and uniformly negative below $T_i$ - $T_C$.

In **NCB76**, the values of $P_S$ were at or below the detection limit up to the solubility limits of both dopants. All the mixtures of (*R*)-**2.1a** showed a uniform texture

with no switching in the SmC* phase, which suggested that $P_S$ is effectively zero in the temperature range of the SmC* phase. In contrast, mixtures of (*S*)-**2.2a** in **NCB76** showed sharp $P_S$ inversion temperatures that varied with the dopant mole fraction $\chi_{2.2a}$. The $P_S$ inversion temperature was determined by applying a low frequency AC field (1 Hz) upon slowly cooling the mixtures (0.5 °C/min) in the SmC* phase and finding the temperature at which no switching could be observed. Remarkably, a linear relationship of the reduced inversion temperature (difference between inversion temperature ($T_i$) and Curie point ($T_C$), $T_i - T_C$) as a function of $\chi_{2.2a}$ was obtained with a good least-squares fit ($R^2$ = 0.993) (Figure 3-9). The polarization is uniformly positive above $T_i - T_C$ and uniformly negative below $T_i - T_C$.

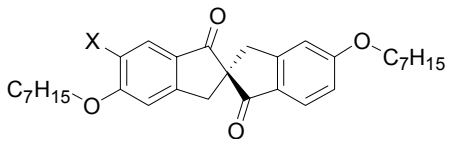


**Table 3-1.** Polarization powers for dopants (*R*)-**1.11a**, (*R*)-**1.14a**, (*R*)-**2.1a** and (*R*)-**2.2a** in four SmC hosts.

| Dopant (X) | $\delta_P$ (nC/cm$^2$)[a,b] | | | |
|---|---|---|---|---|
| | **PhP1** | **PhBz** | **NCB76** | **DFT** |
| (*R*)-**1.11a** (H)[c] | 749 ± 35 (+) | 460 ± 13 (+) | 363 ± 30 (+) | 21 ± 3 (+) |
| (*R*)-**1.14a** (F)[c] | 298 (+) | 144 ± 11 (+) | (–)/(+)[d] | 209 (–) |
| (*R*)-**2.1a** (Cl) | 315 ± 15 (+) | 50 ± 2 (+) | (–)/(+)[d] | 293 ± 24 (–) |
| (*R*)-**2.2a** (Me)[e] | 249 ± 15 (+) | 28 (+)[f] | (–)/(+)[d] | 227 ± 12 (–) |

[a]Uncertainties are ±1 standard error of the least-squares fit. [b]Sign of $P_S$ indicated in parentheses. [c]From ref. 1 and 2. [d]Inversion of polarization was observed upon cooling. [e]Sign of $P_S$ are converted to corresponding (*R*) enantiomer. [f]Extrapolated value from single measurement taken from 5 mol% mixture of dopant in host.

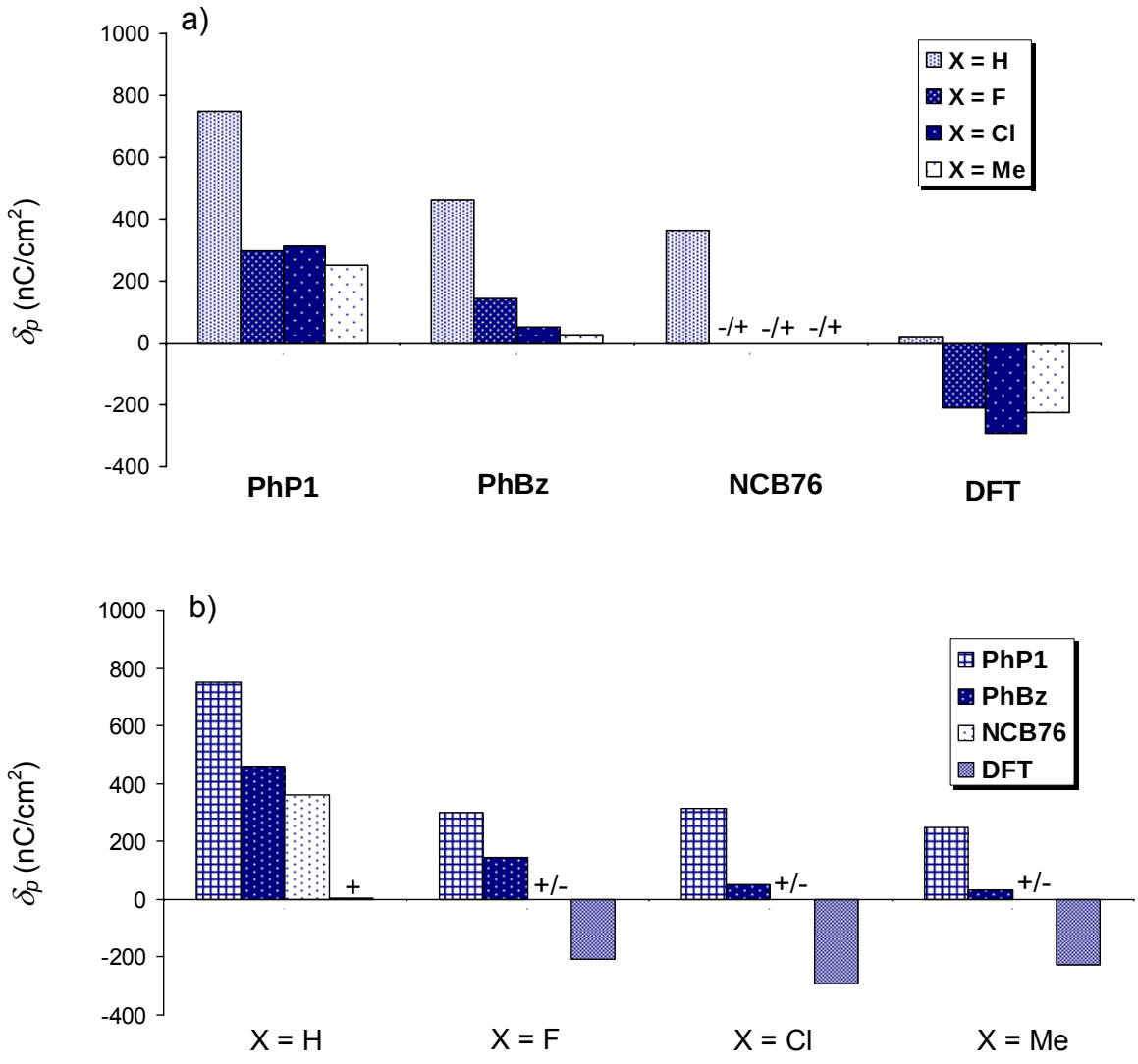


**Figure 3-10**. Comparison of polarization powers of the four 5,5'-diether dopants: (a) as a function of the host, and (b) as a function of the substituent at the 6-position.

A comparative analysis of the data for the four (*R*)-5,5'-diether dopants investigated thus far, which is shown in Table 3-1 and the corresponding bar graphs (Figure 3-10), reveals some interesting trends. First of all, the polarization powers of (*R*)-**2.1a** and (*R*)-**2.2a** vary significantly with the host structure as previously observed with the unsubstituted and fluoro-substituted analogues, but the $\delta_P$ values in any given host are

very similar. In fact, the polarization powers of all three substituted dopants (**1.14a**, **2.1a** and **2.2a**) are relatively similar in any given host. In addition, an inversion of the sign of $P_S$ with temperature was observed for all three dopants in **NCB76**. Dopants **1.14a**, **2.1a** and **2.2a** showed the same trend in $\delta_P$ (host) dependence as that observed with the unsubstituted dopant **1.11a**. However, the polarization powers of the three substituted dopants shift towards more negative values relative to the unsubstituted dopant, which is contrary to our expectation based on the simple conformation distributional model proposed originally.

### *3.2.2. Diester Dopants*

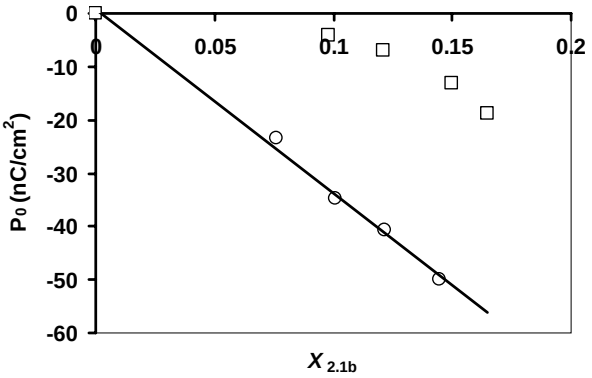


**Figure 3-11**. Reduced polarization $P_0$ versus dopant mole fraction $x_{2.1b}$ for (*R*)-**2.1b** in **PhBz** (□) and **DFT** (○) at $T - T_C$ = -10K.

As shown in Figure 3-11, the plot of $P_0$ versus $\chi_{2.1b}$ for (*R*)-**2.1b** in **DFT** gave a good least-squares fit with an $R^2$ value of 0.996, and a $\delta_P$ value of –345 nC/cm$^2$. With mixtures of (*R*)-**2.1b** in **PhBz**, a non-linear relationship of $P_0$ versus $\chi_{2.1b}$ was obtained, with the absolute value of $P_0$ increasing with $\chi_{2.1b}$. At $\chi_{2.1b}$ = 0.02, $P_S$ was below detection limit and sign inversion of $P_S$ was observed at 63.5 °C; above $\chi_{2.1b}$ = 0.02, measurable $P_S$ values of the mixtures were uniformly negative over the temperature range of the SmC*

phase. In **PhP1**, uniformly positive polarizations were observed for all the mixtures over the temperature range of the SmC* phase, but the polarization induced by (*R*)-**2.1b** was below the detection limit of the instrument (0.3 nC/cm$^2$).

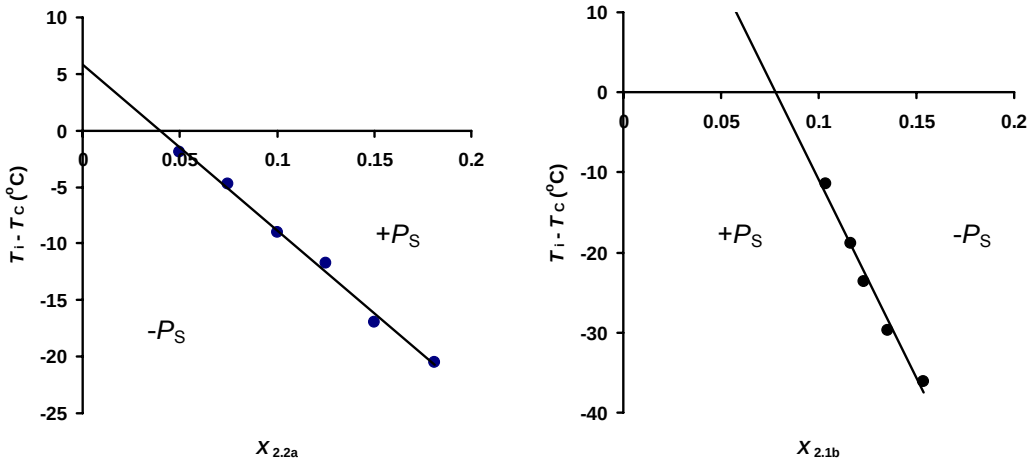


**Figure 3-12**. Reduced Inversion temperature (°C) versus dopant mole fraction $x_d$ for dopant (*S*)-**2.2a** (left) and (*R*)-**2.1b** (right) in **NCB76**.

As with dopant **2.2a**, the $P_S$ values of mixtures of (*R*)-**2.1b** in **NCB76** were at or below detection limit up to the dopant solubility limit, and sign inversion of $P_S$ as a function of temperature was observed. However, the inversion temperature of (*R*)-**2.1b** in **NCB76** proved to be much more sensitive to the dopant mole fraction than with (*S*)-**2.2a**. In the mole fraction range of 0.10–0.15, $P_S$ sign inversion was observed in the temperature range of SmC* phase, and a linear relationship of $T_i - T_C$ versus $\chi_{2.1b}$ was obtained with a good least-squares fit ($R^2$ = 0.982), but the slope of the plot is much steeper than that obtained with (*S*)-**2.2a** (Figure 3-12). The sign of polarization also inverts from negative to positive with decreasing temperature. Above and below the mole fraction range of 0.10–0.15, no inversion of the sign of $P_S$ is evident. At $\chi_{2.1b} < 0.10$ the polarization is positive, and at $\chi_{2.1b} > 0.15$ the polarization is negative, which is consistent

with an extrapolation of the $T_i - T_C$ versus $\chi_{2.1b}$ plot showing the inversion temperature in those ranges of $\chi_{2.1b}$ falling above and below the temperature range of the SmC* phase.

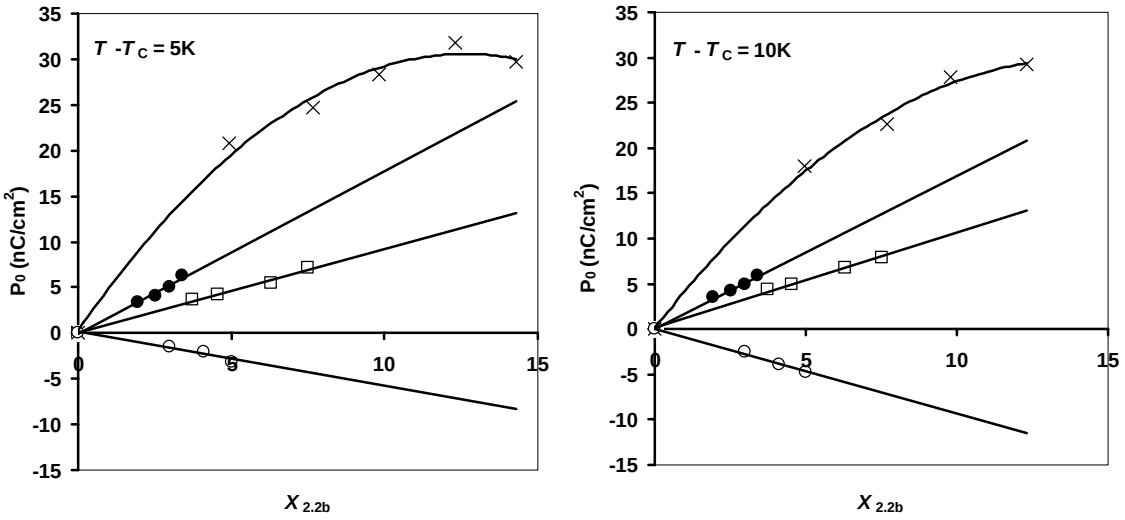


**Figure 3-13**. Reduced polarization $P_0$ versus dopant mole fraction $x_{2.2b}$ for (*R*)-**2.2b** in the four LC hosts at $T - T_C$ = -5K (left) and $T - T_C$ = -10K (right): **PhP1** (●), **PhBz** (□), **NCB76** (×)and **DFT** (○). Note the non-linear relationship between $P_0$ and $x_{2.2b}$ in **NCB76** at both $T - T_C$ = -5K and $T - T_C$ = -10K.

The plots of $P_0$ versus $\chi_{2.2b}$ for (*R*)-**2.2b** in the four hosts are shown in Figure 3-13. The plots gave good least-squares fits in **PhP1**, **PhBz** and **DFT** with $R^2$ values of 0.995–0.996, and $\delta_p$ values of +170, +105 and –94 nC/cm$^2$, respectively. In **NCB76**, however, a non-linear relationship was found between $P_0$ and $\chi_{2.2b}$. A second order fit of the plot gave a good least-squares fit with an $R^2$ value of 0.996, and a $\delta_p$ value of +424 nC/cm$^2$ was calculated based on the slope of the origin. Induced polarizations that scale non-linearly with $\chi_d$ were also observed with other dopants (*e.g.* **1.11b** and **1.14b**) in **NCB76**.[2] One possible explanation is that the mixture has reached a saturation point, despite the fact that the SmC* texture appears uniform by polarized microscopy at $T - T_C$ = –10 K, and that microphase separation may be occurring at the point when the reduced polarization reaches its maximum and starts leveling off. Another possible explanation is

a gradual shift in the conformational distribution of the dopant due to chirality transfer, as it is amplified by a cooperative effect between dopant molecules at higher dopant mole fractions.

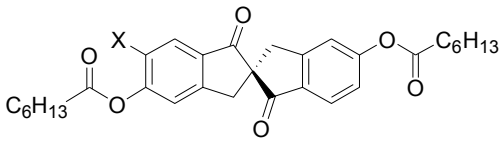

**Table 3-2.** Polarization powers for dopants (*R*)-**1.11b**, (*R*)-**1.14b**, (*R*)-**2.1b** and (*R*)-**2.2b** in four SmC hosts.

| Dopant (X) | $\delta_P$ (nC/cm$^2$)[a,b] | | | |
|---|---|---|---|---|
| | **PhP1** | **PhBz** | **NCB76** | **DFT** |
| (*R*)-**1.11b** (H)[c] | 314 ± 30 (+) | 242 ± 24 (+) | 446 ± 46 (+) | (+)/(–) |
| (*R*)-**1.14b** (F)[c] | 147 ± 18 (+) | (–)/(+) | (–)/(+) | 334 ± 15 (–) |
| (*R*)-**2.1b**(Cl) | < 30 (+)[d] | (–)/(+)[e] | (–)/(+)[e] | 345 ± 13 (–) |
| (*R*)-**2.2b** (Me) | 170 ± 5 (+) | 106 ± 3 (+) | 424 ± 36 (+)[f] | 94 ± 4 (–) |

[a]Uncertainties are ±1 standard error of the least-squares fit. [b]Sign of $P_S$ indicated in parentheses. [c]From ref. 2. [d]The $P_0$ values of the mixtures were at or below the detection limit of our instruments and the upper limit was estimated based on the mixture of highest dopant mole fraction. [e]Inversion of polarization was observed upon cooling. [f]A calculated $\delta_p$ value from a second order fit of the plot based on the slope of the origin.

A summary of the polarization power data for the four 5,5'-diester dopants investigated thus far is given in Table 3-2 and Figure 3-14. In general, the $\delta_p$ values for the diester dopants show less variance with the host structure than their diether analogues. Unlike the four diether dopants, which all exhibit the same $\delta_p$ (host) trend, the diester dopants exhibit two distinct $\delta_p$ (host) trends. Hence, the unsubstituted and methyl-substituted dopants (**1.11b** and **2.2b**) give high positive $\delta_p$ values in **NCB76**, then somewhat lower positive $\delta_p$ values in **PhP1** and **PhBz**, and near zero (inversion of $P_S$) to

low negative $\delta_p$ values in **DFT**. The other two dopants with polar substituents at the 6-position (**1.14b** and **2.1b**) give small positive $\delta_p$ values in **PhP1**, near zero (inversion of $P_S$) in **PhBz** and **NCB76**, and larger negative $\delta_p$ values in **DFT**. As with the diether dopants, the addition of a substituent at the 6-position of one indanone ring does not shift $\delta_p$ values towards more positive values. Even in the case of the methyl-substituted dopant (*R*)-**2.2b**, the $\delta_p$ values are still less positive than (*R*)-**1.11b**, although the effect is less pronounced than dopants with a polar substituent ((*R*)-**1.14b** and (*R*)-**2.1b**).

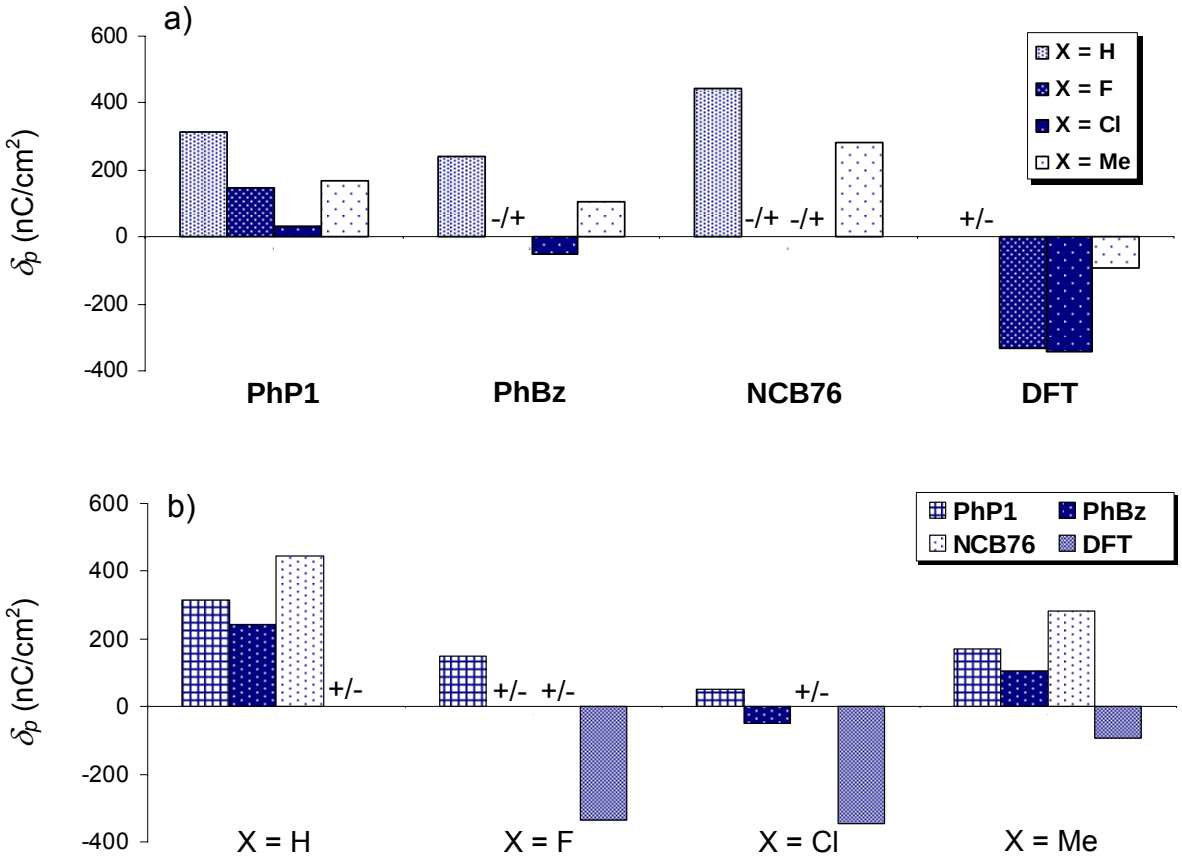


**Figure 3-14**. Comparison of polarization powers of the four 5,5'-diesr dopants: (a) as a function of the host, and (b) as a function of the substituent at 6-position.

## 3.3. Conformational Analysis

To gain more insight on the effect of substituents at the 6-position of the diether and diester dopants on their conformational distributions in the SmC* phase, conformational analyses were performed on two model systems, 6-substituted-5-methoxy-1-indanone (**3.1a–d**), and 6-substituted-5-acetoxy-1-indanone (**3.2a–d**). The analyses were conducted at the B3LYP/6-31G* level using the Spartan'04 software package (Wavefunction Inc.). The energy was minimized as a function of the dihedral angle defined by the atoms C(Me), O, C-5 and C-4 for model compounds **3.1a–d**, and by the atoms C(C=O), O, C-5 and C-4 for model compounds **3.2a–d**.

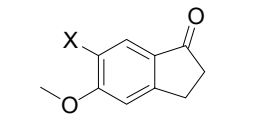

**3.1a**, X = H; **3.1b**, X = F;
**3.1c**, X = Cl; **3.1d**, X = Me

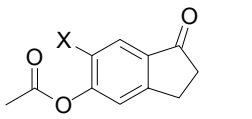

**3.2a**, X = H; **3.2b**, X = F;
**3.2c**, X = Cl; **3.2d**, X = Me

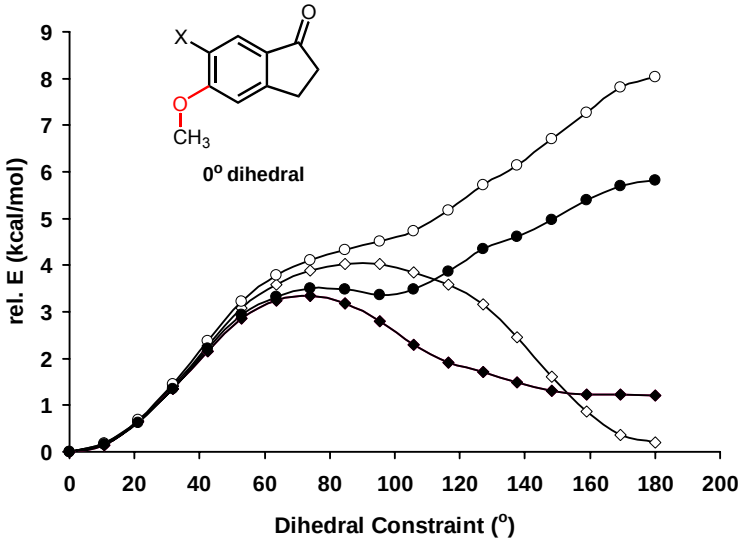


**Figure 3-15.** Energy profiles for 6-substituted 5-methoxyindanone as a function of rotation about the O–C-5 bond, according to B3LYP/6-31G* calculations: X = H (◊); X = F (♦); X = Cl (●) and X = Me (○).

In the case of the ether model compound (**3.1a–d**, Figure 3-15), the unsubstituted compound **3.1a** features two nearly equivalent minima at $\theta = 0^{o}$ and $180^{o}$. The presence of a substituent at the 6-position causes this distribution to shift towards the conformer with the methoxy group *anti* to X (*i.e.* $\theta = 0^{o}$). With X = F, this conformer is favored over the *syn* conformer by *ca*. 1 kcal/mol; with X = Cl and Me, it is favored almost exclusively, except for a very shallow minimum at $\theta \sim 100^{o}$. These results are consistent with differences in the steric demand of X, including the fact that the chloro and methyl groups are nearly isosteric, which is reflected by the similarity in energy profiles obtained for **3.1c** and **3.1d**.

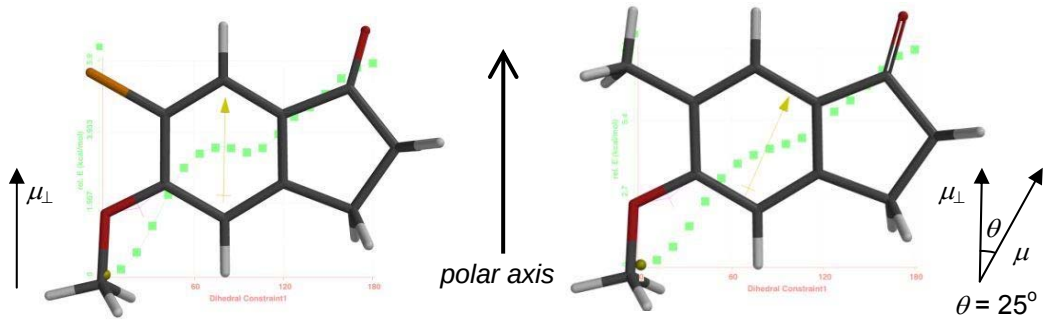


**3.1c** (X = Cl) $\mu_\perp$ = 5.74 D **3.1d** (X = Me) $\mu_\perp$ = 4.62 D

**Figure 3-16.** Calculated molecular transverse dipole moment ($\mu_\perp$) in their lowest energy conformation for the model compounds **3.1c** and **3.1d** at B3LYP/6-31G* level.

Taken together with the conformational analyses, the $\delta_p$ data listed in Table 3-1 for the four diether dopants suggest that the variation in polarization power with X may be explained by a change in conformational distribution of the dopant in the binding site. Furthermore, considering the similarity in conformational energy profiles for **3.1c** (X = Cl) and **3.1d** (X = Me), one might expect similar conformational distributions for dopants **2.1a** and **2.2a** in the binding site. Hence, any difference in $\delta_p$ between **2.1a** and **2.2a** in

any given host should correlate to the difference in transverse dipole moment $\mu_\perp$ of the core. The extent of any such correlation should also scale with the rotational distribution of $\mu_\perp$ with respect to the polar axis, *i.e.*, no difference in $\delta_p$ if the C–X bond lies in the tilt plane, and maximum difference in $\delta_p$ if the C–X bond lies along the polar axis perpendicular to the tilt plane. Interestingly, theoretical calculations of the transverse dipole moment ($\mu_\perp$) of the corresponding substituted alkoxyindanone fragments in their lowest energy conformation (Figure 3-16) give a ratio of $\mu_\perp$ for **3.1c** vs. **3.1d** (5.74/4.62 = 1.24) that is similar to the ratio of $\delta_p$ values for **2.1a** (X = Cl) and **2.2a** (X = Me) in **PhP1** (315/249 = 1.27) and **DFT** (293/227 = 1.29), which suggests that the orientation of the C–X bond may in fact lie perpendicular to the tilt plane, which is inconsistent with the original **P**/**C$_2$** conformational distribution model. In addition, the shift towards more negative $\delta_p$ values observed upon introduction of the substituent X also suggests a shift in conformational distribution *away* from the **P** conformer of the (*R*) enantiomer with the preferred zigzag shape, as proposed originally.

Therefore, the results suggest that dopants in this class may have more complicated conformational distributions than the original **P**/**C$_2$** model and reinforce the notion that results of gas phase calculations must be applied with great caution in the condensed phase. The fact that the C–X bond may not be oriented in the tilt plane suggests that the introduction of the substituent X may not necessarily force the alkoxy group in an *anti* conformation relative to the carbonyl group, and that *gauche* bend conformations may be energetically favored in the SmC* phase in order to provide a better fit to the binding site topography of the host.

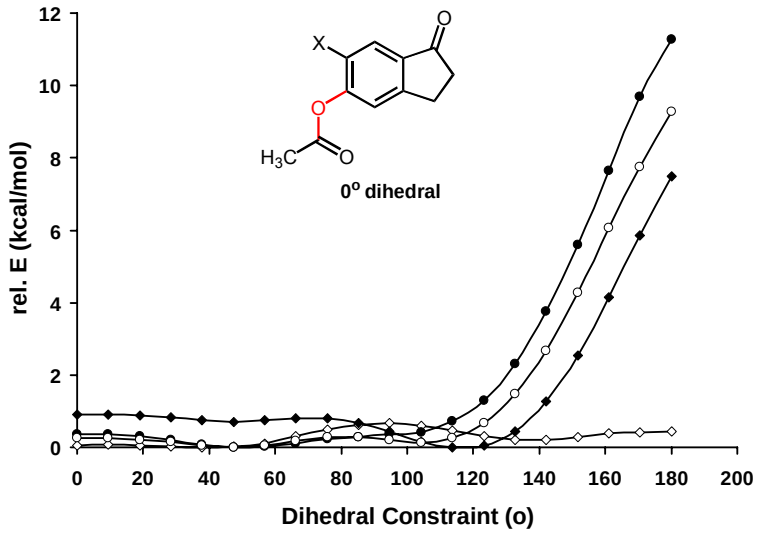


**Figure 3-17.** Energy profiles for 6-substituted 5-acetoxyindanone as a function of rotation about the O–C-5 bond, according to B3LYP/6-31G* calculations: X = H (◊); X = F (♦); X = Cl (●) and X = Me (○).

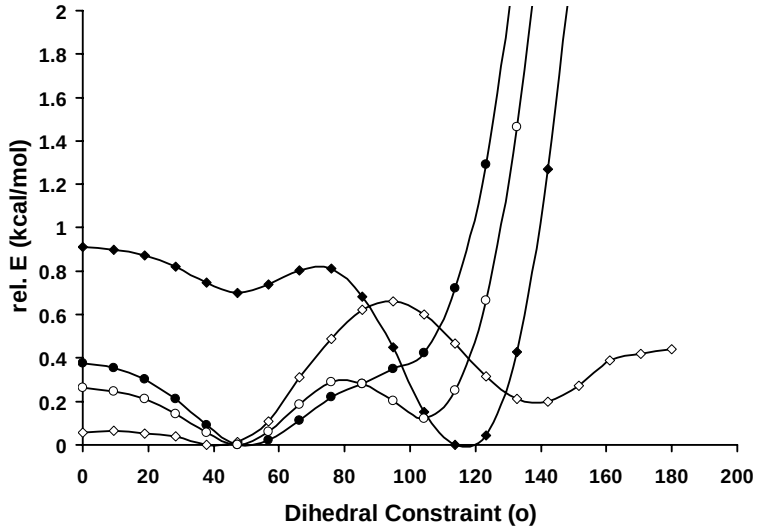


**Figure 3-18.** Expansion of the plot of energy profiles for 6-substituted 5-acetoxyindanone as a function of rotation about the O–C-5 bond, according to B3LYP/6-31G* calculations: X = H (◊); X = F (♦); X = Cl (●) and X = Me (○).

In the case of the ester model compounds (**3.2a–d**), the conformational energy profile for the unsubstituted compound **3.2a** is relatively flat, with two shallow minima at $\theta = 40^{o}$ and $140^{o}$. The presence of a substituent X causes the energy to rise sharply from

$\theta$ = 120° and 180°, but the profiles remain relatively flat otherwise (Figure 3-17). An expansion of the plot (Figure 3-18) reveals finer differences in the profiles of **3.2a–d**.

Nevertheless, these results suggest that any conformational bias for the diester dopants in the binding site of the SmC* phase is likely to be more subtle, and the conformational distribution perhaps more complex than for the diether dopants. This could explain the higher solubility of the diester dopant and the less pronounced host dependence of their polarization powers compared to the diether analogues, considering that the diesters may conform more easily to the zigzag shape of the binding site in the SmC* phase and adapt to changes in its topography.

Given the greater complexity of the conformational energy profiles, we were unable to produce a reliable conformational distribution model for the diester. Nevertheless, the polarization power data of the diester dopants indicates that the addition of a substituent on the 6-position does not result in more positive $\delta_P$ values regardless of the size and polarity of the substituent. Furthermore, unlike the diether dopants, the $\delta_P$ data for the diester dopants show no clear trends, which may be a reflection of a more complex conformational distribution, or more other contributing factors, including chirality transfer.

### 3.4. Inversion of Polarization

An inversion of the sign of polarization as a function of temperature and dopant mole fraction was observed in several dopant/host combinations. A linear relationship of the reduced inversion temperature ($T_i - T_C$) as a function of $\chi_d$ was observed for dopants **2.2a** and **2.1b** in **NCB76**.

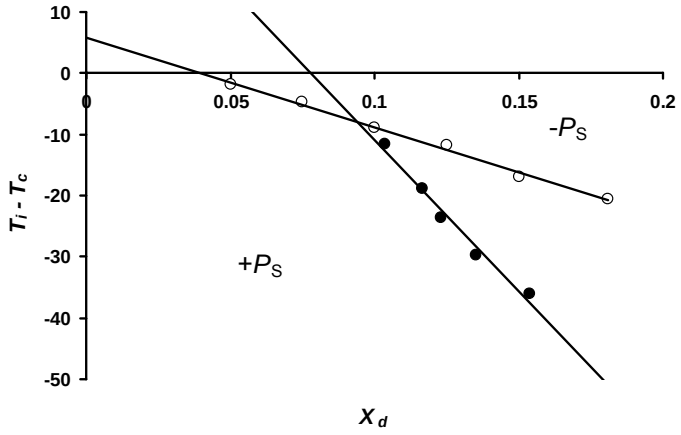


**Figure 3-19**. Reduced Inversion temperature (°C) versus dopant mole fraction $x_d$ for dopant (*R*)-**2.2a** (○) and (*R*)-**2.1b** (●) in **NCB76**. The (*R*) enantiomers of both dopants give positive $P_S$ below the line and negative $P_S$ above the line.

As shown in Figure 3-19, the sign of polarization induced by (*R*)-**2.2a** and (*R*)-**2.1b** inverts from negative to positive on cooling. However, the reduced inversion temperature for dopant **2.1b** is much more sensitive to $\chi_d$ than for dopant **2.2a**. Goodby and co-workers postulated that an inversion of $P_S$ may arise from a temperature-dependent distribution of competing conformations of opposite polarities.[5] Furthermore, Stegemeyer and Fujisawa attributed a dependence of $T_i - T_C$ versus $\chi_d$ to a balance between dopant-host and dopant-dopant interactions, the latter being more pronounced at high $\chi_d$.[6~9]

Goodby's reasoning that a $P_S$ sign inversion arises from a shift in distribution of competing conformational and/or rotational species is quite relevant to our system, and is consistent with our original model suggesting that two or more conformations of opposite polarities are in equilibrium. The fact that the spontaneous polarization of every mixture exhibiting $P_S$ inversion is very close to zero suggests a balance between the polarization contributions of conformers with opposite polarities, and that small perturbations, such as

a change in temperature, might shift the equilibrium in either direction, resulting in a change in the sign of $P_S$.

Based on the work of Stegemeyer and Fujisawa, a dependence of $T_i - T_C$ on $\chi_d$ in this case may be explained by taking chirality transfer into consideration, since dopant-dopant interactions should be more sensitive to $\chi_d$ if the dopant acts as an active guest and exerts a perturbation on its host environment that propagate to other dopant molecules. The stronger the perturbation, the more sensitive the dopant-dopant interactions should be to changes in dopant mole fraction. Therefore, a greater sensitivity of $T_i - T_C$ versus $\chi_d$ may be an indication of a higher degree of (chiral) perturbation exerted by a dopant (**2.1b**) in the SmC* phase.

The consideration of chirality transfer may also explain, at least to some extent, why less positive $\delta_P$ values are observed compared to the unsubstituted dopants **1.11a** and **1.11b** for all 6-substituted derivatives regardless of the size and polarity of the substituent. Based on the CTF model, chirality transfer may increase a conformational bias, resulting in a higher polarization power (*e.g.* dopant **1.4d** in **PhP1**), but it may also decrease a conformational bias depending on the complementarity of the chiral perturbation with the various chiral conformers, resulting in lower polarizations. For both (*R*)-**2.2a** and (*R*)-**2.1b**, the inversion temperature decreases with increasing dopant mole fraction, which indicates that the dopant induces negative polarizations in a broader range of temperature at higher mole fractions, until a uniformly negative $P_S$ is observed over the entire SmC* temperature range. That is to say, the change in nature of the intermolecular interactions at higher dopant mole fractions promotes one or more negative conformations.

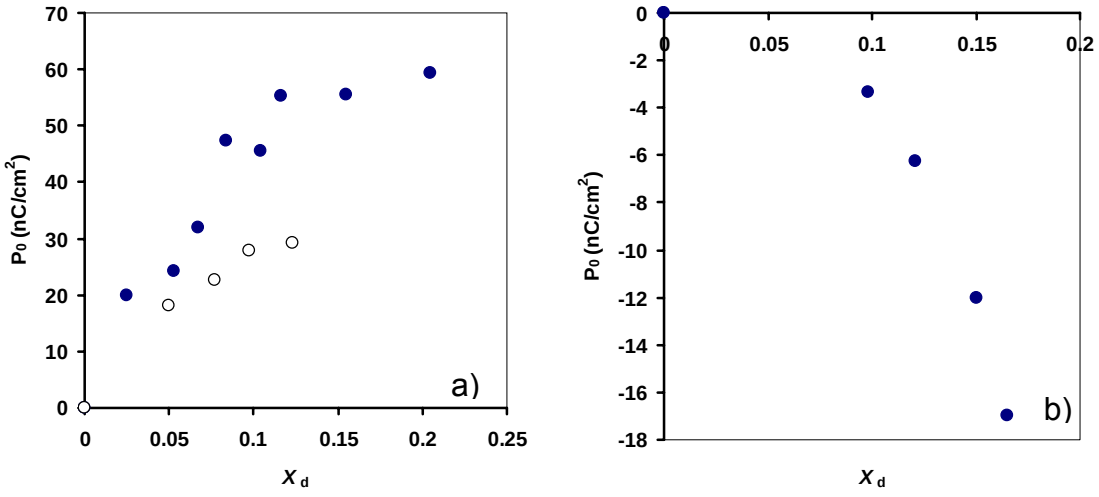


**Figure 3-20**. Examples of non-linear plots of $P_0$ vs. $x_d$. a) (*R*)-**1.11b** (●) and (*R*)-**2.2b** (○) in **NCB76**; b) (*R*)-**2.1b** (●) in **PhBz**.

The postulate that CTF may shift conformational distributions towards conformers with negative polarity in dopants of this class with the (*R*) configuration is further supported by non-linear plots of $P_0$ vs. $\chi_d$ obtained for the diester **1.11b** and **2.2b** in **NCB76**. As shown in Figure 3-20(a), the reduced polarization is positive and levels off at a certain dopant mole fractions, which is consistent with the conformational distribution gradually shifting towards the negative conformers as the chiral perturbations intensify. In the case of the diester **2.1b** in **PhBz**, inversion of polarization is observed for $\chi_d = 0.02$, and a detectable negative $P_0$ increases in a non-linear fashion at $\chi_d > 0.10$, which is also consistent with the proposed effect of the CTF (Figure 3-20(b)).

## 3.5. Detecting CTF by Probe Experiments

Several observations of $P_S$ sign inversion and non-linear $P_0$ vs. $\chi_d$ relationships obtained for the diester dopants in **NCB76** has led us to consider the possible effect of chirality transfer. In the case of the chloro-substituted diester dopant **2.1b** in **NCB76**, the

fact that the reduced inversion temperature is extremely sensitive to $\chi_d$ suggests that the perturbation exerted by the dopant on the liquid crystal host may be long-range in nature.

Previous studies in the Lemieux group have shown that probe experiments are powerful tools in providing direct evidence supporting the chirality transfer feedback (CTF) mechanism.[10,11] An assessment of all the probe experiments performed so far may provide us with guiding principles to select a probe for the present system. Since the outcome of probe experiments is based on the assumption that perturbations exerted by the test dopant in the SmC* phase should affect the $\delta_p$ of the probe, the sensitivity of the latter to those perturbations is a key factor. Therefore, a good probe (i) should be a Type II dopant showing strong host dependence, (ii) it should exert very weak perturbations on its own (*i.e.*, it must be 'passive'), or at least much weaker perturbation than the dopant being 'probed', (iii) perhaps most importantly, the structure of the probe should mimic either the test dopant or the host so as to maximize structural complementarity, and (iv) the probe should have good solubility in the liquid crystal host.

A careful examination of previous probe experiments performed with the 2,2'-spirobiindan-1,1'-dione dopants **1.11a** and **1.13** (see Section 1.7.2 in Chapter 1) reveals a potential flaw: the probe **MDW950** mimics neither the 2,2'-spirobiindan-1,1'-dione dopants nor the host **NCB76**. Therefore, it is possible that **MDW950** is not sensitive enough to detect chiral perturbations exerted by 2,2'-spirobiindan-1,1'-dione dopants because of a lack of structural complementarity.

Previous $^2$H NMR experiments suggest that the unsubstituted 5,5'-diether dopant **1.11a** exerts relatively weak chiral perturbations in the SmC* phase compared to the 6,6'-diether analogue, and it was therefore chosen as the new probe dopant to test the feedback

effect of chirality transfer exerted by the substituted diester dopants. To assess the role played by substitution at the 6-position of the diester dopants in terms of CTF contribution, comparative experiments were performed with the chloro-substituted 5,5'-diester dopant **2.1b** and the unsubstituted analogue **1.11b** in **NCB76**.

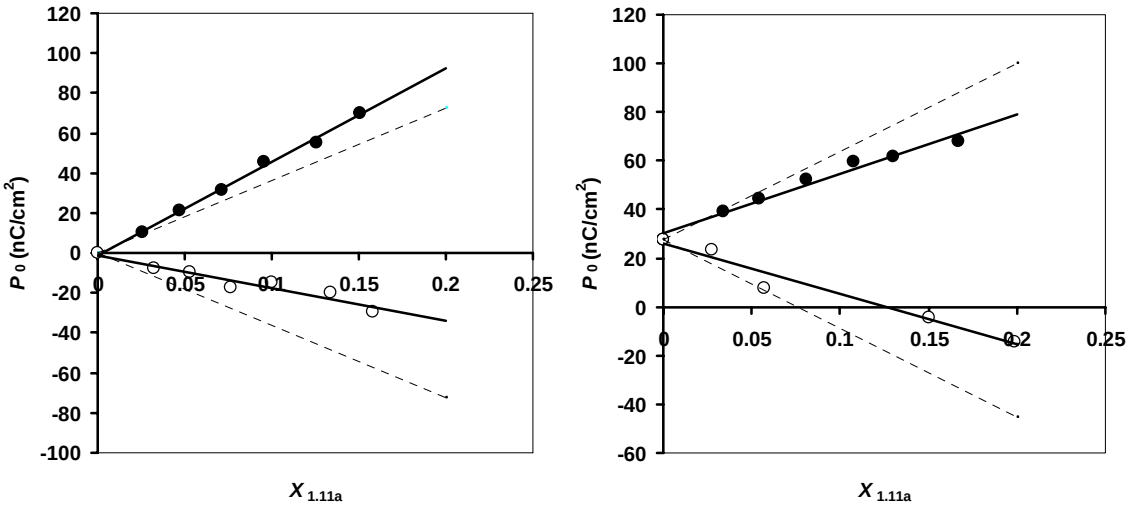


**Figure 3-21.** Reduced polarization ($P_0$) vs. mole fraction for mixtures of (*R*)-**1.11a** (●) and (*S*)-**1.11a** (○) in **NCB76** in the presence of 5 mol% (*S*)-**2.1b** (left) and (*R*)-**1.11b** (right) at 10 K below the SmA*-SmC* transition temperature. The solid lines represent least-squares fits of the two data sets and the dashed lines represent reference plots for (*R*)- and (*S*)-**1.11a** in the absence of a second dopant based on $\delta_p$ values previously measured (ref. 2).

The reduced polarization induced by (*R*)- and (*S*)-**1.11a** was measured at 10K below the Curie point as function of its mole fraction $\chi_{1.11a}$ in the presence of (*S*)-**2.1b** or (*R*)-**1.11b** at a constant mole fraction of 0.05 (5 mol%) in **NCB76**. As shown in Figure 3-21, $P_0$ induced by 5 mol% of (*S*)-**2.1b** is assumed to be zero and $P_0$ induced by 5 mol% of (*R*)-**1.11b** was measured in the absence of the probe **1.11a**. In the absence of a second chiral dopant, the enantiomers of **1.11a** should have equal-but-opposite polarization powers, which are represented by the dashed lines on each plots using the previously determined $\delta_{1.11a}$ value for (*R*)-**1.11a** and (*S*)-**1.11a** in **NCB7**6 ($\delta_{1.11a}$ = +363 and –363

nC/cm$^2$, respectively). The four plots of $P_0$ versus $\chi_{1.11a}$ for (*R*)-**1.11a** and (*S*)-**1.11a** in the presence of (*S*)-**2.1b** and (*R*)-**1.11b** give good least-squares fits ($R^2$ = 0.955–0.995) up to $\chi_{1.11a}$ = 0.15, which is consistent with the probe **1.11a** exerting little or no perturbation in the SmC* phase. In the presence of 5 mol% of (*S*)-**2.1b**, the $\delta_{1.11a}$ values are +468 ± 17 nC/cm$^2$ and –166 ± 20 nC/cm$^2$ for (*R*)- and (*S*)-**1.11a**, respectively, which suggest that (*S*)-**2.1b** exerts a perturbation on the probe, and that the perturbation is chiral. On the other hand, in the presence of (*R*)-**1.11b**, $\delta_{1.11a}$ values decreased by approximately the same amount within error for the (*R*)- and (*S*)-**1.11a** ($\delta_{1.11a}$ = +244 ± 17 nC/cm$^2$ and –207 ± 26 nC/cm$^2$, respectively), which suggests that the unsubstituted diester exerts an achiral perturbation on the probe. These results are consistent with our hypothesis that the addition of a substituent at the 6- position of one indanone ring causes the dopant to exert significant chiral perturbation in the SmC* phase that is long-range.

These results are also consistent with the postulate that the feedback effect of a chiral perturbation exerted by the (*R*) enantiomer of a 2,2'-spirobiindan-1,1'-dione derivative may shift the conformational distribution of the dopant towards conformers with negative polarity. Assuming that dopants of this class share similar conformational distributions, we expect that the presence of (*S*)-**2.1b** would cause $\delta_{1.11a}$ to decrease for the same configuration of dopant/probe pair and increase for the opposite configuration of dopant/probe pair, which is what we observed. In the case of the (*S*)-**2.1b**/(*S*)-**1.11a** combination, $\delta_{1.11a}$ decreases by approximately 55% (–166 nC/cm$^2$ versus –363 nC/cm$^2$); in the case of the (*S*)-**2.1b**/(*R*)-**1.11a** combination, $\delta_{1.11a}$ increases by approximately 30% (+468 nC/cm$^2$ versus +363 nC/cm$^2$).

In summary, these results strongly support the hypothesis that a CTF effect plays a significant, if not unique role in shifting the conformational distribution of the 6-substituted 5,5'-diester dopants towards conformers with negative polarity, and may have similar effect on the 6-substituted 5,5'-diether analogues, resulting in lower polarization powers regardless of the size and polarity of the substituent.

## 3.6. References


1) Boulton, C. J.; Finden, J. G.; Yuh, E.; Sutherland, J. J.; Wand, M. D.; Wu, G.; Lemieux, R. P. *J. Am. Chem. Soc.* **2005**, *127*, 13657-13665.
2) Yuh, E. M.Sc. Thesis, Queen's University, 2005.
3) Miyasato, K.; Abe, S.; Takezoe, H.; Fukuda, A.; Kuze, E. *Jpn. J. Appl. Phys.* **1983**, *22*, L661.
4) Walba, D. M. Ferroelectric Liquid Crystals: A Unique State of Matter. In *Advances in the Synthesis and Reactivity of Solids*; Mallouck, T. E., Ed.; JAI Press, Ltd.: Greenwich, CT, 1991; Vol. 1, pp 173-235.
5) Goodby, J. W.; Chin, E.; Geary, J. M.; Patel, J. S.; Finn, P. L. *J. Chem. Soc., Faraday Trans. I* **1987**, *83*, 3429.
6) Stegemeyer, H.; Meister, R.; Hoffmann, U.; Sprick, A.; Becker, A. *J. Mater. Chem.* **1995**, *5*, 2183.
7) Stegemeyer, H.; Sprick, A.; Osipov, M. A.; Vill, V.; Tunger, H.-W. *Phy. Rev. A* **1995**, *51*, 5721.
8) Fuwa, Y.; Myojin, K.; Moritake, H.; Ozaki, M.; Yoshino, K.; Tani, T.; Fujisawa, K. *Jpn. J. Appl. Phys.* **1994**, *33*, 5488.

9) Ozaki, M.; Fuwa, Y.; Nakayama, K.; Yoshino, K.; Tani, T.; Fujisawa, K. *Ferroelectrics* **1998**, *214*, 51.

10) Lazar, C.; Wand, M. D.; Lemieux, R. P. *J. Am. Chem. Soc.* **2000**, *122*, 12586-12587.

11) Hartley, C. S.; Lazar, C.; Wand, M. D.; Lemieux, R. P. *J. Am. Chem. Soc.* **2002**, *124*, 13513-13518.

# Chapter 4. Conclusions and Future Work

The goal of this project was to further test the conformational distribution model proposed from previous studies of dopants with a substituted 2,2'-spirobiindan-1,1'-dione core, so as to design a new class of Type II dopant capable of inducing large polarizations. A pair of isosteric groups with different polarities, chloro- and methyl-groups, was chosen and dopants **2.1a**, **2.1b**, **2.2a** and **2.2b** were synthesized and characterized in an effort to bias the **P**/$\mathbf{C_2}$ conformational equilibrium proposed in Section 1.7.3.

Both the miscibility of the dopants and their polarization powers show strong host dependence, which is consistent with other dopants in this class. Compared with the ether-linked dopants, the ester-linked dopants are more soluble in LC hosts and show less pronounced host dependence of their polarization powers, suggesting a more complex conformational distribution. For both the ether-linked and ester-linked dopants, the addition of a substituent at the 6-position of one indanone ring results in lower polarization powers regardless of the size and polarity of the substituent, which is contrary to the original conformational distribution model.

A comparative study of the data suggests that the ester-linked dopants exert much stronger perturbations on the host environment than the ether-linked dopants, especially when the 6-position is substituted. Several observations of inversion of the sign of polarization and non-linear relationships of $P_0$ vs. $\chi_d$ obtained for the diester dopants in **NCB76** led us to consider the possible effect of chiral perturbations, and the feedback effect of this perturbation causing a shift in the conformational distribution of the dopant favoring conformers with negative polarity. Using optically pure **1.11a** as probe, new

probe experiments were performed to detect the effect of chirality transfer feedback (CTF) in the case of the chloro-substituted diester dopant (**2.1b**), which showed results consistent with the postulate, as well as underlining the importance of structural complementarity in successful probe experiments.

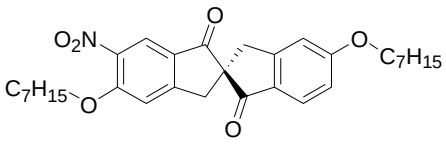


**4.1a**

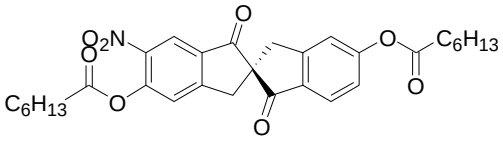


**4.1b**

Further studies on substituted 2,2'-spirobiindan-1,1'-dione systems will focus on two issues: (1) understanding the conformational distribution, and (2) the effect of chirality transfer feedback. Hence, the 6-nitro-substituted dopants **4.1a** and **4.1b** will be investigated, since the nitro group impacts a similar conformational distribution as the methyl and chloro group, but produces a much larger transverse dipole moment. It is hoped that this enhanced transverse dipole moment will be reflected in the polarization powers and host dependence of **4.1a** and **4.1b**, and therefore provides further insight into the conformational distribution of these dopants in the condensed phase. Furthermore, as previous studies showed that the 6,6'-diether dopant **1.13** and the 6,6'-diester dopant **2.23** might exert strong chiral perturbation in **NCB76**, similar probe experiments will be performed to study the chiral perturbation exerted by these two dopants.

# Chapter 5. Experimental

## 5.1. Synthesis and characterization

### *5.1.1. General*

$^{1}H$ and $^{13}C$ NMR spectra were recorded on Bruker Avance 300, 400 or 500 MHz spectrometers using deuterated chloroform or deuterated methanol as solvent. Chemical shifts are reported in δ (ppm) relative to tetramethylsilane as internal standard. Low-resolution EI mass spectra were recorded on a Fisons VG Quattro triple quadrupole mass spectrometer or an Applied Biosystems/MDS Sciex QSTAR XL QqTOF mass spectrometer. Peaks are reported as *m/z* (% intensity relative to base peak). High resolution EI mass spectra were recorded on a Waters/Micromass GCT mass spectrometer, and high resolution ESI mass spectra were recorded on an Applied Biosystems/MDS Sciex QSTAR XL QqTOF mass spectrometer. UV-vis spectra were recorded on a Varian Cary-3 UV-visible spectrometer in hexanes (spectro grade). Circular dichroism spectra were recorded on a Jasco J-715 spectropolarimeter in hexanes (spectro grade). Melting points were obtained on a Fisher-Johns melting point apparatus and are uncorrected. Elemental analyses were obtained from Canadian Microanalytical Service Ltd. (Delta, B.C.). Flash chromatography was performed on 60 Å silica gel (Silicycle Inc., Quebec). Preparative chiral stationary phase HPLC separations were performed with a Daicel Chiralpak AS column (50 cm × 5 cm i.d.) using mixtures of hexanes/EtOH as eluant at a flow rate of 50 mL/min.

*5.1.2. Materials*

All solvents and reagents were obtained from commercial sources and used without further purification unless otherwise noted. Anhydrous $CCl_4$ was obtained from Aldrich. Anhydrous $CH_2Cl_2$ was distilled over $P_2O_5$ under a nitrogen atmosphere. Anhydrous THF, hexane, ether, DMF and toluene were obtained from a Solv-Tek, Inc. solvent purification system. 2-Chloro-5-methylanisole (**2.3**) and 5-methoxyindan (**2.9**) were obtained from Aldrich. Ethoxycarbonyl-5-methoxy-1-indanone (**2.14**)[1], ethyl 2-(bromomethyl)-4-methoxybenzoate (**2.16**)[2] and 1-bromoheptane-1,1-$d_2$[2] and the chiral probe dopants (*R*)- and (*S*)-5,5'-diheptyloxy-2,2'-spirobiindan-1,1'-dione ((*R*)-**1.11a** and ((*S*)-**1.11a**)[2] were synthesized according to literature procedures and were shown to have expected physical and spectral properties. The liquid crystal hosts 4-(4'-heptyl[1,1'-biphenyl]-4-yl)-1-hexylcyclohexanecarbonitrile (**NCB76**) and 2-(4-butoxyphenyl)-5-(ocyloxy)pyrimidine (**PhP1**) were obtained from Clariant. The liquid crystal hosts 4-[(±)-4-methylhexyl)oxy]-phenyl 4-decyloxybenzoate (**PhBz**) and 2',3'-difluoro-4"-heptyl-4-nonyl-[1,1';4',1"]terphenyl (**DFT**) were prepared according to literature procedures by Lemieux group members and were shown to have the expected physical and spectral properties.[3, 4]

**4-Bromo-2-chloro-5-methyphenol (2.4).**[5] A solution of $Br_2$ (14.7 g, 92 mmol) in

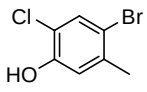


$CHCl_3$ (100 mL) was added dropwise to a solution of 2-chloro-5-methylphenol (**2.3**) (13.1 g, 92 mmol) in $CHCl_3$ (60 mL) at 0 °C. The solution was slowly warmed to r.t. and was stirred for an additional 24 h, then washed with sat. $NaHSO_3$ (2×50 mL), $H_2O$ (3×80 mL), dried ($MgSO_4$) and concentrated to give

19.5g (96%) of **2.4** as a colorless solid: mp 67 – 68 °C (68 °C lit.); $^1$H NMR (300 MHz, $CDCl_3$) δ 7.49 (s, 1H), 6.94 (s, 1H), 5.44 (s, 1H), 2.35 (s, 3H).

**4-Bromo-2-chloro-5-methylanisole (2.5).**[5] Under an argon atmosphere, NaH (60%, 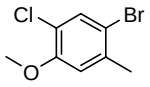

4.52 g, 113 mmol) was added in portions to a solution of **2.4** (19.8 g, 89 mmol) in anhydrous THF (250 mL). The solution was stirred at r.t. for 1 h, MeI (145 mmol) was added and the mixture was heated to reflux for 5 h. The solution was cooled, concentrated and the residue taken up in $H_2O$ (200 mL) and extracted with EtOAc (3×100 mL). The combined organic extracts were washed with $H_2O$ (2×150 mL), brine (2×100 mL), dried ($MgSO_4$) and concentrated to give 21.1 g (100%) of **2.5** as a white solid**:** mp 53 – 55 °C (55 °C lit.); $^1$H NMR (300 MHz, $CDCl_3$) δ 7.52 (s, 1H), 6.81 (s, 1H), 3.89 (s, 3H), 2.38 (s, 3H).

**5-Chloro-4-methoxy-2-methylbenzoic acid (2.6).**[6] Under an argon atmosphere, a 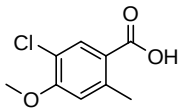

solution of *n*-BuLi (10 mL, 13.6 mmol, 1.36 M in *n*-hexane) was added dropwise to a solution **2.5** (3.00 g, 12.8 mmol) in THF-hexane-$Et_2O$ (6:1:1, 80 mL) cooled to –98 °C. Stirring was continued for 10 min at –98 °C, excess dry-ice was added, and the mixture was allowed to warm to r.t. over 12 h. The solution was concentrated to 30 mL and acidified with 3% aq. HCl and extracted with $CHCl_3$ (3×100 mL). The combined organic extracts were washed with $H_2O$ (2×100 mL), brine (2×100 mL), dried ($MgSO_4$), filtered through a short pad of silica gel, and concentrated to give a white solid. The crude product was washed with hot hexane to give 2.0 g (78%) of

**2.6** as white needles: mp 221 – 222 °C (220 – 222 °C lit.); $^1$H NMR (400 MHz, $CDCl_3$) δ 8.11 (s, 1H), 6.77 (s, 1H), 3.96 (s, 3H), 2.65 (s, 3H).

**Ethyl 5-chloro-4-methoxy-2-methylbenzoate (2.7).** A solution of **2.6** (4.0 g, 20 mmol) in absolute ethanol (150 mL) and $H_2SO_4$ (2.5mL) was heated to reflux overnight. The ethanol was then removed *in vacuo* and the residue was neutralized with sat. $NaHCO_3$ and extracted with EtOAc (3×50 mL). The combined organic layers were washed brine (2×50 mL), dried ($MgSO_4$), filtered through a short pad of silica gel and concentrated to give a white solid. The crude product was recrystalized from hexane to give 3.95 g (87%) of **2.7** as white needles: mp 104 – 105 °C; $^1$H NMR (400 MHz, $CDCl_3$) δ 7.99 (s, 1H), 6.74 (s, 1H), 4.32 (q, *J* = 7 Hz, 2H), 3.94 (s, 3H), 2.61 (s, 3H), 1.38 (t, *J* = 7 Hz, 3H); $^{13}$C NMR (100 MHz, $CDCl_3$) δ 14.6, 22.4, 56.5, 61.0, 114.9, 119.7, 122.7, 133.0, 142.0, 157.6, 166.4; MS (TOF-MS) *m/z* 230 ($[M+2]^+$, 14), 228 ($M^+$, 100), 199 (24), 183 (99), 155 (16); HRMS (TOF-MS) calc'd for $C_{11}H_{13}O_3Cl$: 228.0553, found 228.0548.

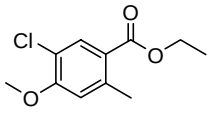


**Ethyl 2-(bromomethyl)-5-chloro-4-methoxybenzoate (2.8).** Under an argon atmosphere, **2.7** (5.00 g, 21.9 mmol), *N*-bromosuccinimide (NBS) (4.34 g, 24.1 mmol) and AIBN (10 mg, 0.06 mmol) in anhydrous $CCl_4$ (200 mL) was heated to reflux. The reaction was monitored by $^1$H NMR every 24 h to determine the percent of conversion. Each time an additional amount of NBS in equivaler proportion to the remaining starting material and AIBN (10 mg, 0.06 mmol) were added, and the solution was heated to reflux under argon for 24 h until the

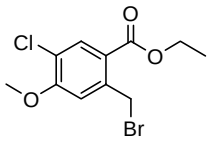

conversion of **2.7** reached a 1:5:1 proportion of starting material, benzylic *mono*-bromo and *di*-bromo products. After cooling, the mixture was washed with sat. $NaHCO_3$ (2×100 mL), brine (2×100 mL), dried ($MgSO_4$) and concentrated. The crude product was purified by flash chromatography on silica gel (19:1 hexanes/EtOAc) to give 4.51 g (67%) of **2.8** as white needles: mp 99 – 100 °C; $^1$H NMR (400 MHz, $CDCl_3$) δ 8.04 (s, 1H), 6.98 (s, 1H), 4.97 (s, 2H), 4.38 (q, *J* = 7 Hz, 2H), 3.98 (s, 3H), 1.42 (t, *J* = 7 Hz, 3H); $^{13}$C NMR (100 MHz, $CDCl_3$) δ 14.3, 31.2, 56.4, 61.3, 114.5, 121.8, 122.4, 133.4, 140.2, 157.8, 165.1; MS (TOF-MS) *m/z* 308 ($[M+2]^+$, 4), 306 ($M^+$, 3), 263 (2), 261 (1), 227 (17), 199 (100), 182 (3), 154 (2); HRMS (TOF-MS) calc'd for $C_{11}H_{12}O_3ClBr$: 305.9658, found 305.9656.

**(*RS*)-2-Ethoxycarbonyl-2-(2-(ethoxycarbonyl)-4-chloro-5-methoxybenzyl)-5-methoxy**

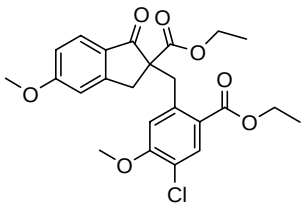


**-1-indanone (2.17).** Under an argon atmosphere, 60% dispersion of NaH (0.36 g, 8.9 mmol) was washed three times with $Et_2O$. A solution of **2.14** (1.61 g, 6.9 mmol) in anhydrous DMF (10 mL) was then slowly added to the NaH as a stirred suspension in anhydrous DMF (10 mL). After gas evolution ceased, the mixture was heated at 60 °C for 1 h and a solution of **2.8** (2.21 g, 7.2 mmol) in anhydrous DMF (30 mL) was slowly added. The solution was stirred at 60 °C for 96 h, then quenched with water and extracted with $CHCl_3$ (3×100 mL). The combined extracts were washed with brine (3×100 mL), dried ($MgSO_4$), filtered through a short pad of silica gel and concentrated to give a pale yellow solid. The crude product was washed with hot hexane (20 mL) to give 2.38 g (75%) of **2.17** as a white solid: mp 115 – 117 °C; $^1$H NMR (500 MHz, $CDCl_3$) δ 7.91 (s, 1H), 7.67

(d, *J* = 9 Hz, 1H), 6.87 (dd, *J* = 9 Hz, 2 Hz, 1H), 6.81 (s, 1H), 6.76 (d, *J* = 2 Hz, 1H), 4.26 (m, 2H), 4.18 (m, 3H), 3.85 (s, 3H), 3.77 (s, 3H), 3.68 (d, *J* = 14 Hz, 1H), 3.54 (d, *J* = 18 Hz, 1H), 2.98 (d, *J* = 18 Hz, 1H), 1.37 (t, *J* = 7 Hz, 3H), 1.22 (t, *J* = 7 Hz, 3H); $^{13}$C NMR (125 MHz, $CDCl_3$) δ 14.4, 14.7, 35.6, 35.7, 56.0, 56.5, 61.5, 62.2, 62.4, 109.6, 115.2, 116.3, 120.9, 124.3, 126.4, 128.9, 133.0, 140.1, 157.5, 157.6, 166.2, 166.6, 171.5, 201.5; MS (TOF-MS) *m/z* 460 ($M^+$, 6), 414 (7), 369 (38), 357 (63), 341 (97), 313 (58), 306 (54), 297 (10), 233 (91), 187 (100); HRMS (TOF-MS) calc'd for $C_{24}H_{25}O_7Cl$: 460.1289, found 460.1292.

**(*RS*)-6-chloro-5,5'-dimethoxy-2,2'-spirobiindan-1,1'-dione (2.19).** A mixture of (*RS*)-**2.17** (2.20 g, 4.78 mmol) was dissolved in 150 mL of a 20:40:40 (v/v/v) solution of $H_2SO_4$, $H_2O$, and EtOH and the reaction mixture was heated to reflux overnight, then cooled to r.t. and filtered. The solid residue was taken up in $CHCl_3$, washed with sat. $NaHCO_3$ (2×100 mL), brine (2×100 mL), dried ($MgSO_4$) and concentrated to give a pale yellow solid. The crude product was washed with hot EtOAc to give 1.50 g (91%) of (*RS*)-**2.19** as a white solid: mp 243 – 244°C; $^1$H NMR (400 MHz, $CDCl_3$) δ 7.75 (s, 1H), 7.68 (d, *J* = 8 Hz, 1H), 7.04 (s, 1H), 6.98 (d, *J* = 2 Hz, 1H), 6.94 (dd, *J* = 8 Hz, 2 Hz, 1H), 4.02 (s, 3H), 3.91 (s, 3H), 3.65 (d, *J* = 17 Hz, 1H), 3.63 (d, *J* = 17 Hz, 1H), 3.12 (d, *J* = 17 Hz, 1H), 3.11 (d, *J* = 17 Hz, 1H); $^{13}$C NMR (100 MHz, $CDCl_3$) δ 38.0, 38.1, 56.0, 56.9, 66.1, 108.6, 109.8, 116.3, 124.2, 126.5, 126.9, 128.7, 129.1, 155.2, 157.1, 160.9, 166.2, 200.5, 200.8; MS (TOF-MS) *m/z* 344 ($[M+2]^+$, 16), 342 ($M^+$, 100), 314 (39), 313 (13), 271 (4); HRMS (TOF-MS) calc'd for $C_{19}H_{15}O_4Cl$: 342.0659, found 342.0650.

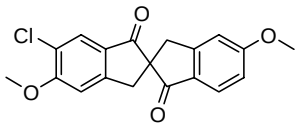

**(*RS*)-6-Chloro-5,5'-dihydroxy-2,2'-spirobiindan-1,1'-dione (2.21).** Under an argon atmosphere, (*RS*)-**2.19** (0.79 g, 2.30 mmol) was added to a stirred solution of $AlCl_3$ (1.53 g, 11.50 mmol) in anhydrous toluene (200 mL). The mixture was refluxed overnight, then quenched with $H_2O$ and filtered. The solid residue was dissolved in EtOH, concentrated to 10 mL, washed with $H_2O$ and filtered again to give 0.51 g (71%) of (*RS*)-**2.21** as a beige solid: mp > 300 °C (dec.); $^1$H NMR (400 MHz, MeOD) δ 7.64 (s, 2H), 7.52 (d, *J* = 8 Hz, 1H), 7.06 (s, 1H), 6.92 (d, *J* = 2 Hz, 1H), 6.86 (dd, *J* = 8 Hz, 2 Hz, 1H), 3.50 (d, *J* = 17 Hz, 1H), 3.47 (d, *J* = 17 Hz, 1H), 3.14 (d, *J* = 17 Hz, 1H), 3.13 (d, *J* = 17 Hz, 1H); $^{13}$C NMR (100 MHz, $CDCl_3$) δ 37.5, 37.6, 65.9, 111.7, 112.6, 116.5, 122.6, 125.8, 126.4, 127.3, 127.9, 155.9, 158.2, 160.5, 165.4, 202.0, 202.5; MS (TOF-MS) *m/z* 316 ($[M+2]^+$, 13), 314 ($M^+$, 100), 286 (39), 285 (18), 251 (6), 223 (11); HRMS (EI) calc'd for $C_{17}H_{11}O_4Cl$: 314.0346, found 314.0358.

**(*R*)- and (*S*)-6-Chloro-5,5'-bis-(heptyloxy-1,1-*d*$_2$)-2,2'-spirobiindan-1,1'-dione ((*R*)-2.1a and (*S*)-2.1a).** Under an argon atmosphere, a solution of (*RS*)-**2.21** (63.2 mg, 0.2 mmol), $Cs_2CO_3$ (260 mg, 0.8 mmol) and 1-bromoheptane-1,1- *d*$_2$ (217 mg, 1.2 mmol) in anhydrous DMF (15 mL) was stirred overnight at r.t., and heated to 70 °C for another 24 h. The reaction mixture was cooled to r.t., poured into water and extracted with EtOAc (3×30 mL). The combined organic extracts were washed with brine (2×50 mL), dried ($MgSO_4$), and concentrated. The residue was purified by flash chromatography on silica gel (9:1 hexanes/EtOAc) and recrystalized from HPLC-grade hexane to give 85 mg (83%) of

(*RS*)-**2.1a** as a white solid: mp 154 – 156 °C; $^{1}$H NMR (400 MHz, $CDCl_3$) δ 7.75 (s, 1H), 7.67 (d, *J* = 8 Hz, 1H), 6.99 (s, 1H), 6.95 (d, *J* = 2 Hz, 1H), 6.92 (dd, *J* = 8 Hz, 2 Hz, 1H), 3.64 (d, *J* = 17 Hz, 1H), 3.61 (d, *J* = 17 Hz, 1H), 3.09 (d, *J* = 17 Hz, 1H), 3.07 (d, *J* = 17 Hz, 1H), 1.89 (quintet, *J* = 7 Hz, 2H), 1.82 (quintet, *J* = 7 Hz, 2H), 1.32 – 1.58 (m, 16H), 0.92 (t, *J* = 7 Hz, 6H); $^{13}$C NMR (100 MHz, $CDCl_3$) δ 14.4, 22.9, 26.1, 26.2, 28.9, 29.1, 29.2, 29.3, 32.0, 38.1, 38.2, 66.1, 109.2, 110.3, 116.6, 124.5, 126.5, 126.8, 128.5, 128.8, 155.1, 157.0, 160.6, 165.8, 200.6, 200.9; MS (TOF-MS) *m/z* 516 ($[M+2]^+$, 12), 514 ($M^+$, 100), 414 (15), 314 (6), 286 (8); HRMS (TOF-MS) calc'd for $C_{31}H_{35}D_4O_4Cl$: 514.2788, found 514.2785; UV (hexanes) $\lambda_{max}$ (log ε) 206 (4.73), 269 (4.61), 289 (4.34), 297 (4.41), 307 (4.17). The racemic mixture was resolved by preparative scale chiral phase HPLC (2% EtOH in hexanes, 50 mL/min) to give (*R*)-**2.1a** and (*S*)-**2.1a** (first and second eluants, respectively) in optically pure form: CD ((*R*)-**2.1a,** hexanes) $\lambda_{ext}$ (Δε) 208 (9.5), 221 (–21.7), 231 (25.8), 258 (–10.2), 272 (6.3), 294(–4.3), 311 (–4.4), 321 (–5.1), 332 (–5.1), 344 (–2.9). Prior to doping into liquid crystal mixtures, the dopant was recrystallized from HPLC hexanes after filtration through a 0.45 μm PTFE filter.

**(*R*)- and (*S*)-6-Chloro-5,5'-diheptoyloxy-2,2'-spirobiindan-1,1'-dione ((*R*)-2.1b and (*S*)-2.1b).** 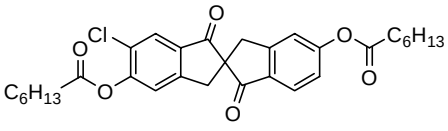

Under an argon atmosphere, DCC (206 mg, 1.00 mmol) was added to a stirred solution of (*RS*)-**2.21** (63.2 mg, 0.2 mmol), DMAP (122 mg, 1.00 mmol) and heptanoic acid (130 mg, 1.00 mmol) in anhydrous $CH_2Cl_2$ (5mL). The solution was stirred at room temperature overnight, then filtered and concentrated. The residue was taken up in EtOAc (30 mL), and washed with 2% aq. HCl (2×10 mL), dried ($MgSO_4$) and

concentrated. The residue was purified by flash chromatography on silica gel (6:1 hexanes/EtOAc) and recrystalized from HPLC-grade hexane to give 74 mg (69%) of (*RS*)-**2.1b** as white needles: mp 130 – 132 °C; $^{1}$H NMR (400 MHz, $CDCl_3$) δ 7.84 (s, 1H), 7.77 (d, *J* = 8 Hz, 1H), 7.36 (s, 1H), 7.32 (d, *J* = 1 Hz, 1H), 7.14 (dd, *J* = 8 Hz, 1 Hz, 1H), 3.70 (d, *J* = 17 Hz, 1H), 3.67 (d, *J* = 17 Hz, 1H), 3.19 (d, *J* = 17 Hz, 1H), 3.17 (d, *J* = 17 Hz, 1H), 2.67 (t, *J* = 7 Hz, 2H), 2.61 (t, *J* = 7 Hz, 2H), 1.80 (m, 4H), 1.36-1.48 (m, 12H), 0.93 (t, *J* = 7 Hz, 6H); $^{13}$C NMR (100 MHz, $CDCl_3$) δ 14.3, 22.8, 25.0, 25.1, 29.0, 31.8, 34.4, 34.7, 37.8, 38.1, 66.1, 119.7, 121.8, 122.4, 126.6, 126.5, 126.7, 128.2, 132.9, 134.1, 152.7, 153.5, 155.7, 156.9, 171.2, 172.0, 200.5, 200.9; MS (TOF-MS) *m/z* 538 ($M^+$, <1); 426 (36), 314 (100), 113 (35), 85 (9); HRMS (TOF-MS) calc'd for $C_{31}H_{35}O_6Cl$: 538.2122, found 538.2137; UV (hexanes) $\lambda_{max}$ (log ε) 210 (4.83), 254 (4.55), 284 (4.00), 293 (4.03). The racemic mixture was resolved by preparative chiral phase HPLC (5% EtOH in hexanes, 50 mL/min) to give (*R*)-**2.1b** and (*S*)-**2.1b** (first and second eluants, respectively) in optically pure form: CD ((*R*)-**2.1b,** hexanes) $\lambda_{ext}$ (Δε) 203 (10.8), 213 (–12.5), 224 (1.51), 232 (5.22), 247 (–6.1), 264 (0.1), 293 (–4.8), 320 (–0.6), 341 (–1.4). Prior to doping into liquid crystal mixtures, the dopant was recrystallized from HPLC hexanes after filtration through a 0.45 μm PTFE filter.

Anal. calc'd for $C_{31}H_{35}ClO_6$: C 69.07, H 6.54; found: C 69.28, H 6.71.

**6-Bromo-5-methoxyindan (2.10).**[7] A solution of $Br_2$ (3.5 mL, 67.5 mmol) in $CH_2Cl_2$ (100 mL) was slowly added at 0 °C to a solution of 5-methoxyindan (**2.9**) (10.0 g, 67.5 mmol) in $CH_2Cl_2$ (100 mL). The solution was stirred at 0 °C for 2 h, then washed with sat. $NaHCO_3$ (3×100 mL), brine (2×100 mL) and dried

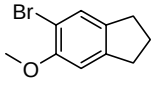

($MgSO_4$). Activated carbon was added to decolorize and the solution, which was filtered through a short pad of silica gel and concentrated to give 15.5 g (100%) of **2.10** as a colorless oil: $^1$H NMR (400 MHz, $CDCl_3$) δ 7.38 (s, 1H), 6.81 (s, 1H), 3.88 (s, 3H), 2.86 (m, 4H), 2.10 (m, 2H).

**5-Methoxy-6-methylindan (2.11).**[8] Under an argon atmosphere, a solution of *n*-BuLi

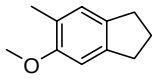

(33 mL, 44.9 mmol, 1.36 M in *n*-hexane) was added dropwise to a solution of **2.10** (8.57g, 37.8 mmol) in anhydrous THF (100 mL) cooled to –78 °C. Stirring was continued for 10 min at –78 °C and excess MeI (10 mL, 184 mmol) was added. The mixture was allowed to warm to r.t., and then concentrated, diluted with $H_2O$ (80 mL) and extracted with $CHCl_3$ (3×100 mL). The combined extracts were washed with brine (2×100 mL), dried ($MgSO_4$) and concentrated. The crude product was distilled under reduced pressure to give 5.56 g (91%) of **2.11** as a colorless liquid: $^1$H NMR (300 MHz, $CDCl_3$) δ 7.02 (s, 1H), 6.76 (s, 1H), 3.83 (s, 3H), 2.90 (t, $J$ = 7 Hz, 2H), 2.85 (t, $J$ = 7 Hz, 2H), 2.21 (s, 3H), 2.09 (m, 2H).

**5-Methoxy-6-methylindanone (2.12).**[9] Equal amounts of potassium permanganate and

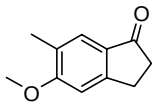

copper sulfate pentahydrate were groud together in a mortar. The resulting purple powder (32 g) was added to a solution **2.11** (2.27 g, 14.0 mmol) in $CH_2Cl_2$ (200 mL) and the mixture was stirred vigorously under gentle reflux for 48 h. The product was filtered through a Celite pad and the residue washed successively with $CH_2Cl_2$ (3×200 mL) and $Et_2O$ (3×200 mL). Evaporation of the solvent and recrystalization from hexane gave 0.86 g (35%) of **2.12** as light yellow needles: mp 114 –

116 °C (114 – 115 °C lit.); $^{1}$H NMR (400 MHz, $CDCl_3$) δ 7.53 (s, 1H), 6.84 (s, 1H), 3.92 (s, 3H), 3.08 (t, *J* = 6 Hz, 2H), 2.66 (t, *J* = 6 Hz, 2H), 2.23 (s, 3H); $^{13}$C NMR (100 MHz, $CDCl_3$) δ 16.7, 26.1, 36.7, 55.9, 106.7, 125.5, 127.5, 130.1, 156.6, 164.1, 205.8; MS (TOF-MS) *m/z* 176 ($M^+$, 100), 148 (27), 133 (25), 117 (7), 105 (7); HRMS (TOF-MS) calc'd for $C_{11}H_{12}O_2$: 176.0837, found 176.0835.

**2-Ethoxycarbonyl-5-methoxy-6-methyl-1-indanone (2.15).** Under an argon

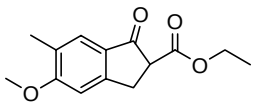

atmosphere, a 60% dispersion of NaH (0.90 g, 22 mmol) was washed three times with $Et_2O$. Diethyl carbonate (2 mL, 17 mmol) in anhydrous toluene (20 mL) were then added to the NaH and the resulting solution was stirred and heated to reflux. A solution of **2.12** (1.20 g, 6.8 mmol) in toluene (20 mL) was added slowly to the refluxing solution over 4h and the reaction mixture was refluxed overnight. Acetic acid and $H_2O$ were added until all the solid dissolved and the aqueous layer reached a pH of 5. The aqueous layer was extracted with EtOAc (3×50 mL) and the combined extracts were washed with brine (2×100 mL), and dried ($MgSO_4$). Activated carbon was added to decolorize the solution, which was filtered through a short pad of silica gel and concentrated to give 1.55 g (92%) of **2.15** as a yellow solid: mp 93 – 95 °C; $^{1}$H NMR (400 MHz, $CDCl_3$) δ 7.52 (s, 1H), 6.85 (s, 1H), 4.23 (q, *J* = 7 Hz, 2H), 3.92 (s, 3H), 3.67 (dd, *J* = 8 Hz, 2 Hz, 1H), 3.47 (dd, *J* = 17 Hz, 4Hz, 1H), 3.28 (dd, *J* = 17 Hz, 8Hz, 1H), 2.21 (s, 3H), 1.30 (t, *J* = 7 Hz, 3H); $^{13}$C NMR (100 MHz, $CDCl_3$) δ 14.5, 16.7, 30.6, 53.8, 56.0, 61.9, 106.6, 126.3, 128.1, 128.2, 155.3, 164.6, 169.9, 198.1; MS (TOF-MS) *m/z* 248 ($M^+$, 46), 202 (21), 174 (100), 147 (10), 115 (7); HRMS (TOF-MS) calc'd for: $C_{14}H_{16}O_4$ 248.1049, found 248.1055.

**(*RS*)-5,5'-Dimethoxy-6-methyl-2,2'-spirobiindan-1,1'-dione (2.20).** A 60% dispersion of NaH (0.42g, 10.5 mmol) was washed three times with $Et_2O$. Under an argon atmosphere, a solution of **2.15** (1.55 g, 6.2 mmol) in anhydrous DMF (15 mL) was slowly added to the NaH as a stirred suspension in anhydrous DMF (5 mL). After gas evolution ceased, the mixture was heated at 60 °C for one hour and a solution of **2.16** (1.86 g, 6.8 mmol) in anhydrous DMF (30 mL) was slowly added. The solution was stirred at 60 °C for 96 hours, then quenched with water and extracted with $Et_2O$ (3×100 mL). The combined extracts were washed with brine (2×100 mL), dried ($MgSO_4$) and concentrated. The resulting (*RS*)-2-ethoxycarbonyl-2-(2-(ethoxycarbonyl)-5-methoxybenzyl)-5-methoxy-6-methyl-1-indanone (**2.18**) was dissolved in a 20:40:40 (v/v/v) solution of $H_2SO_4$, $H_2O$, and EtOH (150 mL) and the reaction mixture was heated to reflux overnight. After cooling, the reaction mixture was concentrated, neutralized with 20% aq. NaOH and extracted with $CHCl_3$ (3×100 mL). The combined extracts were washed with brine (2×100 mL), dried ($MgSO_4$) and concentrated to give a pale yellow solid. The crude product was washed with hot hexane to give 1.15 g (57%, two steps) of (*RS*)-**2.20** as a white solid: mp 223 – 225 °C; $^1$H NMR (400 MHz, $CDCl_3$) δ 7.69 (d, *J* = 8 Hz, 1H), 7.53 (s, 1H), 6.98 (d, *J* = 2 Hz, 1H), 6.94 (dd, *J* = 8 Hz, 2Hz, 1H), 3.95 (s, 3H), 3.92 (s, 3H), 3.66 (d, *J* = 17 Hz, 1H), 3.63 (d, *J* = 17 Hz, 1H), 3.11 (d, *J* = 17 Hz, 1H), 3.09 (d, *J* = 17 Hz, 1H); $^{13}$C NMR (100 MHz, $CDCl_3$) δ 16.7, 38.2, 38.3, 56.0 (2C), 65.9, 106.6, 109.8, 116.2, 126.5, 126.7, 128.1, 128.3, 129.1, 155.4, 157.3, 164.5, 166.0, 201.5, 201.6; MS (TOF-MS) *m/z* 322 ($M^+$, 100), 294 (39), 279 (12), 251 (10); HRMS (TOF-MS) calc'd for $C_{20}H_{18}O_4$: 322.1205, found 322.1212.

**(*RS*)-5,5'-Dihydroxy-6-methyl-2,2'-spirobiindan-1,1'-dione (2.22).** Under an argon

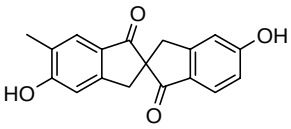


atmosphere, $AlCl_3$ (1.03 g, 7.75 mmol) was added to a stirred solution of (*RS*)-**2.20** (500 mg, 1.55 mmol) in anhydrous toluene (120 mL). The mixture was heated to reflux overnight, then carefully quenched with water and filtered. The solid residue was dissolved in EtOH, concentrated to 5 mL, washed with $H_2O$ and filtered again to give 420 mg (92%) of (*RS*)-**2.22** as an off white solid: mp > 300 °C (dec.); $^1$H NMR (400 MHz, MeOD) δ 7.56 (d, *J* = 8 Hz, 1H), 7.43 (s, 1H), 6.90 (d, *J* = 2 Hz, 1H), 6.89 (s, 1H), 6.84 (dd, *J* = 8 Hz, 2 Hz, 1H), 3.48 (d, *J* = 17 Hz, 1H), 3.45 (d, *J* = 17 Hz, 1H), 3.13 (d, *J* = 17 Hz, 1H), 3.10 (d, *J* = 17 Hz, 1H); MS (TOF-MS) *m/z* 294 ($M^+$, 100), 267 (4), 249 (11), 238 (2), 194 (3); HRMS (TOF-MS) calc'd for $C_{18}H_{14}O_4$: 294.0892, found 294.0900.

**(*R*)- and (*S*)-5,5'-(Diheptyloxy-1,1-*d*$_2$)-6-methyl-2,2'-spirobiindan-1,1'-dione ((*R*)-**

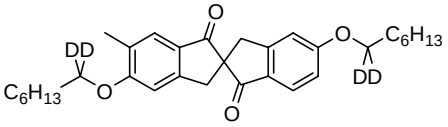


**2.2a and (*S*)-2.2a).** Under an argon atmosphere, a solution of (*RS*)-**2.22** (150 mg, 0.51 mmol), $Cs_2CO_3$ (331 mg, 1.02 mmol) and 1-bromoheptane-1,1-*d*$_2$ (320 mg, 1.77 mmol) in anhydrous DMF (30 mL) was stirred at r.t for 24 h and heated to 70 °C overnight. After cooling, the solution was poured into water and extracted with $Et_2O$ (3×50 mL). The combined organic extracts were washed with brine (2×50 mL), dried ($MgSO_4$) and concentrated. The residue was purified by flash chromatography on silica gel (9:1 hexanes/EtOAc) and recrystalized from HPLC-grade hexane to give 140 mg (55%) of (*RS*)-**2.2a** as a white solid: mp 139 – 141 °C; $^1$H NMR (400 MHz, $CDCl_3$) δ 7.67 (d, *J* = 8 Hz, 1H), 7.52 (s, 1H), 6.95 (d, *J* = 2 Hz, 1H), 6.92 (dd, *J* = 8 Hz, 2 Hz, 1H), 6.89 (s, 1H), 3.64 (d, *J* = 17 Hz, 1H), 3.61 (d, *J* = 17 Hz, 1H ), 3.09 (d, *J* = 17 Hz, 1H), 3.07 (d, *J* = 17 Hz, 1H), 2.23

(s, 3H), 1.80 – 1.87 (m, 4H), 1.33 – 1.50 (m, 16H), 0.92 (t, $J$ = 7 Hz, 6H); $^{13}$C NMR (100 MHz, $CDCl_3$) δ14.4, 16.8, 22.9, 26.2, 26.3, 29.2, 29.3, 32.1, 38.3, 38.4, 65.8, 107.2, 110.3, 116.5, 126.5, 126.7, 128.1, 128.2, 128.9, 155.4, 157.2, 164.1, 165.7, 201.6, 201.7; MS (TOF-MS) *m/z* 494 ($M^+$, 100.0), 394 (2.8), 366 (1.5), 266 (2.9); HRMS (TOF-MS) calc'd for $C_{32}H_{38}D_4O_4$: 494.3334, found 494.3346; UV (hexanes) $\lambda_{max}$ (log ε) 208 (4.68), 221 (4.58), 269 (4.58), 290 (4.35), 296 (4.39). The racemic mixture was resolved by preparative scale chiral phase HPLC (2% EtOH in hexanes, 50 mL/min) to give (*R*)-**2.2a** and (*S*)-**2.2a** (first and second eluants, respectively) in optically pure form: CD ((*R*)-**2.2a**, hexanes) $\lambda_{ext}$ (Δε) 207 (10.4), 221 (–21.1), 230 (21.8), 258 (–9.8), 271 (5.4), 294 (–3.0), 301 (–0.9), 308 (–4.3), 318 (–5.4), 332 (–5.3), 343 (–3.1). Prior to doping into liquid crystal mixtures, the dopant was recrystallized from HPLC hexanes after filtration through a 0.45 μm PTFE filter.

**(*R*)- and (*S*)-5,5'-Diheptoyloxy-6-methyl-2,2'-spirobiindan-1,1'-dione ((*R*)-2.2b and (*S*)-2.2b).** Under an argon atmosphere, DCC (349 mg, 1.7 mmol) was added to a stirred solution of (*RS*)-**2.22** (100 mg, 0.34 mmol), DMAP (207 mg, 1.7 mmol) and heptanoic acid (220 mg, 1.7 mmol) in anhydrous $CH_2Cl_2$ (10 mL). The solution was stirred at room temperature overnight, then filtered and concentrated. The residue was taken up in EtOAc (50 mL), washed with 2% aq. HCl (3×30 mL), dried ($MgSO_4$) and concentrated. The residue was purified by flash chromatography on silica gel (6:1 hexanes/EtOAc) and recrystallized from HPLC-grade hexane to give 107 mg (45%) of (*RS*)-**2.2b** as white needles: mp 148 – 149 °C; $^1$H NMR (400 MHz, $CDCl_3$) δ 7.77 (d, $J$ = 8 Hz, 1H), 7.64 (s, 1H), 7.31 (d, $J$ = 2 Hz, 1H), 7.24 (s, 1H), 7.13 (dd, $J$ = 8 Hz, 2 Hz, 1H), 3.69 (d, $J$ = 17 Hz, 1 H), 3.66 (d, $J$ =

17 Hz, 1 H), 3.18 (d, *J* = 17 Hz, 1H), 3.15 (d, *J* = 17 Hz, 1H), 2.63 (t, *J* = 7 Hz, 2H), 2.61 (t, *J* = 8 Hz, 2H), 2.24 (s, 3H), 1.76 – 1.82 (m, 4H), 1.34 – 1.46 (m, 12H), 0.93 (t, *J* = 7 Hz, 6H); $^{13}$C NMR (100 MHz, $CDCl_3$) δ 14.3, 16.7, 22.8, 25.1, 25.2, 29.0, 29.1, 31.7, 34.6, 34.8, 38.0, 38.3, 65.9, 119.7, 120.0, 122.2, 126.4, 127.4, 131.2, 133.2, 133.3, 153.3, 155.6, 155.8, 156.8, 171.8, 172.0, 201.6, 201.7; MS (TOF-MS) *m/z* 541 ($[M+Na]^+$), 519 ($[M+H]^+$), 431, 239, 186, 139; HRMS (TOF-MS) calc'd for $C_{32}H_{39}O_6$: 519.2747; found 519.2736; UV (hexanes) $\lambda_{max}$ (log ε) 206 (4.86), 255 (4.58), 292 (4.08). The racemic mixture was resolved by preparative chiral phase HPLC (5% EtOH in hexanes, 50 mL/min) to give (*R*)-**2.2b** and (*S*)-**2.2b** (first and second eluants, respectively) in optically pure form: CD ((*R*)-**2.2b**, hexanes) $\lambda_{ext}$ (Δε) 204 (13.7), 212 (–19.9), 221 (–0.6), 234 (7.6), 249 (–5.6), 263 (1.2), 292 (–4.2), 320 (–0.2), 342 (–1.6). Prior to doping into liquid crystal mixtures, the dopant was recrystallized from HPLC hexanes after filtration through a 0.45 μm PTFE filter.

Anal. calc'd for $C_{32}H_{38}O_6$: C 74.11, H 7.39; found C 74.12, H 7.60.

### 5.2. Determination of Transition Temperatures by Polarized Microscopy

Phase transition temperatures of liquid crystal mixtures were determined upon cooling by viewing thin films of the samples in 4 μm polyimide-coated ITO glass cells (E.H.C. Co., Japan), and on untreated glass slides with a cover slip using a Nikon Eclipse E600 POL filled with a Linkam LTS 350 hot stage. The I-N*, N*-SmA* and SmC*-Cr phase transition temperatures were determined based on changes in texture as observed between crossed polarizers. The SmA*-C* phase transition temperature was determined by extrapolation of the plot of $P_S$ versus temperature as the temperature where $P_S = 0$, and/or by observation of the appearance of zigzag defects.

## 5.3. Ferroelectric Polarization Measurements

### *5.3.1. Sample preparation*

Mixtures for ferroelectric polarization measurements were prepared by weighing appropriate amounts of material into conical glass vials and mixing in the isotropic phase. Capillary action was used to load each mixture into polyimide-coated ITO glass cells (4 µm x 0.160 $cm^2$) supplied by E.H.C. Co. Cell thicknesses were determined by capacitance measurement of an empty cell using a Displaytech APT-III polarization testbed (Displaytech Inc., Longmont, CO). Ferroelectric polarization measurements were carried out using the APT-III in conjunction with a Nikon Eclipse E600 POL and a Linkam LTS 350 hot stage. Each cell was heated to the isotropic phase under an AC triangular wave (100 Hz, 6 V/µm) unless otherwise noted and held until any bubbles in the addressed area disappeared. Good alignment was obtained by applying a high frequency AC field (100 Hz) to a filled cells while slowly cooling the mixtures from the isotropic phase via the N* and SmA* phases (2 °C /min).

### *5.3.2. Polarization measurements*

Spontaneous polarizations ($P_S$) were measured as a function of temperature by the triangular wave method (100 Hz, 6 V/µm) unless otherwise noted.[10] The sign of $P_S$ along the polar axis was assigned from the relative configuration of the electrical field and the switching position of the sample according to the established convention.[11] Tilt angles, $\theta$, were measured as a function of temperature between crossed polarizers as half the rotation between two extinction positions corresponding to opposite polarization orientations. The reduced polarization, $P_0$, was calculated for each mixture at $T - T_C = -10$ K according to equation (1-3).

## 5.4. Determination of Polarization Inversion Temperatures

Inversion of polarization was observed in some cases in the SmC phase, and the $P_S$ inversion temperature was determined by applying a low frequency AC field (1 Hz) upon slowly cooling the mixtures (0.5 °C/min) in the SmC* phase and finding the temperature at which no switching could be observed.

## 5.5. References


1) Nieman, J. A.; Keay, B. A. *Tetrahedron: Asymmetry* **1995**, *6*, 1575.
2) Boulton, C. J.; Finden, J. G.; Yuh, E.; Sutherland, J. J.; Wand, M. D.; Wu, G.; Lemieux, R. P. *J. Am. Chem. Soc.* **2005**, *127*, 13657.
3) Keller, P. *Ferroelectrics* **1984**, *58*, 3.
4) Gray, G. W.; Hird, M.; Lacey, D.; Toyne, K. *J. Chem. Soc., Perkin Trans. 2* **1989**, 2041.
5) Speicher, A.; Kolz, J.; Sambanje, R. P. *Synthesis*, **2002**, *17*, 2503.
6) Wyrick, S. D.; Smith, F. T.; Kemp, W. E.; Grippo, A. A. *J. Med. Chem*. **1987**, *30*, 1798.
7) Han, W.; Lu, Y.; Zhao, H.; Dutt, M.; Biehl, E. R. *Synthesis*, **1996**, *1*, 59.
8) Dean, R. E.; Midgley, A.; White, E. N.; McNeil, D. *J. Chem. Soc.***1961**, 2773.
9) Johnson, M. P.; Frescas, S. P.; Oberlender, R.; Nichols, D. E. *J. Med. Chem.* **1991**, *34*, 1662.
10) Miyasato, K.; Abe, S.; Takezoe, H.; Fukuda, A.; Kuze, E. *Jpn. J. Appl. Phys.* **1983**, *22*, L661.
11) Walba, D. M. In *Advances in the Synthesis and Reactivity of Solids*; Mallouck, T. E., Ed.; JAI Press, Ltd.: Greenwich, CT, 1991; Vol. 1, p 173.

# Appendix 1. $^{1}$NMR Spectra of Novel Compounds

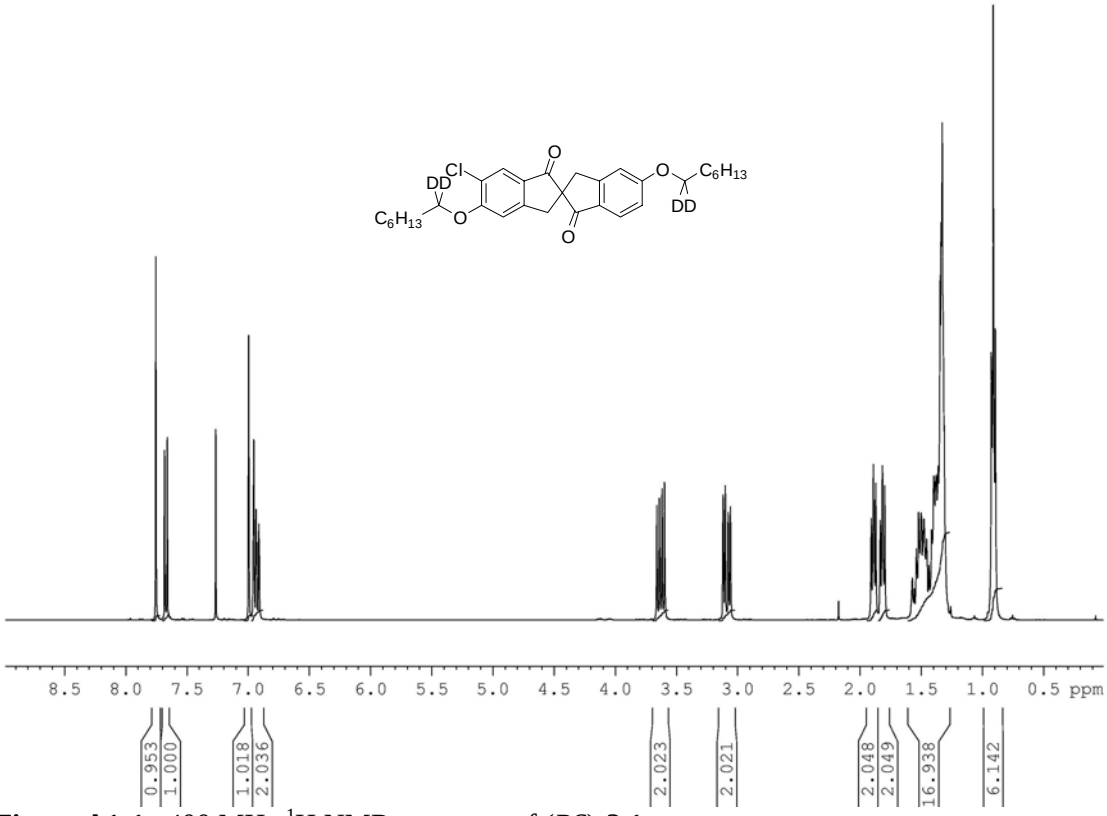


**Figure A1-1.** 400 MHz $^{1}$H NMR spectrum of (*RS*)-**2.1a**.

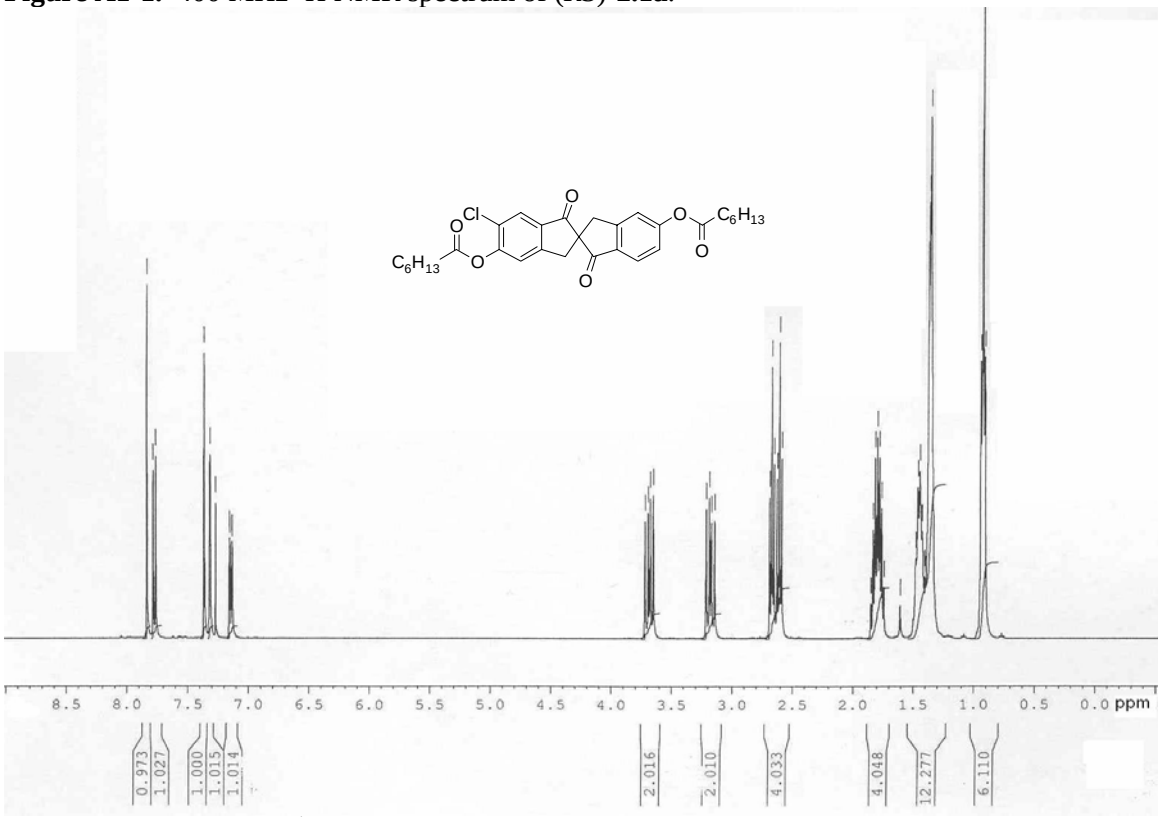


**Figure A1-2.** 400 MHz $^{1}$H NMR spectrum of (*RS*)-**2.1b**.

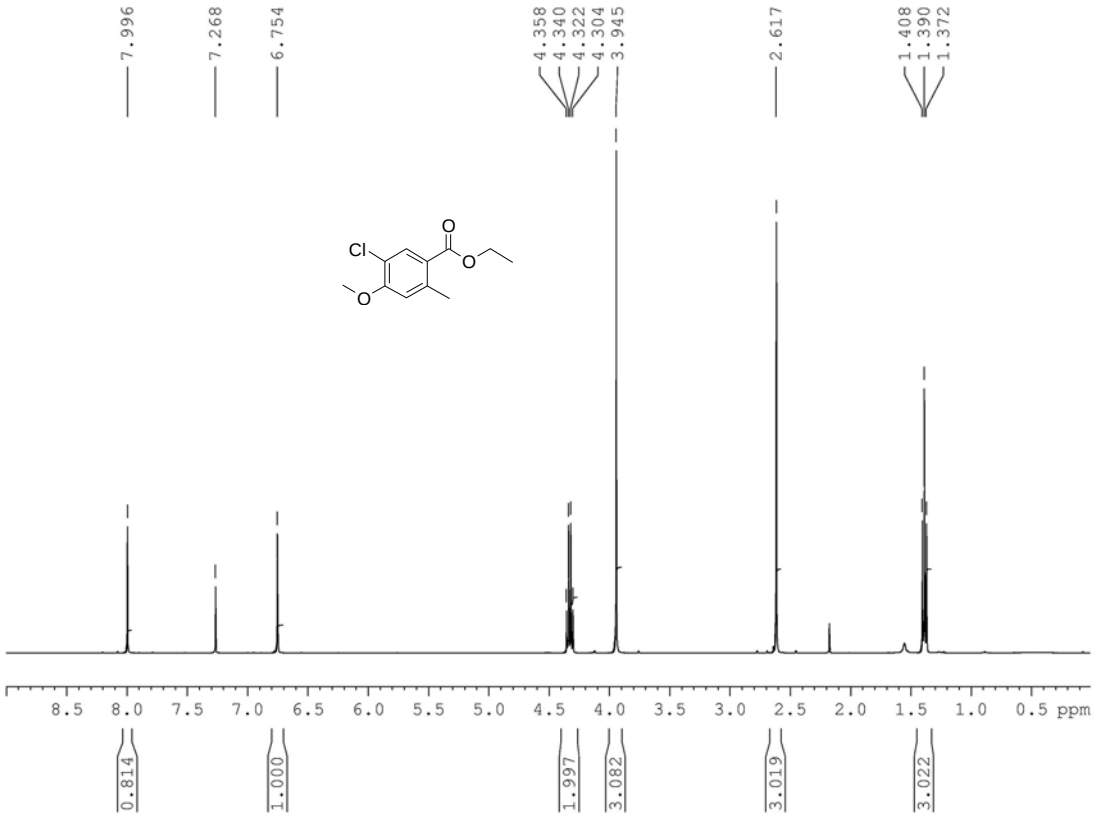


**Figure A1-3.** 400 MHz $^{1}$H NMR spectrum of **2.7**.

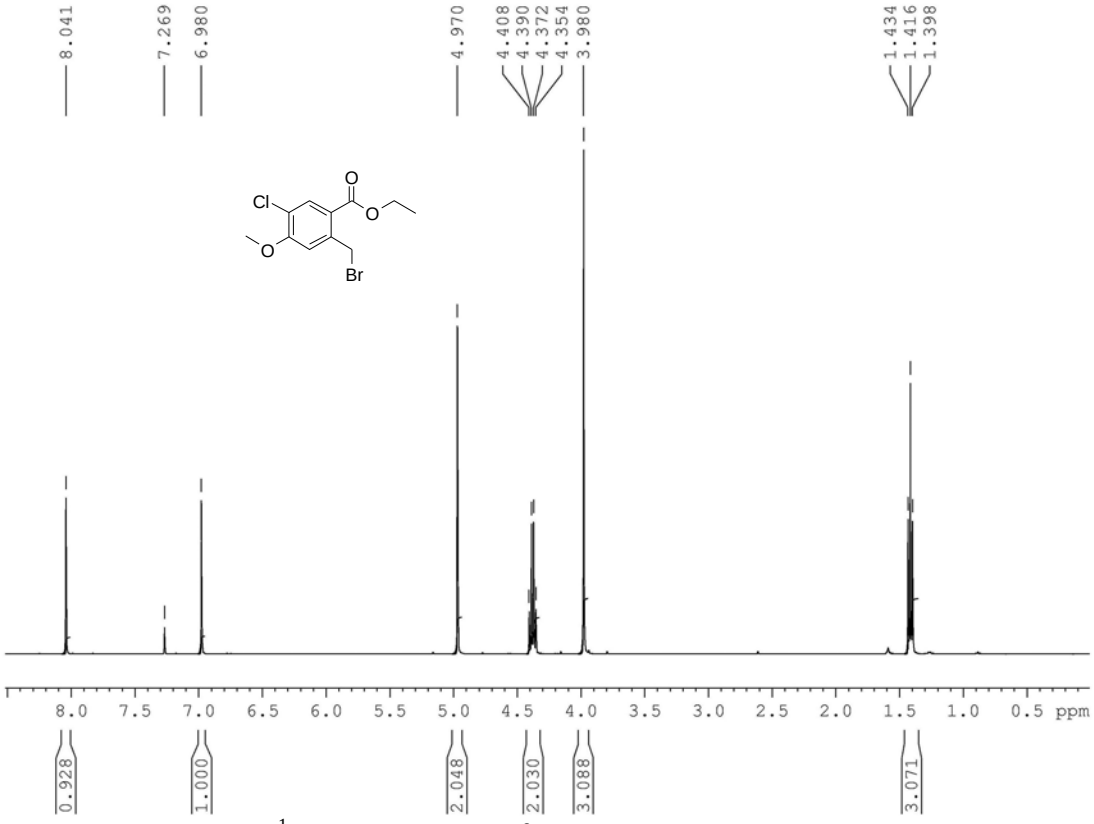


**Figure A1-4.** 400 MHz $^{1}$H NMR spectrum of **2.8**.

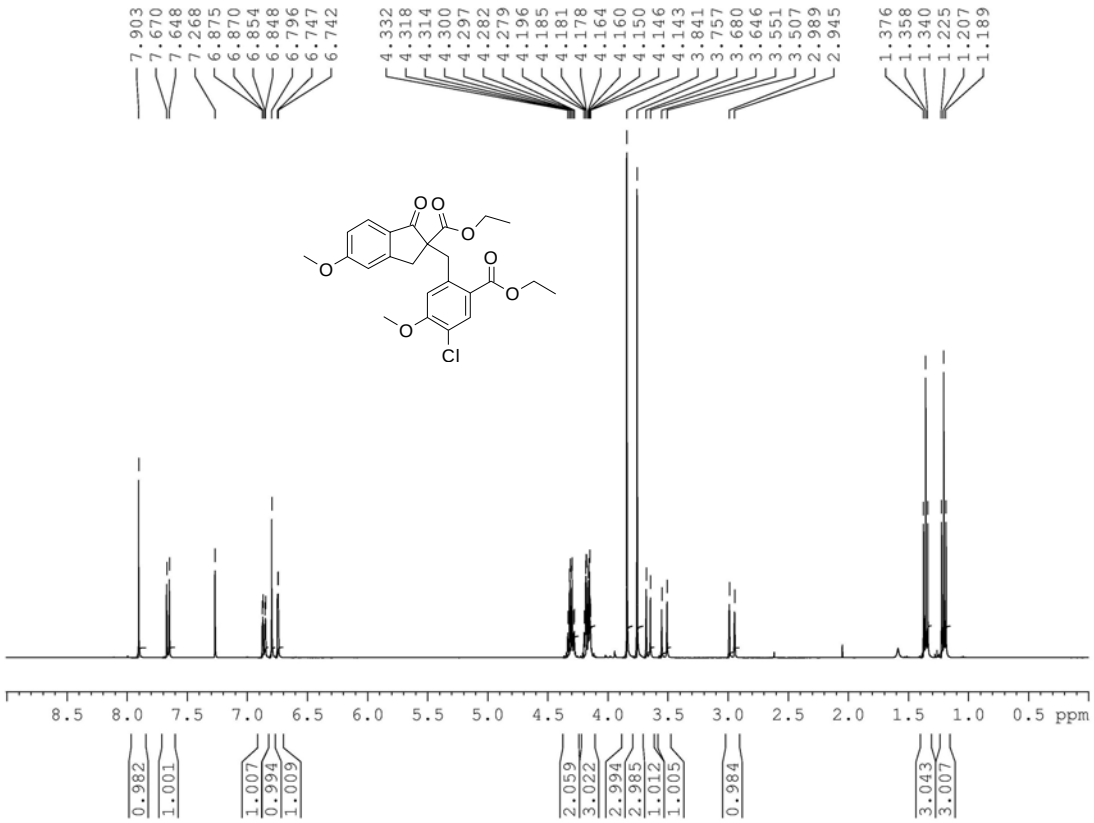


**Figure A1-5.** 400 MHz $^{1}$H NMR spectrum of (*RS*)-**2.17**.

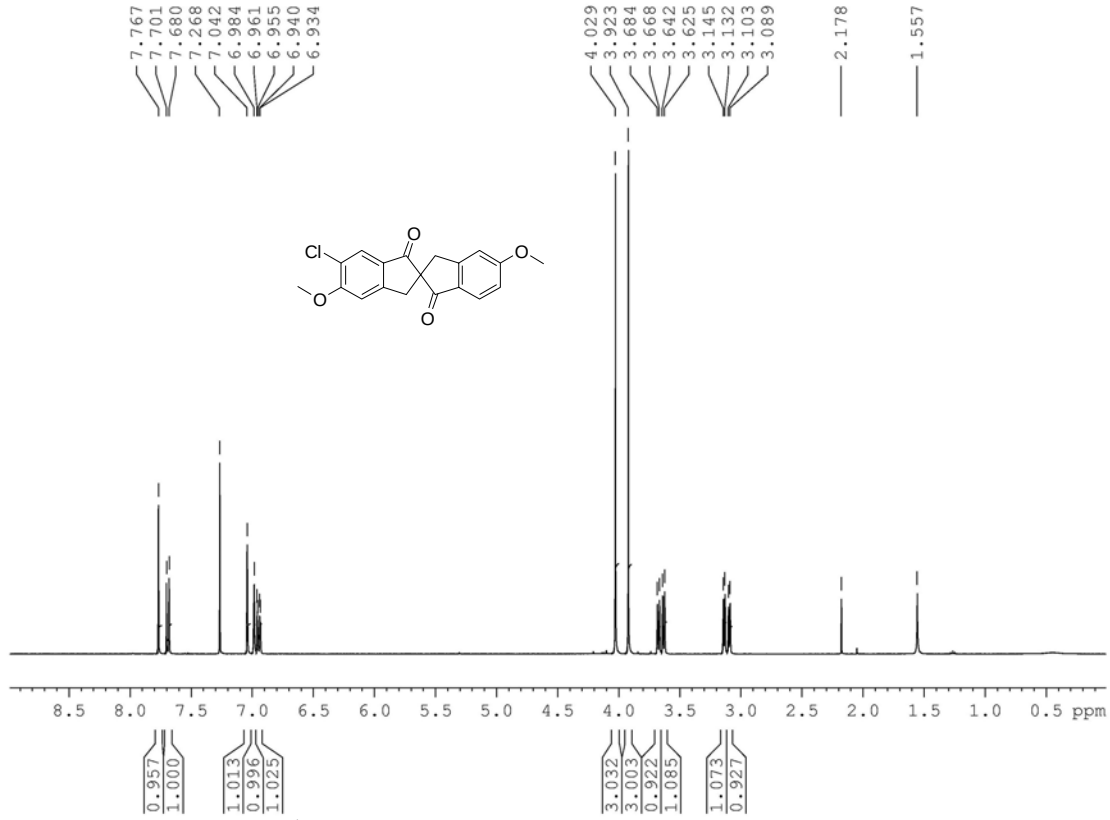


**Figure A1-6.** 400 MHz $^{1}$H NMR spectrum of (*RS*)-**2.19**.

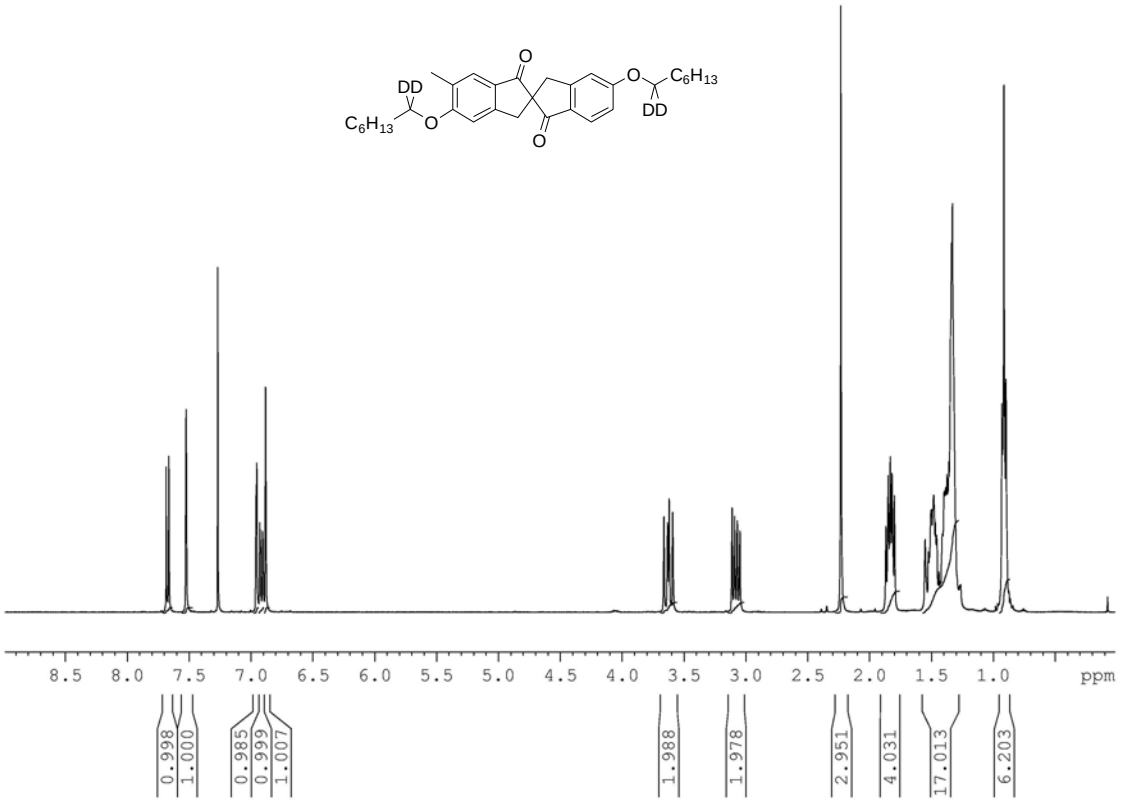


**Figure A1-7.** 400 MHz $^{1}$H NMR spectrum of (*RS*)-**2.2a**.

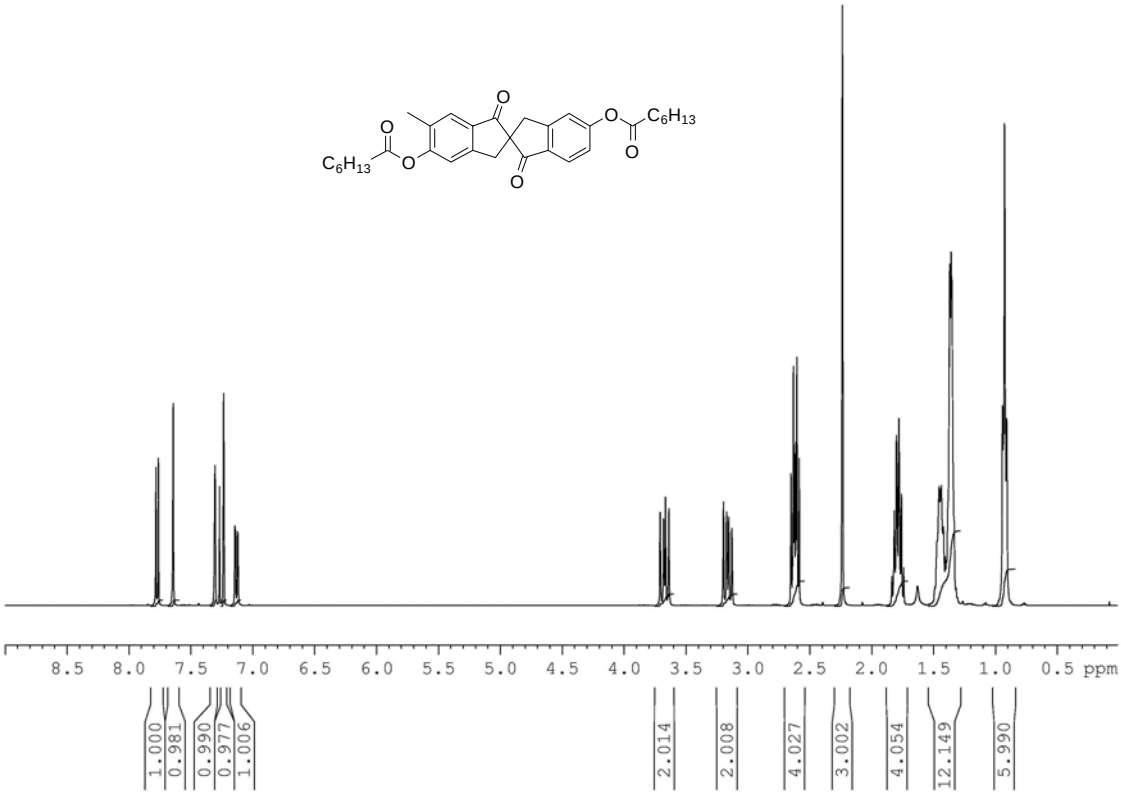


**Figure A1-8.** 400 MHz $^{1}$H NMR spectrum of (*RS*)-**2.2b**.

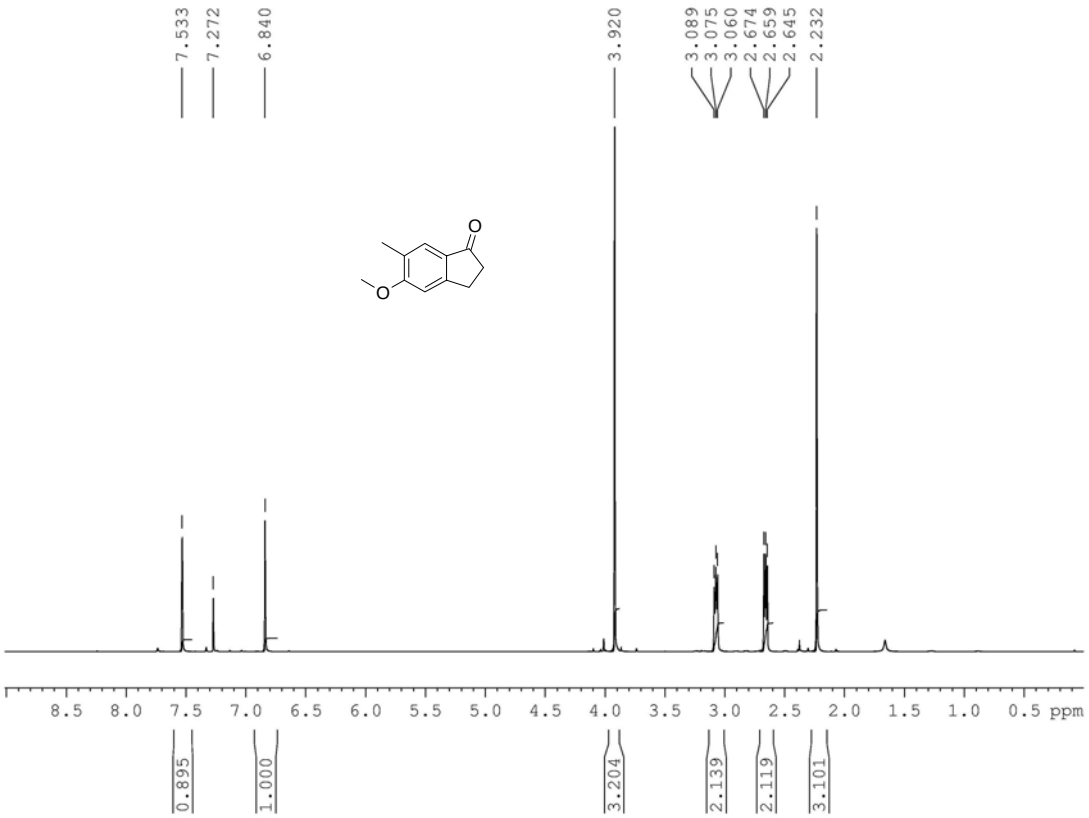


**Figure A1-9.** 400 MHz $^{1}$H NMR spectrum of **2.12**.

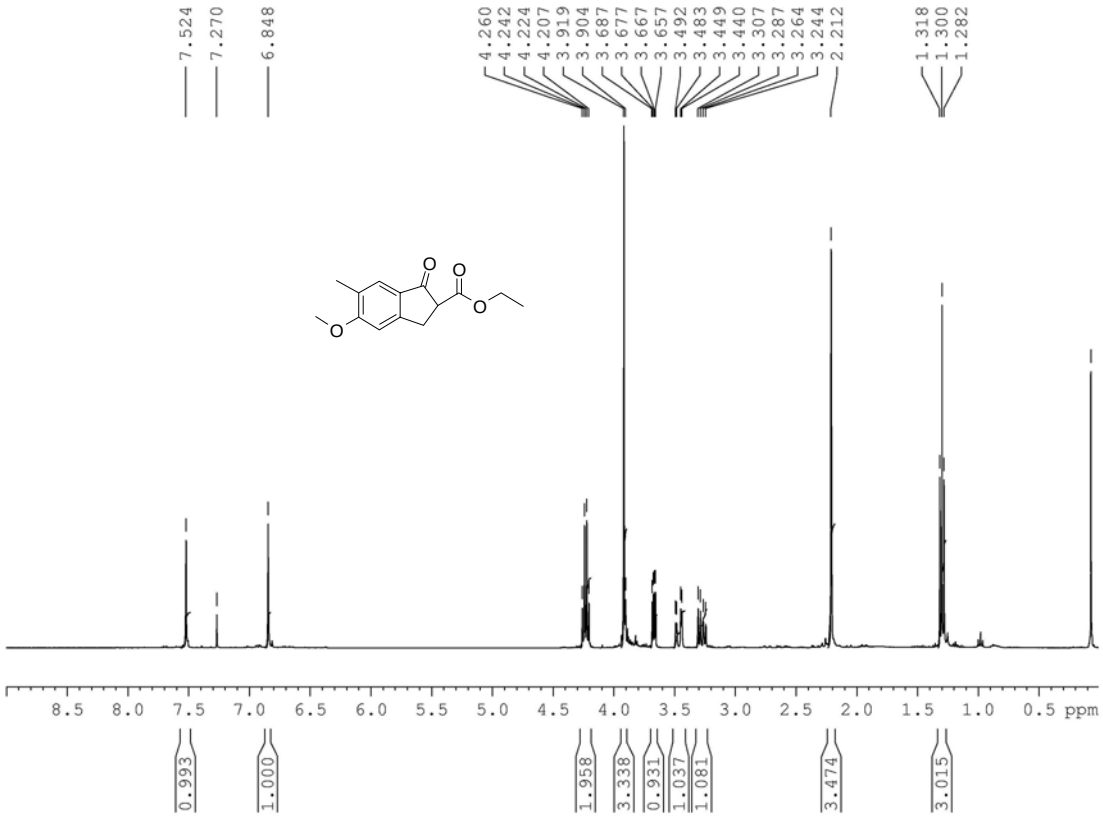


**Figure A1-10.** 400 MHz $^{1}$H NMR spectrum of **2.15**.

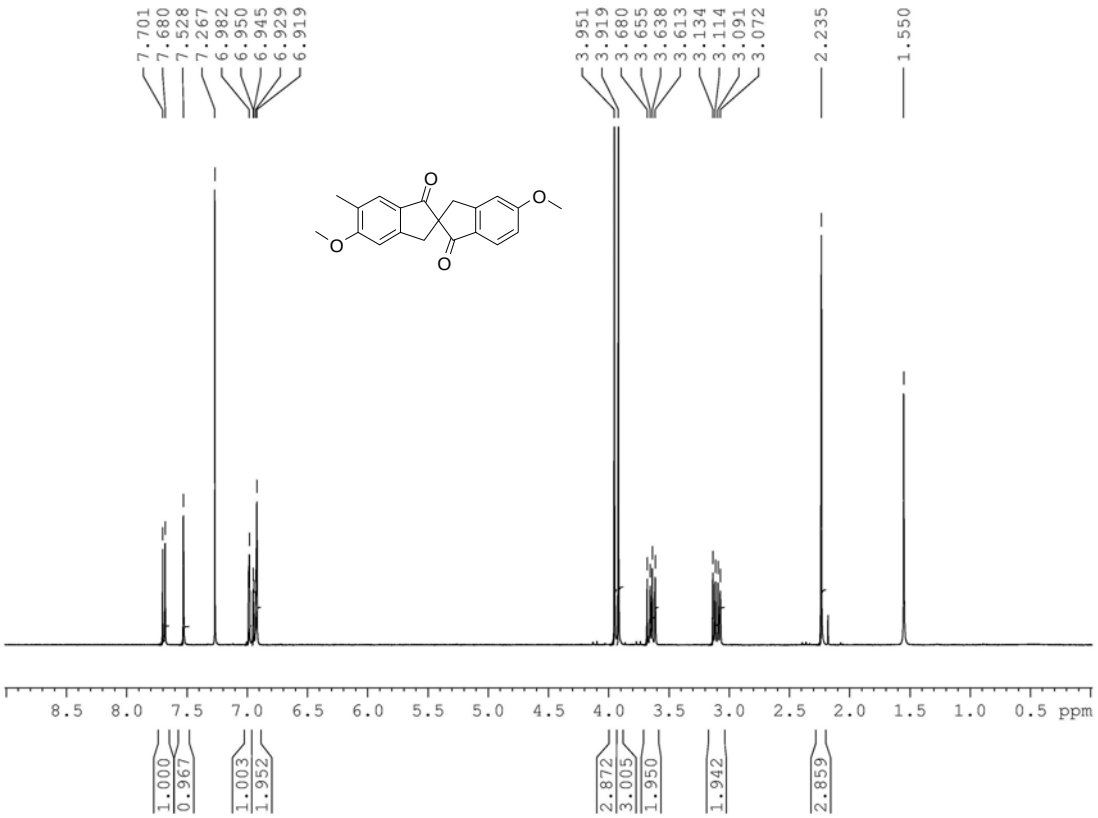


**Figure A1-11.** 400 MHz $^{1}$H NMR spectrum of (*RS*)-**2.20**.

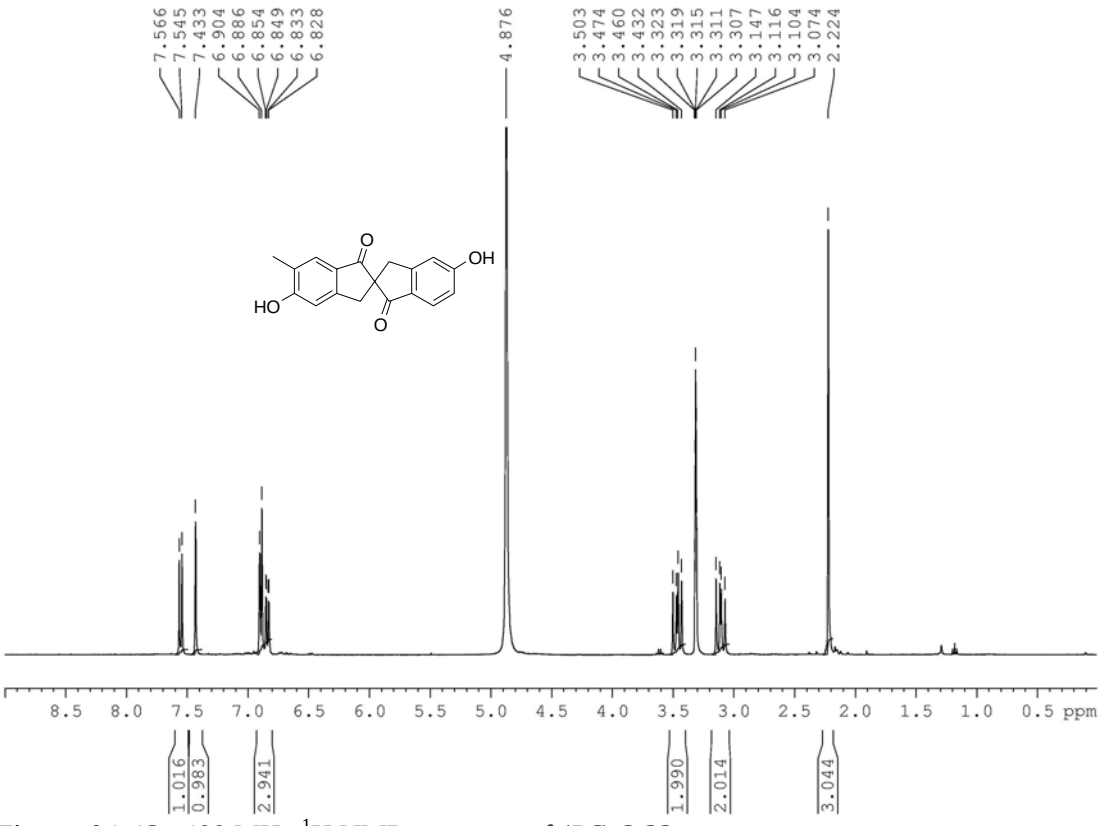


**Figure A1-12.** 400 MHz $^{1}$H NMR spectrum of (*RS*)-**2.22**.

# Appendix 2. Polarization Power Data

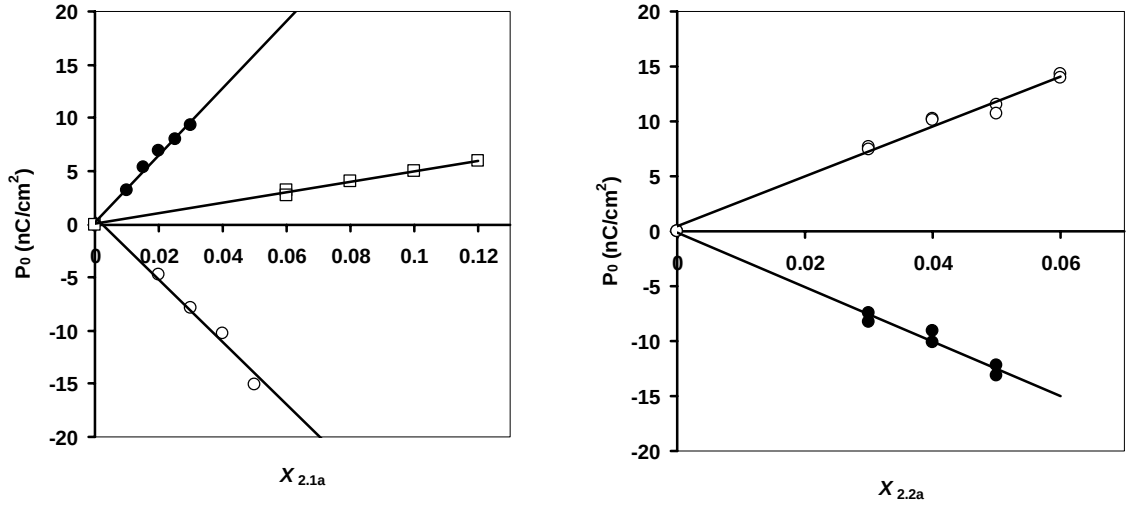


**Figure 3-8**. Reduced polarization $P_o$ versus dopant mole fraction $x_d$ in **PhP1** (●), **PhBz** (□), and **DFT** (○) at $T - T_C$ = -10K for dopant (*R*)-**2.1a** (left) and dopant (*S*)-**2.2a** (right).

(*R*)-**2.1a** in **DFT** ($T - T_C$ = –5K)

| $\chi$ (*R*)-**2.1a** | $P_S$(nC/cm$^2$) | $\theta$(°) | $P_0$ (nC/cm$^2$) |
|---|---|---|---|
| 0 | | | 0 |
| 2.0 | – 0.87 | 12.1 | – 4.15 |
| 3.0 | – 1.67 | 13.7 | – 7.05 |
| 4.0 | – 2.15 | 13.3 | – 9.35 |
| 5.0 | – 3.22 | 15.6 | – 12.0 |

(*R*)-**2.1a** in **DFT** ($T - T_C$ = –10K)

| $\chi$ (*R*)-**2.1a** | $P_S$(nC/cm$^2$) | $\theta$(°) | $P_0$ (nC/cm$^2$) |
|---|---|---|---|
| 0 | | | 0 |
| 2.0 | – 1.25 | 15.4 | – 4.72 |
| 3.0 | – 2.39 | 17.6 | – 7.90 |
| 4.0 | – 3.00 | 17.0 | – 10.3 |
| 5.0 | – 4.47 | 17.2 | – 15.1 |

(*R*)-**2.1a** in **PhP1*** ($T - T_C$ = –5K)

| $\chi$ (*R*)-**2.1a** | $P_S$(nC/cm$^2$) | $\theta$(°) | $P_0$ (nC/cm$^2$) |
|---|---|---|---|
| 0 | | | 0 |
| 0.01 | + 0.83 | 13.2 | + 3.62 |
| 0.015 | + 1.27 | 14.2 | + 5.20 |
| 0.02 | + 1.72 | 14.8 | + 6.71 |
| 0.025 | + 2.14 | 16.2 | + 7.65 |
| 0.03 | + 2.58 | 16.6 | + 9.03 |
| 0.04 | + 4.05 | 17.6 | + 13.4 |

* Measurements were performed at 80 Hz, 6 V/μm.

(*R*)-**2.1a** in **PhP1*** ($T - T_C$ = –10K)

| $\chi$ (*R*)-**2.1a** | $P_S$(nC/cm$^2$) | $\theta$(°) | $P_0$ (nC/cm$^2$) |
|---|---|---|---|
| 0 | | | 0 |
| 0.01 | + 0.85 | 15.7 | + 3.14 |
| 0.015 | + 1.53 | 16.8 | + 5.31 |
| 0.02 | + 2.16 | 18.2 | + 6.90 |
| 0.025 | + 2.64 | 19.2 | + 8.01 |
| 0.03 | + 3.20 | 20.2 | + 9.28 |

* Measurements were performed at 80 Hz, 6 V/μm.

(*R*)-**2.1a** in **PhBz** ($T - T_C$ = –5K)

| $\chi$ (*R*)-**2.1a** | $P_S$(nC/cm$^2$) | $\theta$(°) | $P_0$ (nC/cm$^2$) |
|---|---|---|---|
| 0 | | | 0 |
| 0.06 | + 0.83 | 20.2 | + 2.37 |
| 0.06 | + 0.72 | 23.6 | + 1.80 |
| 0.08 | + 1.04 | 22.2 | + 2.75 |
| 0.1 | + 1.26 | 24.0 | + 3.10 |
| 0.12 | + 1.42 | 21.8 | + 3.82 |
| 0.15* | + 1.62 | 24.8 | + 3.86 |

* $P_0$ of 15 mol% mixture remains the same as $\chi_{2.1a}$ = 0.12, although no sign of dopant's crystallization out of the mixture was observed.

(*R*)-**2.1a** in **PhBz** ($T - T_C = -10$K)

| $\chi$ (*R*)-**2.1a** | $P_S$(nC/cm$^2$) | $\theta$(°) | $P_0$ (nC/cm$^2$) |
|---|---|---|---|
| 0 | | | 0 |
| 0.06 | + 1.27 | 23.4 | + 3.20 |
| 0.06 | + 1.25 | 27.0 | + 2.75 |
| 0.08 | + 1.76 | 26.2 | + 3.99 |
| 0.1 | + 2.21 | 26.5 | + 4.95 |
| 0.12 | + 2.49 | 24.8 | + 5.94 |
| 0.15* | + 2.76 | 27.0 | + 6.07 |

* $P_0$ of 15 mol% mixture remains the same as $\chi_{2.1a} = 0.12$, although no sign of dopant's crystallization out of the mixture was observed.

(*S*)-**2.2a** in **PhP1** ($T - T_C = -5$K)

| $\chi$ (*S*)-**2.2a** | $P_S$(nC/cm$^2$) | $\theta$(°) | $P_0$ (nC/cm$^2$) |
|---|---|---|---|
| 0 | | | 0 |
| 0.03 | – 1.88 | 13.3 | – 8.17 |
| 0.03 | – 1.90 | 14.4 | – 7.59 |
| 0.04 | – 2.51 | 16.2 | – 9.00 |
| 0.04 | – 2.53 | 14.1 | – 10.4 |
| 0.05 | – 3.42 | 15.8 | – 12.6 |
| 0.05 | – 3.37 | 14.4 | – 13.6 |

(*S*)-**2.2a** in **PhP1** ($T - T_C = -10$K)

| $\chi$ (*S*)-**2.2a** | $P_S$(nC/cm$^2$) | $\theta$(°) | $P_0$ (nC/cm$^2$) |
|---|---|---|---|
| 0 | | | 0 |
| 0.03 | – 2.17 | 15.2 | – 8.28 |
| 0.03 | – 2.25 | 17.5 | – 7.48 |
| 0.04 | – 3.07 | 19.8 | – 9.06 |
| 0.04 | – 2.99 | 17.2 | – 10.1 |
| 0.05 | – 3.97 | 18.9 | – 12.3 |
| 0.05 | – 3.85 | 17.0 | – 13.2 |

(*S*)-**2.2a** in **DFT** ($T - T_C$ = –5K)

| $\chi$ (*S*)-**2.2a** | $P_S$(nC/cm$^2$) | $\theta$(°) | $P_0$ (nC/cm$^2$) |
|---|---|---|---|
| 0 | | | 0 |
| 0.03 | + 1.37 | 13.5 | + 5.87 |
| 0.03 | + 1.34 | 12.6 | + 6.17 |
| 0.04 | + 2.04 | 14.0 | + 8.43 |
| 0.04 | + 1.96 | 13.5 | + 8.40 |
| 0.05 | + 2.20 | 12.8 | + 9.93 |
| 0.05 | + 2.14 | 14.3 | + 8.86 |
| 0.06 | + 2.81 | 13.8 | + 11.8 |
| 0.06 | + 2.66 | 14.0 | + 11.0 |

(*S*)-**2.2a** in **DFT** ($T - T_C$ = –10K)

| $\chi$ (*S*)-**2.2a** | $P_S$(nC/cm$^2$) | $\theta$(°) | $P_0$ (nC/cm$^2$) |
|---|---|---|---|
| 0 | | | 0 |
| 0.03 | + 2.15 | 16.4 | + 7.64 |
| 0.03 | + 2.04 | 16.0 | + 7.40 |
| 0.04 | + 3.12 | 17.8 | + 10.2 |
| 0.04 | + 3.07 | 17.6 | + 10.2 |
| 0.05 | + 3.37 | 17.1 | + 11.5 |
| 0.05 | + 3.30 | 18.0 | + 10.7 |
| 0.06 | + 4.24 | 17.8 | + 13.9 |
| 0.06 | + 4.12 | 16.7 | + 14.3 |

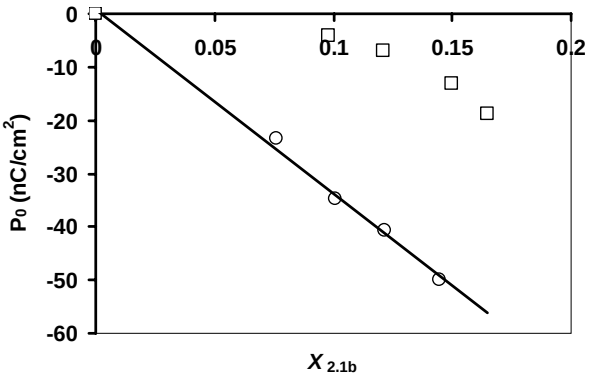


**Figure 3-11**. Reduced polarization $P_0$ versus dopant mole fraction $x_{2.1b}$ for (*R*)-**2.1b** in **PhBz** (□) and **DFT** (○) at $T - T_C$ = -10K.

(*R*)-**2.1b** in **DFT** ($T - T_C$ = -5K)

| $\chi$ (*R*)-**2.1b** | $P_S$(nC/cm$^2$) | $\theta$(°) | $P_0$ (nC/cm$^2$) |
|---|---|---|---|
| 0 | | | 0 |
| 0.076 | – 4.40 | 13.2 | – 19.3 |
| 0.101 | – 6.51 | 13.2 | – 28.4 |
| 0.122 | – 8.28 | 13.3 | – 36.0 |
| 0.144 | – 9.80 | 14.2 | – 40.0 |

(*R*)-**2.1b** in **DFT** ($T - T_C$ = -10K)

| $\chi$ (*R*)-**2.1b** | $P_S$(nC/cm$^2$) | $\theta$(°) | $P_0$ (nC/cm$^2$) |
|---|---|---|---|
| 0 | | | 0 |
| 0.076 | – 6.58 | 16.4 | – 23.3 |
| 0.101 | – 9.86 | 16.5 | – 34.7 |
| 0.122 | – 12.5 | 17.8 | – 40.8 |
| 0.144 | – 14.9 | 17.4 | – 49.9 |

(*R*)-**2.1b** in **PhBz** ($T - T_C$ = -5K)

| $\chi$ (*R*)-**2.1b** | $P_S$(nC/cm$^2$) | $\theta$(°) | $P_0$ (nC/cm$^2$) |
|---|---|---|---|
| 0 | | | 0 |
| 0.098 | – 1.17 | 20.5 | – 3.34 |
| 0.121 | – 2.39 | 22.4 | – 6.27 |
| 0.150 | – 4.78 | 23.4 | – 12.0 |
| 0.165 | – 6.78 | 23.5 | – 17.0 |

(*R*)-**2.1b** in **PhBz** ($T - T_C$ = -10K)

| $\chi$ (*R*)-**2.1b** | $P_S$(nC/cm$^2$) | $\theta$(°) | $P_0$ (nC/cm$^2$) |
|---|---|---|---|
| 0 | | | 0 |
| 0.098 | – 1.56 | 22.4 | – 4.09 |
| 0.121 | – 2.98 | 25.3 | – 6.97 |
| 0.150 | – 5.98 | 26.8 | – 13.3 |
| 0.165 | – 8.28 | 26.0 | – 18.9 |

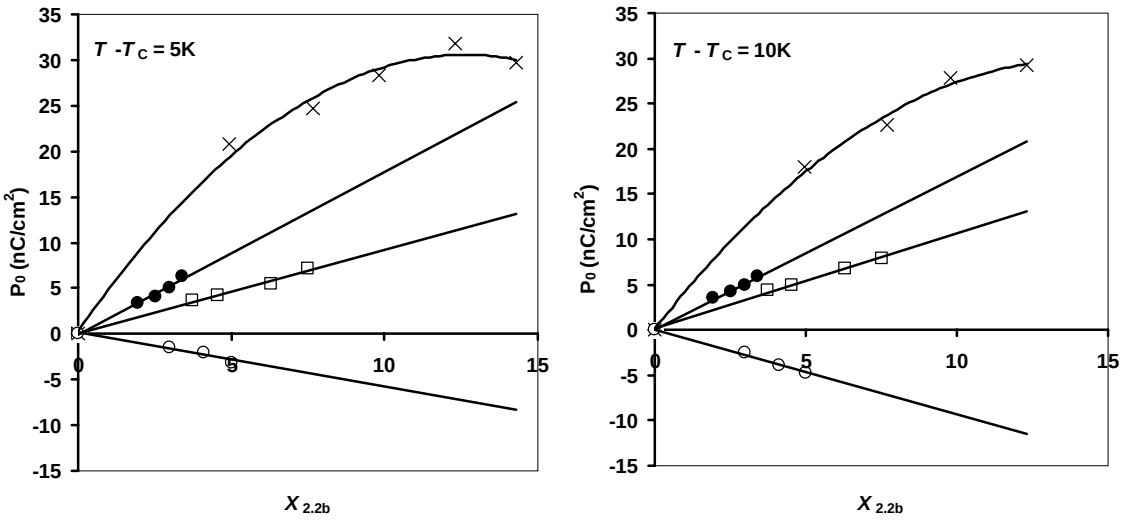


**Figure 3-13**. Reduced polarization $P_0$ versus dopant mole fraction $x_{2.2b}$ for (*R*)-**2.2b** in the four LC hosts at $T - T_C$ = -5K (left) and $T - T_C$ = -10K (right): **PhP1** (●), **PhBz** (□), **NCB76** (×)and **DFT** (○). Note the non-linear relationship between $P_0$ and $x_{2.2b}$ in **NCB76** at both $T - T_C$ = -5K and $T - T_C$ = -10K.

(*R*)-**2.2b** in **NCB76*** ($T - T_C$ = -5K)

| $\chi$ (*R*)-**2.2b** | $P_S$(nC/cm$^2$) | $\theta$(°) | $P_0$ (nC/cm$^2$) |
|---|---|---|---|
| 0 | | | 0 |
| 0.050 | + 4.04 | 11.2 | + 20.8 |
| 0.077 | + 5.21 | 12.2 | + 24.6 |
| 0.098 | + 5.83 | 11.9 | + 28.3 |
| 0.123 | + 6.66 | 12.1 | + 31.8 |
| 0.143 | + 6.88 | 13.4 | + 29.7 |

* Measurements were performed at 80 Hz, 6 V/μm.

(*R*)-**2.2b** in **NCB76*** ($T - T_C$ = -10K)

| $\chi$ (*R*)-**2.2b** | $P_S$(nC/cm$^2$) | $\theta$(°) | $P_0$ (nC/cm$^2$) |
|---|---|---|---|
| 0 | | | 0 |
| 0.050 | + 4.40 | 14.1 | + 18.1 |
| 0.077 | + 6.04 | 15.5 | + 22.6 |
| 0.098 | + 7.33 | 15.3 | + 27.8 |
| 0.123 | + 8.42 | 16.7 | + 29.3 |

* Measurements were performed at 80 Hz, 6 V/μm.

(*R*)-**2.2b** in **PhBz** ($T - T_C$ = -5K)

| $\chi$ (*R*)-**2.2b** | $P_S$(nC/cm$^2$) | $\theta$(°) | $P_0$ (nC/cm$^2$) |
|---|---|---|---|
| 0 | | | 0 |
| 0.037 | + 1.27 | 19.9 | + 3.73 |
| 0.046 | + 1.49 | 20.7 | + 4.22 |
| 0.063 | + 2.01 | 21.7 | + 5.44 |
| 0.075 | + 2.49 | 20.3 | + 7.18 |

(*R*)-**2.2b** in **PhBz** ($T - T_C$ = -10K)

| $\chi$ (*R*)-**2.2b** | $P_S$(nC/cm$^2$) | $\theta$(°) | $P_0$ (nC/cm$^2$) |
|---|---|---|---|
| 0 | | | 0 |
| 0.037 | + 1.73 | 21.6 | + 4.43 |
| 0.046 | + 2.00 | 23.7 | + 4.96 |
| 0.063 | + 2.60 | 22.8 | + 6.71 |
| 0.075 | + 3.12 | 23.1 | + 7.95 |

(*R*)-**2.2b** in **PhP1** ($T - T_C$ = -5K)

| $\chi$ (*R*)-**2.2b** | $P_S$(nC/cm$^2$) | $\theta$(°) | $P_0$ (nC/cm$^2$) |
|---|---|---|---|
| 0 | | | 0 |
| 0.020 | + 0.48 | 8.2 | + 3.37 |
| 0.025 | + 0.72 | 10.3 | + 4.03 |
| 0.030 | + 1.08 | 12.3 | + 5.07 |
| 0.034 | + 1.04 | 9.4 | + 6.37 |

(*R*)-**2.2b** in **PhP1** ($T - T_C$ = -10K)

| $\chi$ (*R*)-**2.2b** | $P_S$(nC/cm$^2$) | $\theta$(°) | $P_0$ (nC/cm$^2$) |
|---|---|---|---|
| 0 | | | 0 |
| 0.020 | + 0.64 | 10.6 | + 3.48 |
| 0.025 | + 0.92 | 12.7 | + 4.18 |
| 0.030 | + 1.22 | 14.4 | + 4.91 |
| 0.034 | + 1.15 | 11.5 | + 5.95 |

(*R*)-**2.2b** in **DFT** ($T - T_C$ = -5K)

| $\chi$ (*R*)-**2.2b** | $P_S$(nC/cm$^2$) | $\theta$(°) | $P_0$ (nC/cm$^2$) |
|---|---|---|---|
| 0 | | | 0 |
| 0.030 | – 0.28 | 11.3 | – 1.43 |
| 0.041 | – 0.42 | 11.8 | – 2.05 |
| 0.050 | – 0.64 | 11.8 | – 3.13 |

(*R*)-**2.2b** in **DFT** ($T - T_C$ = -10K)

| $\chi$ (*R*)-**2.2b** | $P_S$(nC/cm$^2$) | $\theta$(°) | $P_0$ (nC/cm$^2$) |
|---|---|---|---|
| 0 | | | 0 |
| 0.030 | – 0.58 | 13.1 | – 2.56 |
| 0.041 | – 0.98 | 14.6 | – 3.89 |
| 0.050 | – 1.26 | 15.5 | – 4.71 |

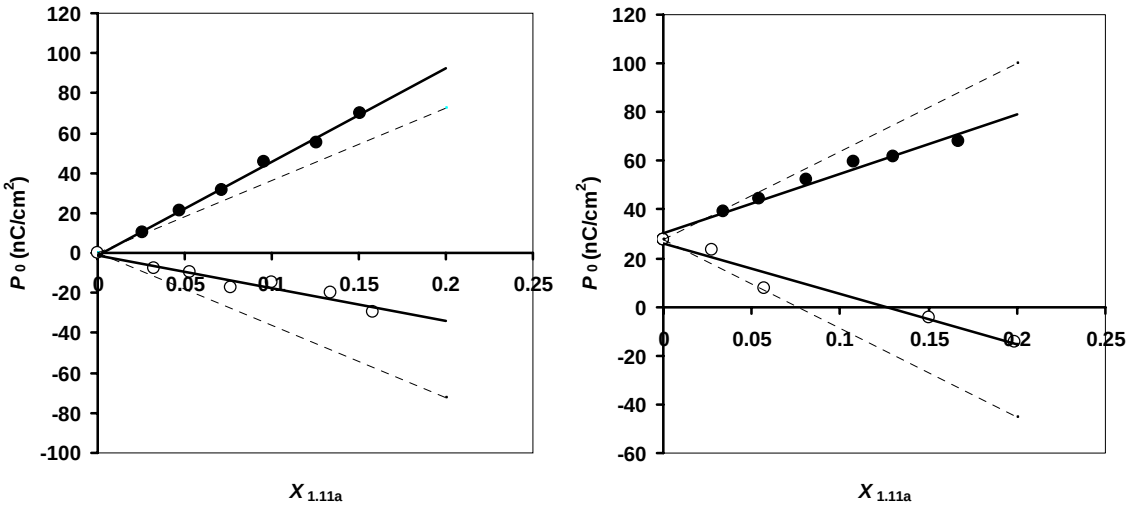


**Figure 3-21.** Reduced polarization ($P_0$) vs. mole fraction for mixtures of (*R*)-**1.11a** (●) and (*S*)-**1.11a** (○) in **NCB76** in the presence of 5 mol% (*S*)-**2.1b** (left) and (*R*)-**1.11b** (right) at 10 K below the SmA*-SmC* transition temperature. $P_0$ induced by 5 mol% of (*S*)-**2.1b** was considered to be zero and $P_0$ induced by 5 mol% of (*R*)-**1.11b** was measured in the absence of the probe dopant **1.11a**. The solid lines represent least-squares fits of the two data sets and the dashed lines represent reference plots for (*R*)- and (*S*)-**1.11a** in the absence of a second dopant based on $\delta_p$ values previously measured (ref. 2).

(*R*)-**1.11b** in **and** (*S*)-**1.11a** in **NCB76** ($T - T_C$ = -5K**)**

| $\chi$ (*R*)-**1.11b** | $\chi$ (*R*)-**1.11a** | $P_S$ (nC/cm$^2$) | $\theta$ (°) | $P_0$ (nC/cm$^2$) |
|---|---|---|---|---|
| 0.050 | 0 | | | + 27.5 |
| 0.050 | 0.027 | + 3.72 | 11.2 | + 19.2 |
| 0.050 | 0.057 | + 2.11 | 13.4 | + 9.10 |
| 0.050 | 0.150 | – 0.69 | 13.2 | – 3.02 |
| 0.050 | 0.198 | – 2.86 | 15.1 | – 11.0 |

(*R*)-**1.11b** in **and** (*S*)-**1.11a** in **NCB76** ($T - T_C$ = -10K**)**

| $\chi$ (*R*)-**1.11b** | $\chi$ (*R*)-**1.11a** | $P_S$ (nC/cm$^2$) | $\theta$ (°) | $P_0$ (nC/cm$^2$) |
|---|---|---|---|---|
| 0.050 | 0 | | | + 27.5 |
| 0.050 | 0.027 | + 5.65 | 14.0 | + 23.4 |
| 0.050 | 0.057 | + 2.09 | 16.2 | + 7.49 |
| 0.050 | 0.150 | – 1.19 | 16.7 | – 4.14 |
| 0.050 | 0.198 | – 4.45 | 17.8 | – 14.6 |

(*R*)-**1.11b** in **and** (*R*)-**1.11a** in **NCB76** ($T - T_C$ = -5K**)**

| $\chi$ (*S*)-**2.1b** | $\chi$ (*R*)-**1.11a** | $P_S$ (nC/cm$^2$) | $\theta$ (°) | $P_0$ (nC/cm$^2$) |
|---|---|---|---|---|
| 0.050 | 0 | | | + 27.5 |
| 0.050 | 0.034 | + 7.30 | 12.4 | + 34.0 |
| 0.050 | 0.054 | + 8.38 | 13.2 | + 36.7 |
| 0.050 | 0.081 | + 10.2 | 13.1 | + 44.8 |
| 0.050 | 0.108 | + 11.7 | 13.1 | + 51.6 |
| 0.050 | 0.130 | + 12.1 | 13.3 | + 52.6 |
| 0.050 | 0.167 | + 13.6 | 13.7 | + 57.3 |

(*R*)-**1.11b** in **and** (*R*)-**1.11a** in **NCB76** ($T - T_C$ = -10K**)**

| $\chi$ (*R*)-**1.11b** | $\chi$ (*R*)-**1.11a** | $P_S$ (nC/cm$^2$) | $\theta$ (°) | $P_0$ (nC/cm$^2$) |
|---|---|---|---|---|
| 0.050 | 0 | | | + 27.5 |
| 0.050 | 0.034 | + 10.4 | 15.4 | + 39.2 |
| 0.050 | 0.054 | + 12.4 | 16.2 | + 44.6 |
| 0.050 | 0.081 | + 14.9 | 16.6 | + 52.1 |
| 0.050 | 0.108 | + 17.1 | 16.7 | + 59.5 |
| 0.050 | 0.130 | + 18.1 | 17.0 | + 62.0 |
| 0.050 | 0.167 | + 20.4 | 17.4 | + 68.2 |

(*S*)-**2.1b** in **and** (*S*)-**1.11a** in **NCB76** ($T - T_C$ = -5K**)**

| $\chi$ (*S*)-**2.1b** | $\chi$ (*S*)-**1.11a** | $P_S$ (nC/cm$^2$) | $\theta$ (°) | $P_0$ (nC/cm$^2$) |
|---|---|---|---|---|
| 0.050 | 0 | | | 0 |
| 0.050 | 0.033 | – 1.25 | 13.4 | – 5.39 |
| 0.050 | 0.053 | – 1.92 | 12.9 | – 8.60 |
| 0.050 | 0.076 | – 3.45 | 14.7 | – 13.6 |
| 0.050 | 0.100 | – 3.19 | 13.5 | – 13.7 |
| 0.050 | 0.134 | – 4.31 | 13.0 | – 19.2 |
| 0.050 | 0.158 | – 5.72 | 13.8 | – 24.0 |

(*S*)-**2.1b** in **and** (*S*)-**1.11a** in **NCB76** ($T - T_C$ = -10K**)**

| $\chi$ (*S*)-**2.1b** | $\chi$ (*S*)-**1.11a** | $P_S$ (nC/cm$^2$) | $\theta$ (°) | $P_0$ (nC/cm$^2$) |
|---|---|---|---|---|
| 0.050 | 0 | | | 0 |
| 0.050 | 0.033 | – 2.09 | 16.4 | – 7.40 |
| 0.050 | 0.053 | – 2.66 | 16.6 | – 9.31 |
| 0.050 | 0.076 | – 5.19 | 17.5 | – 17.3 |
| 0.050 | 0.100 | – 4.09 | 15.9 | – 14.9 |
| 0.050 | 0.134 | – 5.71 | 16.5 | – 20.1 |
| 0.050 | 0.158 | – 8.71 | 17.1 | – 29.6 |

(*S*)-**2.1b** in **and** (*R*)-**1.11a** in **NCB76** ($T - T_C$ = -5K**)**

| $\chi$ (*S*)-**2.1b** | $\chi$ (*R*)-**1.11a** | $P_S$ (nC/cm$^2$) | $\theta$ (°) | $P_0$ (nC/cm$^2$) |
|---|---|---|---|---|
| 0.050 | 0 | | | 0 |
| 0.050 | 0.026 | + 1.84 | 10.6 | + 10.0 |
| 0.049 | 0.047 | + 3.72 | 10.6 | + 22.2 |
| 0.049 | 0.071 | + 5.17 | 11.1 | + 26.8 |
| 0.049 | 0.095 | + 7.03 | 10.4 | + 38.9 |
| 0.049 | 0.125 | + 9.28 | 10.6 | + 50.4 |
| 0.050 | 0.151 | + 10.7 | 10.8 | + 57.2 |

(*S*)-**2.1b** in **and** (*R*)-**1.11a** in **NCB76** ($T - T_C$ = -10K**)**

| $\chi$ (*S*)-**2.1b** | $\chi$ (*R*)-**1.11a** | $P_S$ (nC/cm$^2$) | $\theta$ (°) | $P_0$ (nC/cm$^2$) |
|---|---|---|---|---|
| 0.050 | 0 | | | 0 |
| 0.050 | 0.026 | + 2.32 | 13.1 | + 10.2 |
| 0.049 | 0.047 | + 5.10 | 13.9 | + 21.2 |
| 0.049 | 0.071 | + 7.86 | 14.5 | + 31.4 |
| 0.049 | 0.095 | + 10.5 | 13.2 | + 45.9 |
| 0.049 | 0.125 | + 14.1 | 14.8 | + 55.3 |
| 0.050 | 0.151 | + 16.2 | 13.4 | + 70.0 |

# Appendix 3. Inversion of Polarizations

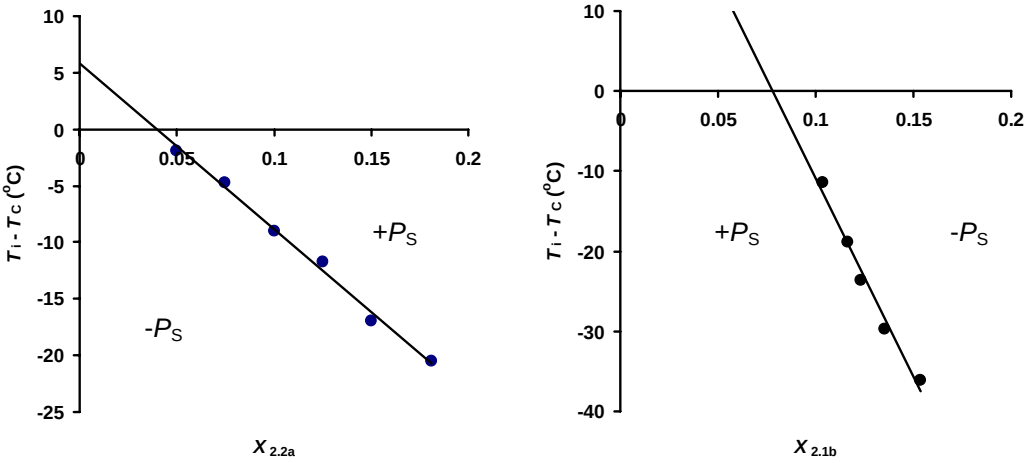


**Figure 3-12**. Reduced Inversion temperature (°C) versus dopant mole fraction $x_d$ for dopant (*S*)-**2.2a** (left) and (*R*)-**2.1b** (right) in **NCB76**.

(*S*)-**2.2a** in **NCB76**

| $\chi$ (*S*)-**2.2a** | $T_C$ (°C) | $T_i$ (°C) | $T_i - T_C$ (°C) |
|---|---|---|---|
| 0.050 | 68.4 | 66.5 | – 1.9 |
| 0.075 | 67.5 | 62.8 | – 4.7 |
| 0.100 | 66.9 | 57.9 | – 9.0 |
| 0.125 | 66.0 | 54.3 | – 11.7 |
| 0.150 | 64.7 | 47.7 | – 17.0 |
| 0.181 | 64.5 | 44 | – 20.5 |

(*R*)-**2.1b** in **NCB76**

| $\chi$ (*R*)-**2.1b** | $T_C$ (°C) | $T_i$ (°C) | $T_i - T_C$ (°C) |
|---|---|---|---|
| 0.1037 | 75.0 | 63.5 | – 11.5 |
| 0.1164 | 76.0 | 57.2 | – 18.8 |
| 0.1232 | 77.2 | 53.6 | – 23.6 |
| 0.1354 | 78.5 | 48.8 | – 29.7 |
| 0.1538 | 80.0 | 43.9 | – 36.1 |